AD-A053 693 WASHINGTON STATE UNIV PULLMAN SHOCK DYNAMICS LAB F/G 14/2
ELECTRICAL RESPONSE OF A BIMETALLIC JUNCTION TO SHOCK COMPRESSI--ETC(U)
MAR 78 D D BLOOMQUIST, G E DUVALL, J J DICK F49620-77-C-0034
UNCLASSIFIED AFOSR-TR-78-0728 NL

1 OF 2
AD A053 693

AFOSR-TR- 78-0728

AD A053693

DDC FILE COPY

Shock Dynamics Laboratory

Department of Physics

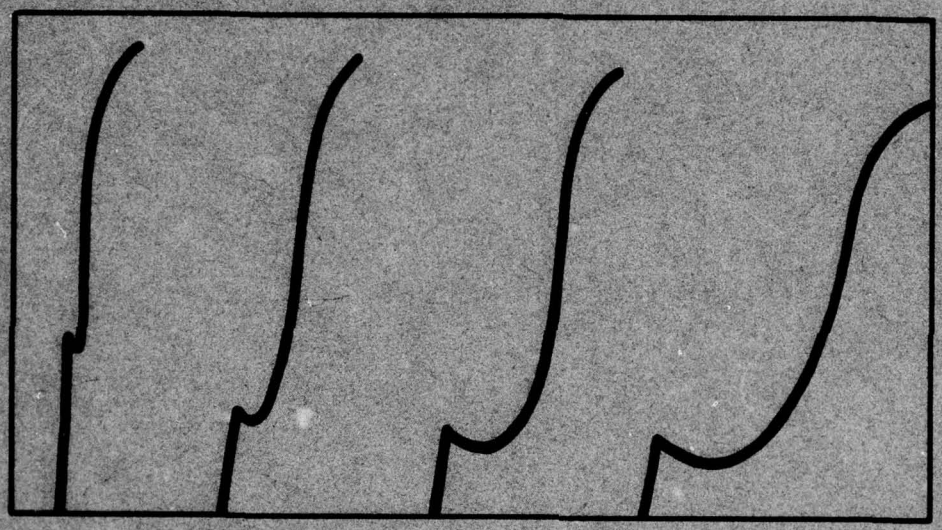

Washington State University

Pullman, Washington 99163

DISTRIBUTION STATEMENT A
Approved for public release;
Distribution Unlimited

DDC
RECEIVED
MAY 10 1978
B

The front cover shows stress time profiles for LiF. Specimen thicknesses are, from left to right, .478mm, 1.078mm, 4.066mm, 5.592mm. Vertical scale, 4 kbar/cm; horizontal scale, 0.1μsec/cm.

ELECTRICAL RESPONSE OF A BIMETALLIC JUNCTION TO SHOCK COMPRESSION

FINAL REPORT

F49620-77-C-0034

by

Douglas D. Bloomquist

George E. Duvall

and

Jerry J. Dick

Washington State University
Department of Physics
Pullman, WA 99164

Research sponsored by the Air Force Office of Scientific Research, Air Force Systems Command, USAF, under Contract No. F49620-77-C-0034. The United States Government is authorized to reproduce and distribute reprints for Governmental purposes notwithstanding any copyright notation hereon.

Approved for public release; distribution unlimited.

March 1978

DDC
RECEIVED
MAY 10 1978
B

(19) REPORT DOCUMENTATION PAGE

READ INSTRUCTIONS BEFORE COMPLETING FORM

1. REPORT NUMBER (18) AFOSR TR- 78-0728	2. GOVT ACCESSION NO.
3. RECIPIENT'S CATALOG NUMBER	
4. TITLE (and Subtitle) (6) Electrical Response of a Bimetallic Junction to Shock Compression.	5. TYPE OF REPORT & PERIOD COVERED Final Report, 11/1/76 - 12/31/77
	6. PERFORMING ORG. REPORT NUMBER
7. AUTHOR(s) (10) Douglas D. Bloomquist, George E. Duvall, Jerry J. Dick	8. CONTRACT OR GRANT NUMBER(s) (15) F49620-77-C-0034
9. PERFORMING ORGANIZATION NAME AND ADDRESS Department of Physics Washington State University Pullman, WA 99164	10. PROGRAM ELEMENT, PROJECT, TASK AREA & WORK UNIT NUMBERS 61102F (16) 2306 2306/A1 (17) A1
11. CONTROLLING OFFICE NAME AND ADDRESS Air Force Office of Scientific Research Bolling AFB / NE Washington D.C. 20332	12. REPORT DATE (11) March 1978 13. NUMBER OF PAGES 136 (12) 139p.
14. MONITORING AGENCY NAME & ADDRESS (if different from Controlling Office) (9) Final rept. 1 Nov 76 - 31 Dec 77,	15. SECURITY CLASS. (of this report) UNCLASSIFIED
	15a. DECLASSIFICATION/DOWNGRADING SCHEDULE

16. DISTRIBUTION STATEMENT (of this Report)

Approved for public release; distribution unlimited.

17. DISTRIBUTION STATEMENT (of the abstract entered in Block 20, if different from Report)

18. SUPPLEMENTARY NOTES

19. KEY WORDS (Continue on reverse side if necessary and identify by block number)

Shock Waves
Shock Compression
Thermoelectric Effect
Thermocouple
Bimetallic Junction

20. ABSTRACT (Continue on reverse side if necessary and identify by block number)

The electrical response of a copper-constantan junction to shock compression has been studied over a pressure range from 145 kbars to 360 kbars. Four possible sources of anomalous response were found; electrical noise due to circuit closure at impact, shock demagnetization of a ferromagnetic material, high local temperature at the junction interface due to shock compression of a surface damage layer, and two-dimensional flow in the pressurized region due to pressure relief from the edges. Using a diffusion welded junction the emf

20.

measured is within 20% of the predicted emf based on normal thermocouple response to shock compression temperatures. In a geometry in which a guard ring was used to maintain the pressure behind the shock front, the observed voltage-time profile was a step with constant plateau. In a similar configuration where radial pressure relief was allowed behind the shock front, the initial step, which compares directly in amplitude to the above results, is followed by a marked positive ramping. This ramping was directly correlated with the two-dimensional flow due to radial pressure relief. The results indicate thay any fundamental anomaly which exists for one-dimensional strain is less than 10-20% of the observed signals in the pressure range studied.

ACCESSION for
NTIS White Section
DDC Buff Section
UNANNOUNCED
JUSTIFICATION
BY
DISTRIBUTION/AVAILABILITY CODES
Dist. AVAIL. and/or SPECIAL
A

TABLE OF CONTENTS

	Page
LIST OF ILLUSTRATIONS	v
LIST OF TABLES	vii
INTRODUCTION	1
1. THE SEEBECK EFFECT AND APPLICATION TO THE SHOCK COMPRESSED BIMETALLIC JUNCTION	3
1.1 Thermoelectric Power of Metals	3
1.2 Shock Compression in a Thermoelectric Circuit	13
1.3 Temperature in a Shocked Copper-Constantan Couple	23
2. REVIEW OF PREVIOUS WORK	28
3. SOURCES OF ANOMALOUS EMF	41
3.1 *Electrical Noise Observed when Circuit is Completed* During Shock Experiment	41
3.2 Effect of Shock Demagnetization	42
3.3 Effect of Surface Layer Between Elements	46
4. EXPERIMENTAL TECHNIQUE	60
4.1 Experimental Configuration	61
4.2 Materials	62
4.3 Preparation Techniques	64
4.4 Impact Technique	69
4.5 Comparison of the Actual Experiments with the Idealized Experiment	73
5. EXPERIMENTAL RESULTS AND DISCUSSION	76
5.1 Results of Experiments without Guard Ring	76
5.2 Results of Experiments with Guard Ring	81
5.3 Comparison of Results with Theory and Discussion	83

Page

5.4 Conclusions and Recommendations 90

5.4.1 Conclusions 90
5.4.2 Recommendations 93

REFERENCES 94

APPENDIX
A. MEASUREMENT OF THE THERMOELECTRIC POWER OF AN OFHC COPPER AND A-CONSTANTAN THERMOCOUPLE 98

B. TEMPERATURE CALCULATIONS 101

C. ELECTRICAL NOISE AT IMPACT 106

D. SHOCK DEMAGNETIZATION 110

E. CALCULATIONS AND EXPERIMENTS INVOLVING THE SURFACE LAYER AT THE JUNCTION 120

F. THE EFFECTS OF A CHANGING INDUCTANCE AND SPECIAL RELATIVITY WHEN RADIAL PRESSURE RELIEF IS ALLOWED 127

LIST OF ILLUSTRATIONS

Figure		Page
1.1	Thermoelectric Circuit Through Temperatures T and T + ΔT	5
1.2	Idealized Configuration for Bimetallic Junction Experiments	14
1.3	Temperature Profile for Idealized Experiment	16
1.4	Thermoelectric Circuit Through Pressurized Region	18
1.5	Copper-Constantan Thermoelectric Circuit Through Temperatures T_o and T	21
1.6	Temperature Profile Near Junction just after Shock Compression	27
3.1	Illustration of Experiments by Bowden and Tabor on Friction	48
3.2	Pressure-Particle Velocity Diagram for Shock Wave Interactions in a Porous Layer between Solid Regions	49
3.3	Position-Time Diagrams for Shock Wave Interactions with a Porous Layer between Solid Regions	50
3.4	Temperature Profile Just After the Shock Compression of a Porous Layer	53
3.5	Temperature vs. Time in a Porous Layer Heated by Shock Compression	56
3.6	Thermoelectric Circuit and Associated Temperature Profile with Porous Interface Layer	57
4.1	Configuration for Uniaxial Strain Experiments	63
4.2	Exploded View of Target Assembly	65
4.3	Concentration of Nickel in Copper Near the Welded Junction of Copper and Constantan	68
4.4	Illustration of Impact Experiments	70
4.5	Schematic Drawing of Recording System	71

Figure		Page
4.6	Actual Experimental Configuration Compared with the Idealized Configuration	74
5.1	Voltage-Time Profiles for Shots 77-005, 77-026, 77-037, and 77-074	77
5.2	Voltage-Time Profiles for Shots 77-064, 77-076, and 77-079	84
5.3	Voltage-Time Profiles for Shots 77-084, 77-085, and 77-092	85
5.4	Comparison of Measured Emf Data with the Predicted Emf as a Function of Pressure	87
A.1	Thermopower Data for Copper-Constantan Thermocouple at Zero Pressure	100
C.1	Concentric Ring Experimental Configuration	107
C.2	Voltage-Time Profiles for Shots 76-073, 76-075, 76-078, and 76-086	108
D.1	Voltage-Time Profiles for Shots 76-032, 76-037, 76-039, and 76-040	112
D.2	Modified Concentric Ring Configuration used in Shots 76-037 and 76-039	114
D.3	Experimental Configuration used in Shot 76-040	115
D.4	Experimental Configuration used in Shots 76-051 and 76-054	116
D.5	Voltage-Time Profiles for Shots 76-051, 76-054, 76-052, and 76-062	118
E.1	Experimental Configuration used in Shots 77-038, 77-039, and 76-052	123
E.2	Voltage-Time Profiles for Shots 77-038 and 77-039	126

LIST OF TABLES

Table		Page
2.1	Results of Previous Investigations	29
3.1	Temperature Rise in Shocked Porous Copper	54
4.1	Materials Used	63
5.1	Results of Experiments with Radial Pressure Relief	78
5.2	Results of Experiments with Uniaxial Strain	82
5.3	Comparison of Calculated and Measured Temperature	88
A.1	Thermopower Data at Zero Pressure	98
B.1	Constants Used in Temperature Calculations	104
B.2	Temperature Rise in a Shock	105
D.1	Summary of Data on Shock Demagnetization	111
E.1	Summary of Data on Surface Preparation Studies	125

INTRODUCTION

Numerous investigations undertaken since 1959 have shown that when a shock wave passes through a junction of dissimilar metals, an emf is observed between the unshocked extremities of the metals. Since the temperature is elevated in the shocked region, an emf is expected if the metal pair behaves as a normal thermocouple. In every case the observed emf was of the appropriate sign but greater in magnitude than would be expected from normal thermoelectric response to shock compression temperatures. In most studies the emf was observed to be between 3 and 6 times too large. A great deal of confusion exists as to the source of the abnormally large response and the cause of the general nonreproducibility among experiments.

Initially such studies were motivated by the need for a transducer which would continuously indicate shock strength as a function of time. Attempts were made to calibrate the voltage output with pressure or temperature but nonreproducibility among investigators has made this impossible. In some investigations primary emphasis was placed on determining the cause of the abnormally large emf. Some progress has been made but no general resolution of the problem now exists.

The objective of this study was to bring some order into the study of this effect by carefully measuring the response of a bimetallic junction to a step pressure pulse using a light gas gun and modern high resolution recording equipment. The experimental program developed in two phases, the first of which was to develop an experimental configuration in which conditions such as junction quality and shock pressure could be completely determined. It was also

necessary to show that no parasitic signals were inadvertently being measured due to sources other than the junction response. The objective of the second phase of this program was to use the experimental configuration so developed to study the junction response over a range in pressures from 145 kbars to 360 kbars, and to compare it to anticipated response based on conventional static calibrations.

Throughout the course of this investigation, the primary question to be answered in light of the previous state of confusion was whether the anomalously high emf and nonreproducibility previously reported were due to fundamental principles or experimental artifacts. The results reported here indicate not only that anomalously large emfs were indeed due to experimental artifacts, but also that the simple measurement of shock compression temperature with a thermoelectric circuit may be possible.

CHAPTER 1

THE SEEBECK EFFECT AND APPLICATION TO THE SHOCK COMPRESSED BIMETALLIC JUNCTION

1.1 Thermoelectric Power of Metals.

The present theory of thermoelectricity is neither exact nor complete. The basic relationship between causes and effects involved are embodied in the simple linear Onsager relations, but an exact theoretical understanding of the coefficients is precluded by complexities of real materials on the atomic scale. The thermoelectric phenomena, which include the Seebeck, Peltier and Thomson effects, are combinations of more than one process involving electron diffusion as well as electron-electron, electron-phonon, and electron-impurity interactions. Although each of these processes can be treated in a general way with the use of modern quantum mechanics and statistical mechanics, it is not possible, except in rare cases, to predict quantitative results as accurately as they may be measured. At this point in the development of the general theory, experimental results of thermoelectric phenomena are being interpreted in terms of the general formalism in order to gain a fuller understanding of both the theory and the specific properties of the materials. The objective of the following treatment is to give a working understanding of mechanisms known to be active in the materials of interest in order to evaluate the experimental results of the current investigation in terms of results of previous work under normal laboratory conditions. This

discussion will be limited to the Seebeck effect in metals with particular attention given to constantan, an alloy of 55% copper and 45% nickel.*

The Seebeck effect or Seebeck potential is the electric potential difference, $\Delta\phi$, which exists between the ends of a material in which a temperature gradient is maintained. The common measurement of this effect is made using a circuit as in Fig. 1.1 in which two materials with different properties are used and no current is allowed to flow. The thermoelectric power of the couple is defined by

$$S_{A-B} = \lim_{\Delta T \to 0} (\Delta\phi/\Delta T). \qquad (1.1)$$

It is not possible under normal conditions to measure the potential difference due to a temperature gradient in a single material because the measurement itself involves other materials. It is possible, however, to define an absolute thermopower by the relation

$$\vec{E} = \overleftrightarrow{S}\nabla T, \qquad (1.2a)$$

where $\vec{E}$ is the electric field in the material and ∇T is the temperature gradient. In general $\overleftrightarrow{S}$ is a second rank tensor. In any further treatment here, except where noted, it will be assumed that the materials of interest are isotropic, and S can be written as a scalar. Since

$$\vec{E} = -\nabla\phi$$

Eq. (1.2a) becomes

$$d\phi = -S\, dT \qquad (1.2b)$$

where ϕ is the electric potential.

---

*The name constantan is commonly used for a class of copper-nickel alloys ranging in composition from 60%-40% to 50%-50%, and sometimes including 1% manganese.

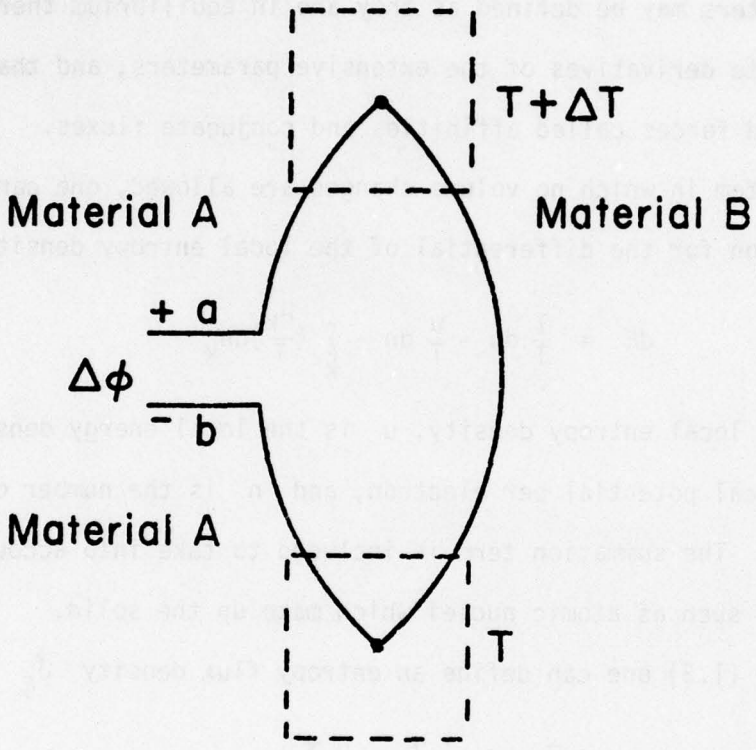

Fig. 1.1.--Thermoelectric Circuit through Temperatures T and T + ΔT.

The absolute thermopower and associated Seebeck effect represent only one part of a more complex interdependence among temperature gradients, electric potential gradients, heat flux, and electric current. The formal relationships among these quantities are known as the Onsager relations and will be treated here within the framework of irreversible thermodynamics (see Callen[1]). In the theory of irreversible thermodynamics it is assumed that the intensive parameters may be defined as they are in equilibrium thermodynamics as the appropriate derivatives of the extensive parameters, and that there exist generalized forces called affinities and conjugate fluxes.

In a system in which no volume changes are allowed, one can write a general expression for the differential of the local entropy density as

$$d\xi = \frac{1}{T} du - \frac{\mu}{T} dn - \sum_k \left(\frac{\mu_k}{T}\right) dn_k \tag{1.3}$$

where ξ is the local entropy density, u is the local energy density, μ is the electrochemical potential per electron, and n is the number of electrons per unit volume. The summation term is included to take into account any other components such as atomic nuclei which make up the solid.

From Eq. (1.3) one can define an entropy flux density $\vec{J}_\xi$ as

$$\vec{J}_\xi = \frac{1}{T} \vec{J}_u - \frac{\mu}{T} \vec{J}_n, \tag{1.4}$$

where $\vec{J}_u$ and $\vec{J}_n$ are the energy and electron flux density, respectively. The other components, n_k, are neglected in the further development as they are considered immobile and thus do not contribute fluxes to Eq. (1.4). In this way we are neglecting effects due to material motion in this treatment. The rate of local entropy production is equal to the amount of entropy leaving the region plus the rate of local entropy increase. Therefore,

$$\dot{\xi} = \frac{\partial \xi}{\partial t} + \nabla \cdot \vec{J}_\xi, \tag{1.5}$$

where $\dot{\xi}$ is the rate of local entropy production, and $\partial\xi/\partial t$ is the rate of local entropy increase. The appropriate continuity equations for energy and number of electrons are

$$0 = \frac{\partial u}{\partial t} + \nabla\cdot\vec{J}_u \tag{1.6a}$$

$$0 = \frac{\partial n}{\partial t} + \nabla\cdot\vec{J}_n \ . \tag{1.6b}$$

From Eq. (1.3) the first term of Eq. (1.5) can be evaluated as

$$\frac{\partial \xi}{\partial t} = \frac{1}{T}\frac{\partial u}{\partial t} - \frac{\mu}{T}\frac{\partial n}{\partial t} \ . \tag{1.7}$$

By taking the divergence of Eq. (1.4) and using (1.7), Eq. (1.5) becomes

$$\dot{\xi} = \frac{1}{T}\left(\frac{\partial u}{\partial t} + \nabla\cdot\vec{J}_u\right) - \frac{\mu}{T}\left(\frac{\partial n}{\partial t} + \nabla\cdot\vec{J}_n\right)$$

$$+ \left(\nabla\left(\frac{1}{T}\right)\right)\cdot\vec{J}_u - \left(\nabla\left(\frac{\mu}{T}\right)\right)\cdot\vec{J}_n \ . \tag{1.8}$$

The first two terms are zero from the continuity Eqs. (1.6), so that

$$\dot{\xi} = \left(\nabla\left(\frac{1}{T}\right)\right)\cdot\vec{J}_u - \left(\nabla\left(\frac{\mu}{T}\right)\right)\cdot\vec{J}_n \ . \tag{1.9}$$

In a continuous system the affinities of irreversible thermodynamics are defined as gradients of the entropy representation intensive parameters. In this system the affinities, or generalized forces, are $\nabla(1/T)$ and $\nabla(\mu/T)$. The fluxes are $\vec{J}_u$ and $-\vec{J}_n$. The preceding argument is given to identify the form of the fluxes and affinities so that the general relation between fluxes and affinities may be introduced. If it is assumed that the fluxes at a given instant depend only on the affinities at that instant, the fluxes can be expanded in a power series of the instantaneous affinities as

$$\vec{J}_i = \sum_j L_{ij}\vec{F}_j + \frac{1}{2!}\sum_{jk}\sum L_{ijk}\vec{F}_j\vec{F}_k + \ldots \ , \tag{1.10}$$

where $\vec{F}_j$ represents the affinity conjugate to the flux $\vec{J}_j$. Taking only the linear term, Eq. (1.10) becomes for the present case

$$-\vec{J}_n = L'_{11}\nabla(\frac{\mu}{T}) + L'_{12}\nabla(\frac{1}{T}) \tag{1.11a}$$

$$\vec{J}_u = L'_{21}\nabla(\frac{\mu}{T}) + L'_{22}\nabla(\frac{1}{T}) \ . \tag{1.11b}$$

It is easier to work with the flow of heat than with the flux of total internal energy. Following the same procedure used to define the fluxes in Eq. (1.4), a heat flux can be defined as

$$\vec{J}_Q = T\vec{J}_\xi \ , \tag{1.12}$$

and by Eq. (1.4),

$$\vec{J}_Q = \vec{J}_u - \mu\vec{J}_n \ . \tag{1.13}$$

The rate of entropy production can now be written as

$$\dot{\xi} = \nabla(\frac{1}{T})\cdot\vec{J}_Q - (\frac{1}{T})\nabla\mu\cdot\vec{J}_n \ . \tag{1.14}$$

The fluxes and affinities are now reselected and Eq. (1.11) becomes

$$-\vec{J}_n = L_{11}(\frac{1}{T})\nabla\mu + L_{12}\nabla(\frac{1}{T}) \tag{1.15a}$$

$$\vec{J}_Q = L_{21}(\frac{1}{T})\nabla\mu + L_{22}\nabla(\frac{1}{T}) \ . \tag{1.15b}$$

The Onsager theorem, where no externally applied magnetic field is present, states that $L_{12} = L_{21}$. For a discussion of the effects of an external magnetic field on this relation see Ziman,[2] Chapter XII.

The coefficients L_{ij} may be determined in terms of familiar quantities such as heat conductivity by comparing special cases of Eq. (1.15) with

established physical laws. Using the Onsager theorem, one can then discuss the more complex combinations of fluxes and forces in terms of well known phenomena. As an example, one can find a relation between the coefficients L_{ij} and the heat conductivity κ by solving Eqs. (1.15) under the conditions that the electric current J_n is zero and

$$\kappa \equiv -\vec{J}_Q/\nabla T \ . \tag{1.16}$$

The resulting relation is

$$\kappa = (L_{11}L_{22} - L_{12}^2)/T^2L_{11} \ . \tag{1.17}$$

In this way, the three independent coefficients can be determined in terms of the electric conductivity σ, the heat conductivity κ, and the absolute thermopower S. Equation (1.15) can now be written

$$-\vec{J}_n = (\frac{T\sigma}{e^2})(\frac{1}{T})\nabla\mu - (\frac{T^2\sigma S}{e})\nabla(\frac{1}{T}) \tag{1.18a}$$

$$\vec{J}_Q = -(\frac{T^2\sigma S}{e})(\frac{1}{T})\nabla\mu + (T^3\sigma S^2 + T^2\kappa)\nabla(\frac{1}{T}) \ , \tag{1.18b}$$

where e (<0) is the charge of an electron.

The thermopower expression, Eq. (1.2b), can be regained from Eq. (1.18) by using the first of the two expressions and letting the current J_n be zero, which yields

$$0 = \frac{T\sigma}{e^2}(\frac{1}{T})d\mu - (\frac{T^2\sigma S}{e})d(\frac{1}{T}) \tag{1.19}$$

or

$$\frac{1}{e}\,d\mu = -S\,dT \ . \tag{1.20}$$

The electrochemical potential, μ, can be written as a sum of two components, the electric part and the chemical part, as

$$\mu = \mu_e + \mu_c \ , \tag{1.21}$$

where $\mu_e = e\phi$, and μ_c depends on temperature and electron concentration. Equation (1.20) becomes

$$\left(\frac{1}{e}\right) d\mu_c + d\phi = -S\, dT \tag{1.22a}$$

or

$$d\phi = -S\, dT - \left(\frac{1}{e}\right) d\mu_c \ . \tag{1.22b}$$

The extra term in Eq. (1.22) as compared with Eq. (1.2b) gives rise to the contact potential or the difference in electric potential across a material boundary. This can be seen by integrating Eq. (1.22b) along a small path across the boundary between two metals I and II so that

$$\phi_{II} - \phi_I = -\frac{1}{e}\left(\mu_c^{II} - \mu_c^{I}\right) \ . \tag{1.23}$$

Since temperature is continuous, the other term vanishes in the limit as the integration path length goes to zero. This contact potential is not measured explicitly in any thermoelectric circuit as can be seen in the following example. Consider the circuit of Fig. 1.1. The materials A and B have absolute thermopowers S_A and S_B, respectively. The difference in the electrochemical potential between point a and b is given by the integration of Eq. (1.20).

$$\mu^a - \mu^b = e\int_{T_b}^{T} (-S_A)dT' + e\int_{T}^{T+\Delta T} (-S_B)dT' + e\int_{T+\Delta T}^{T_a} (-S_A)dT' \ . \tag{1.24}$$

Since the temperature and the material are the same at a and b, the chemical potential μ_c is the same at a and b, so that from Eq. (1.21)

$$\mu^a - \mu^b = \mu_e^a - \mu_e^b = e(\phi^a - \phi^b) \tag{1.25}$$

and therefore

$$\phi^a - \phi^b = \int_T^{T+\Delta T} (-S_B)dT' + \int_{T+\Delta T}^{T} (-S_A)dT' \ . \tag{1.26}$$

This can be compared with the defining equation for the thermoelectric power of such a couple, (Eq. 1.1). By combining the integrals, Eq. (1.26) becomes

$$\Delta\phi = \phi^a - \phi^b = \int_T^{T+\Delta T} (S_A - S_B)dT \tag{1.27}$$

and by comparison with Eq. (1.1)

$$S_{A-B} = S_A - S_B \ . \tag{1.28}$$

It is important to note here that the current which flows in a thermoelectric circuit is in the opposite direction from that of the net external electric field. This has led to a great deal of confusion as to the sign of the thermoelectric voltage. As is the case in any emf source such as a voltaic cell or thermocouple, there is an opposing force within the source which drives the current in the opposite direction from that of the external electric field. In a thermocouple the confusion seems to arise because, unlike other emf sources, it is not obvious that the source is anything but a resistive element of a circuit. In a circuit such as in Fig. 1.1 the entire circuit, apart from the measuring apparatus, can be considered an emf source with an associated internal resistance much like a battery.

The two basic mechanisms which give rise to the absolute thermopower in metals, and are represented by the Onsager relations, are thermal diffusion of electrons and what is called phonon drag. The thermopower is usually written as a sum of two terms

$$S = S_d + S_g \tag{1.29}$$

where S_d and S_g refer to the diffusion and phonon drag thermopowers, respectively. The diffusion process accompanies heat transport by the mobile electrons, and the phonon drag term is due to an interaction of the electrons with heat transport through the crystalline lattice.

The phonon drag thermopower is negligible above room temperature.[3] The diffusion part of the thermopower may be discussed in terms of Boltzman transport theory. For a more complete discussion of this subject see Ziman[2] or Mott and Jones.[4] The significant result is that the parameters σ, κ, and S can be determined in terms of the Fermi energy, ζ, the Boltzman constant, k, and the temperature, T. It can be shown that

$$\sigma = e^2 K_o \tag{1.30a}$$

$$\kappa = (1/T)(K_2 - K_1^2 K_o^{-1}) \tag{1.30b}$$

$$S = \frac{1}{eT} K_1 K_o^{-1} \tag{1.30c}$$

where

$$K_n = \{(\varepsilon-\zeta)^n \frac{\sigma(\varepsilon)}{e^2} + \frac{\pi^2}{6} k^2 T^2 \frac{\partial^2}{\partial \varepsilon^2} [(\varepsilon-\zeta)^n \frac{\sigma(\varepsilon)}{2} + \ldots\}_{\varepsilon=\zeta}. \tag{1.31}$$

Here $\sigma(\varepsilon)$ is to mean the electrical conductivity which one would calculate if the Fermi energy of the metal were ε. The Mott expression for the thermopower is obtained by substituting K_1 and K_o into Eq. (1.30c) and

retaining only the terms to first order in kT/ζ. The result is

$$S_d = \frac{\pi^2 k^2 T}{3e} \left(\frac{\partial \ln\sigma(\varepsilon)}{\partial \varepsilon}\right)_{\varepsilon=\zeta} . \tag{1.32}$$

It has been shown[2] that for a free-electron metal the logarithmic derivative in Eq. (1.32) is just $1/\zeta$ for $T \ll \theta_D$ and $3/\zeta$ for $T > \theta_D$ where θ_D is the Debye temperature. Equation (1.32) becomes

$$S_d = \frac{\pi^2 k^2 T}{3e\zeta} \qquad T \ll \theta_D \tag{1.33}$$

$$S_d = \frac{\pi^2 k^2 T}{e\zeta} \qquad T > \theta_D \tag{1.34}$$

This expression gives a thermopower of about 1 μvolt/°K at room temperature for reasonable values of the Fermi energy. The linear dependence of S on T has been shown for high temperatures (above θ_D) in most metals. Although more accurate expressions for the thermopower can be derived by considering the electron-lattice interaction more carefully, one cannot at this time predict the thermopower quantitatively to the accuracy of experimental results above room temperature.

1.2 Shock Compression in a Thermoelectric Circuit.

Consider the experimental configuration illustrated in Fig. 1.2. A shock wave is propagating away from the junction in both copper and constantan. It will be assumed that no pressure relief takes place from the edges behind the shock although no means of support is shown. The junction will be considered as a perfect plane dividing the two materials. The following discussion will be based on this rather unrealistic configuration and a comparison will be made later with the experiments actually performed.

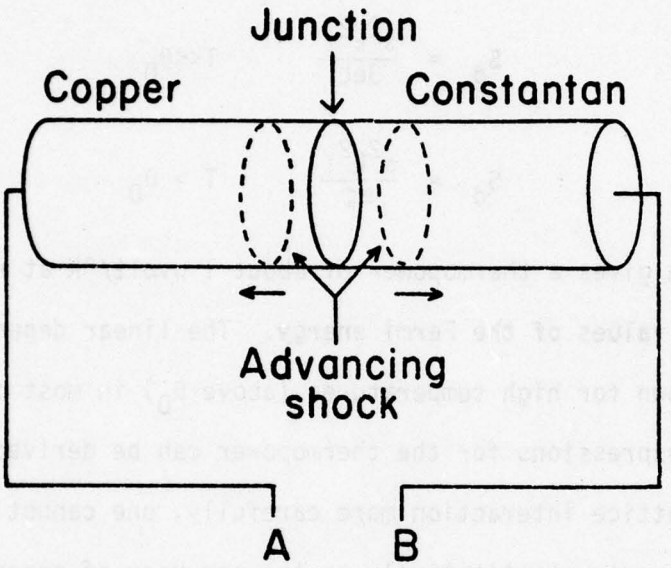

Fig. 1.2.--Idealized Configuration for Bimetallic Junction Experiments. The shock waves are produced by plane impact of the two components.

The measured quantities in this idealized experiment are the emf between A and B (Fig. 1.2), and the velocity of the impactor. The velocity of the impactor is used with the Rankine-Hugoniot jump conditions, and known empirical relations between shock velocity and particle velocity for each material, to obtain the pressure behind the shock front. Pressures and temperatures obtained for various impactor velocities will be discussed in the following section. At this point it will be assumed that the temperature is elevated in the metals due to shock compression so that an emf of thermoelectric origin is expected.

The predicted thermoelectric emf can be obtained from an integration of Eq. (1.2b), where $S = S(T,P)$ is a function of temperature and pressure. Figure 1.3 illustrates the temperature profile for this idealized experiment. Since $S(T,P)$ will be different for the two metals, the integration from A to B of Eq. (1.2b) can be written as

$$\phi_{B-A} \equiv \phi_B - \phi_A = \underbrace{-\int_{T_o}^{T_J} S_{Cu}(T',P)\, dT'}_{\text{region I}} \underbrace{-\int_{T_J}^{T_o} S_{Co}(T',P)\, dT'}_{\text{region II}}$$

$$\underbrace{-\int_{T_o}^{T_o} S_{Cu}(T',P)\, dT'}_{\text{region III}} \tag{1.35}$$

where T_o is the temperature of the materials before the experiments, and T_J is the temperature at the junction measured in degrees Kelvin. The subscripts Cu and Co refer to copper and constantan, respectively, and ϕ_{B-A} is defined as the potential difference $\phi_B - \phi_A$. If $S(T,P)$ were known for each region along with the functional relationship between pressure and

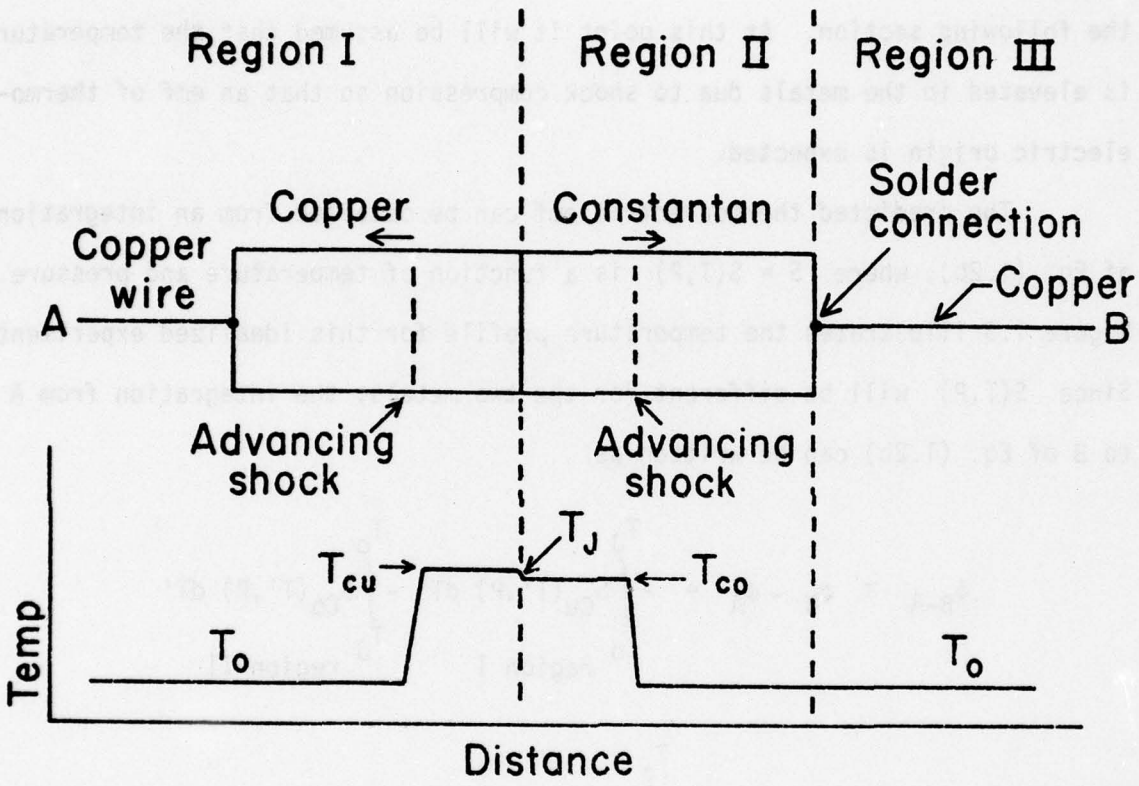

Fig. 1.3.--Temperature Profile for Idealized Experiment.

temperature, the integration could be performed and the results compared directly with experimental results. However, empirical relations which are available for thermopower as a function of pressure and temperature involve particular thermoelectric circuits, so that $S(T,P)$ can be obtained only by careful examination of these circuits.

To understand the dependence of the thermopower on pressure, consider the thermoelectric circuit of Fig. 1.4 made up of a wire of a single material. Using Eq. (1.2b) the measured emf can be written as

$$\phi_{C-D} = -\int_{D}^{C} S(T',P)\, dT' \tag{1.36a}$$

or

$$\phi_{C-D} = -\int_{T_o}^{T_1} S(T',P=0)dT' - \int_{T_1}^{T_2} S(T',P=P_1)dT' - \int_{T_2}^{T_o} S(T',P=0)dT'. \tag{1.36b}$$

Combining terms the equation becomes

$$\phi_{C-D} = -\int_{T_2}^{T_1} S(T',P=0)dT' - \int_{T_1}^{T_2} S(T',P=P_1)dT'. \tag{1.37}$$

If we assume a linear dependence of S on pressure in the form

$$S(T,P) = S(T,0) + \eta P \tag{1.38}$$

where η is a constant, Eq. (1.37) reduces to

$$\phi_{C-D} = -\int_{T_2}^{T_1} S(T',0)dT' - \int_{T_1}^{T_2} S(T',0)dT' - \int_{T_1}^{T_2} \eta P_1 dT' \tag{1.39a}$$

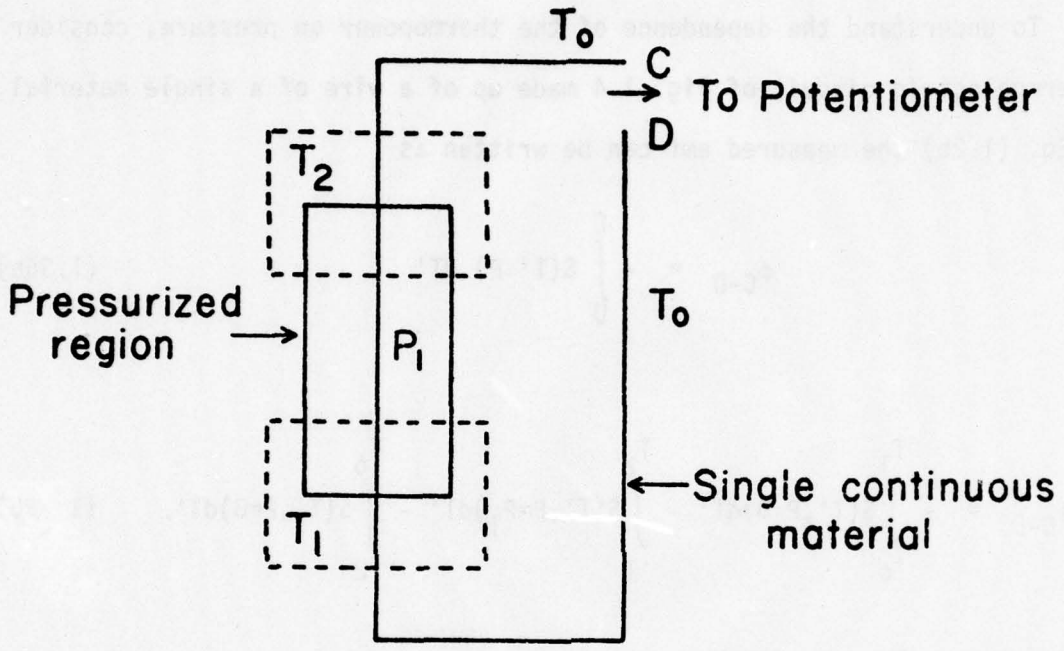

Fig. 1.4.--Thermoelectric Circuit through Pressurized Region.

or
$$\phi_{C-D} = -\eta P_1 \cdot (T_2 - T_1) \ . \qquad (1.39b)$$

From experiments done by Bridgman[5] up to 12 kbars and Bundy[6] up to 72 kbars, the constant η can be evaluated for both copper and constantan as

$$\eta_{Co} = 0.026 \ \mu v/kbar°K$$
$$\eta_{Cu} = -0.002 \ \mu v/kbar°K \ .$$

Equation (1.35) can now be simplified in terms of this pressure dependence as

$$\phi_{B-A} = -\int_{T_1}^{T_J} [\eta_{Cu} P + S_{Cu}(T',0)]dT' - \int_{T_j}^{T_o} [\eta_{Co} P + S_{Co}(T',0)]dT' \ . \qquad (1.40)$$

Since in the shock front the system is not in thermodynamic equilibrium, it is not clear that a temperature-pressure dependence is meaningful. However, as an approximation, the irreversible thermodynamic definition of temperature as the local derivative of internal energy will be assumed, and a linear dependence of temperature on pressure will be used in the form

$$T - T_o = \frac{T_F - T_o}{P_F} P \ . \qquad (1.41)$$

Here T_F and P_F are the equilibrium values behind the shock. Equation (1.40) becomes

$$\phi_{B-A} = -\int_{T_o}^{T_{Cu}} \eta_{Cu} P_{Cu} \frac{(T'-T_o)}{(T_{Cu}-T_o)} dT' - \int_{T_{Cu}}^{T_J} \eta_{Cu} P_{Cu} dT'$$
$$- \int_{T_{Co}}^{T_o} \eta_{Co} P_{Co} \frac{(T'-T_o)}{(T_{Co}-T_o)} dT' - \int_{T_J}^{T_{Co}} \eta_{Co} P_{Co} dT'$$
$$- \int_{T_o}^{T_J} [S_{Cu}(T',0) - S_{Co}(T',0)]dT' \qquad (1.42)$$

where $P_{Cu} = P_{Co}$ = final shock pressure; T_{Cu} and T_{Co} are the shock temperatures in copper and constantan respectively. The first and third terms are integrations over the shock front where the above temperature-pressure dependence applies. The second and fourth integrals are along the temperature gradient due to the difference in shock compression temperatures of the two metals where the pressure is constant. This expression can now be simplified as

$$\phi_{B-A} = -\eta_{Cu}P_{Cu}(T_J - \frac{T_{Cu}}{2} - \frac{T_o}{2}) + \eta_{Co}P_{Co}(T_J - \frac{T_{Co}}{2} - \frac{T_o}{2}) - \int_{T_o}^{T_J} S_{Cu-Co}(T',0)dT' \qquad (1.43)$$

where $S_{Cu-Co}(T',0) = S_{Cu}(T',0) - S_{Co}(T',0)$ is the thermopower defined for a copper-constantan thermocouple at zero pressure as in Eq. (1.1). The correction calculated in this way for the pressure effect corresponds to about an 8% decrease in the expected emf at 300 kbars. It remains only to find the temperatures T_{Co}, T_{Cu}, and T_J as functions of other shock parameters and $S_{Cu-Co}(T)$ in terms of a known empirical relation to estimate the emf observable in shock experiments. The temperatures involved will be treated separately in section 1.3 and $S_{Cu-Co}(T)$ can be easily obtained by the following argument.

Consider the thermoelectric circuit of Fig. 1.5. The emf at the potentiometer is given by

$$\phi_{E-F} = \int_{T_o}^{T} S_{Cu-Co}(T')dT' \qquad (1.44)$$

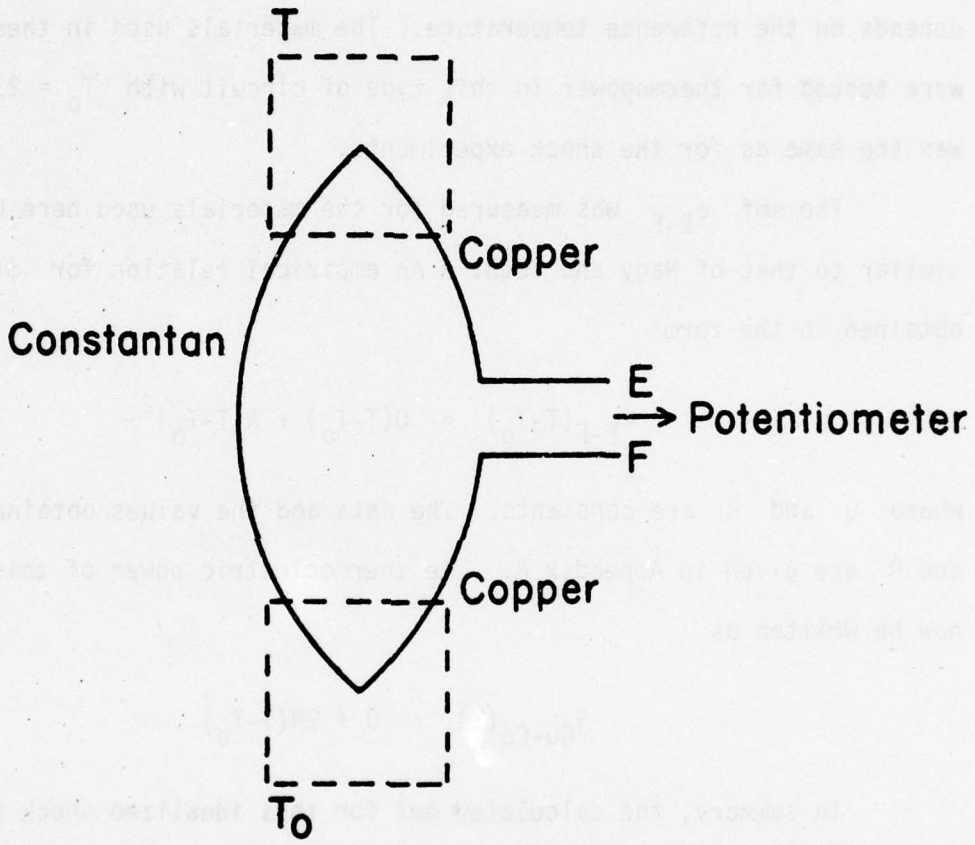

Fig. 1.5.--Copper-Constantan Thermoelectric Circuit through Temperatures T_0 and T.

from Eq. (1.1) so that

$$S_{Cu-Co}(T) = \frac{d}{dT} \int_{T_o}^{T} S_{Cu-Co}(T')dT' = \frac{d}{dT} (\phi_{E-F}) . \qquad (1.45)$$

It is assumed here that T_o is a constant, which implies that $S_{Cu-Co}(T)$ depends on the reference temperature. The materials used in these experiments were tested for thermopower in this type of circuit with $T_o = 23 \pm 2°C$ which was the same as for the shock experiments.

The emf ϕ_{E-F} was measured for the materials used here by a method similar to that of Nagy and Toth.[7] An empirical relation for $\phi(T)$ was obtained in the form

$$\phi_{E-F}(T-T_o) = Q(T-T_o) + R(T-T_o)^2 \qquad (1.46)$$

where Q and R are constants. The data and the values obtained for Q and R are given in Appendix A. The thermoelectric power of this couple can now be written as

$$S_{Cu-Co}(T) = Q + 2R(T-T_o) . \qquad (1.47)$$

In summary, the calculated emf for this idealized shock experiment can be obtained by evaluating Eq. (1.43) where η_{Cu}, η_{Co}, and S_{Cu-Co} can be determined in independent experiments and T_o, T_J, T_{Cu}, T_{Co}, P_{Cu}, and P_{Co} are known or can be estimated from measured quantities. A method for estimating T_o, T_J, and T_{Cu} is given in the next section. This idealized experiment will be compared to the actual experiments when they are described in Chapter 4.

1.3 Temperature in Shocked Copper-Constantan Couple.

In this section an estimate will be made of the temperatures T_{Co}, T_{Cu}, and T_J indicated in Fig. 1.3, based on a modified Christian and Walsh technique.[8] The temperature at the junction will be treated in terms of an initial step temperature profile with subsequent heat flow to produce a fixed temperature at the interface which depends on the diffusivities of the materials.

The temperature rise due to shock compression of a material may be estimated by inverting and integrating the expression

$$d\xi = \left(\frac{\partial \xi}{\partial T}\right)_v dT + \left(\frac{\partial \xi}{\partial v}\right)_T dv \tag{1.48}$$

or

$$d\xi = \frac{1}{T} C_v \, dT + \frac{1}{v} C_v \, \gamma dv \tag{1.49}$$

where ξ is the entropy density and γ is the Grüneisen parameter.

In a shock process there is entropy production due to plastic deformation as well as hydrodynamic compression, so that

$$d\xi = d\xi_1 + d\xi_2 \tag{1.50}$$

where

$$d\xi_1 = \frac{1}{T} \frac{4}{3} \tau \left(dv - v \frac{d\tau}{\mu}\right) \qquad \text{(plastic deformation}^9\text{)} \tag{1.51}$$

and

$$d\xi_2 = \frac{1}{2} \frac{(P_x - P_{x_{HEL}})}{T} \left[1 - \frac{v_{HEL} - v}{P_x - P_{x_{HEL}}} \left(- \frac{dP_x}{dv}\right)\right] dv \qquad \text{(hydrodynamic)} \tag{1.52}$$

where p_x is the component of pressure in the shock propagation direction and the subscript HEL refers to the Hugoniot elastic limit. In the first

expression τ is the maximum resolved shear stress, and μ is the shear modulus. The second expression is the direct result of the Rankine-Hugoniot relation

$$(E - E_o) = (P_x + P_o)(v_o - v)/2 \tag{1.53}$$

and the general thermodynamic relation

$$d\xi = \frac{1}{T} dE + \frac{P}{T} dv \ . \tag{1.54}$$

Using the expression for $d\xi$ along with Eq. (1.49) and differentiating with respect to v, one obtains

$$\frac{dT}{dv} + \frac{\gamma}{v} T = \frac{4}{3} \frac{\tau}{C_v} \left(1 - \frac{v}{\mu} \frac{d\tau}{dv}\right)$$

$$+ \frac{1}{2C_v} (P_x - P_{x_{HEL}}) \left[1 - \frac{v_{HEL} - v}{P_x - P_{x_{HEL}}} \left(- \frac{dP_x}{dv}\right)\right] \ . \tag{1.55}$$

To integrate this differential equation one must assume a dependence of γ and C_v on volume. For this estimation it will be assumed that γ/v and C_v remain constant. The constant γ/v will be designated as G, thus

$$G \equiv \gamma/v = \gamma_o/v_o \ . \tag{1.56}$$

The right side of Eq. (1.55) will be designated as $F(v)$ so that the equation can be written simply as

$$\frac{dT}{dv} + GT = F(v) \ . \tag{1.57}$$

This equation has the solution

$$T = e^{-G(v-v_o)} T_o + e^{-Gv} \int_{v_o}^{v} e^{Gv'} F(v') dv' \ . \tag{1.58}$$

Integration of this expression was done numerically by the application of Simpson's Rule. The pressure as a function of volume along the Hugoniot is calculated point by point using published U_s-U_p relations and the Rankine-Hugoniot jump conditions.[10] (See Appendix B.)

Work hardening during the shock process could be included by letting τ be a function of volume. If one assumes the same dependence of τ as would be observed for quasistatic strain to low pressure, τ has the form

$$\tau = \tau_o + \frac{H}{3}[\ln(v/v_o)] \tag{1.59}$$

which is derived from the single yield equation

$$Y = Y_o + H(\varepsilon_s - \varepsilon_{so}). \quad \text{(See Appendix B)} \tag{1.60}$$

Here ε_s is strain in uniaxial stress, Y is the yield stress, and H is a constant. In Appendix B a comparison is made of temperature estimates with and without a work hardening correction. The correction is only about 1% at 300 kbars. The values of H measured here are 15.5 and 3.74 for copper and constantan, respectively. The Hugoniot elastic limit for copper was taken from published measurements of elastic precursor amplitudes. In constantan, the Hugoniot elastic limit was estimated from the quasistatic yield stress and elastic constants obtained from ultrasonic sound speed measurements. For a linear elastic isotropic solid

$$P_{x_{HEL}} = Y\frac{1-\nu}{1-2\nu} \quad \text{(Ref. 9)} \tag{1.61}$$

where Y is again the yield stress in uniaxial stress and ν is Poisson's ratio. Appendix B includes the values for all of the parameters necessary in these calculations, as well as resultant temperature estimates for various

pressures. The temperature estimates for shocked copper of Rice, et al.[10] are also listed in Appendix B for comparison.

In the region very near the junction, a step temperature profile exists just after the shock transit through the junction as illustrated in Fig. 1.6. The temperature at the interface is time independent and given by Carslaw and Jaeger[11] as

$$T_J = T_{Cu} - \frac{T_{Cu} - T_{Co}}{1 + \beta} \tag{1.62}$$

where β is given by

$$\beta = \frac{\kappa_{Cu}}{\kappa_{Co}} \left(\frac{D_{Co}}{D_{Cu}}\right)^{1/2} \simeq \left(\frac{\kappa_{Cu}}{\kappa_{Co}}\right)^{1/2} . \tag{1.63}$$

In this expression κ and D are heat conductivity and diffusivity, respectively. The approximation holds where the density and specific heat are nearly equal, which is true for copper and constantan. The conductivities for copper and constantan at 100°C are 3.88 watts/cm°C and 0.212 watts/cm°C, respectively, so that β, which will be assumed independent of temperature is

$$\beta \simeq 4.3 \tag{1.64}$$

The temperature at the junction is now

$$T_J = T_{Cu} - \frac{T_{Cu} - T_o}{5.3} \tag{1.65}$$

The temperatures necessary to predict the thermoelectric response of a shocked junction of copper and constantan are estimated by using Eq. (1.58) for the temperature behind the shock, T_{Co} and T_{Cu}, and by using Eq. (1.65) for the junction temperature T_J.

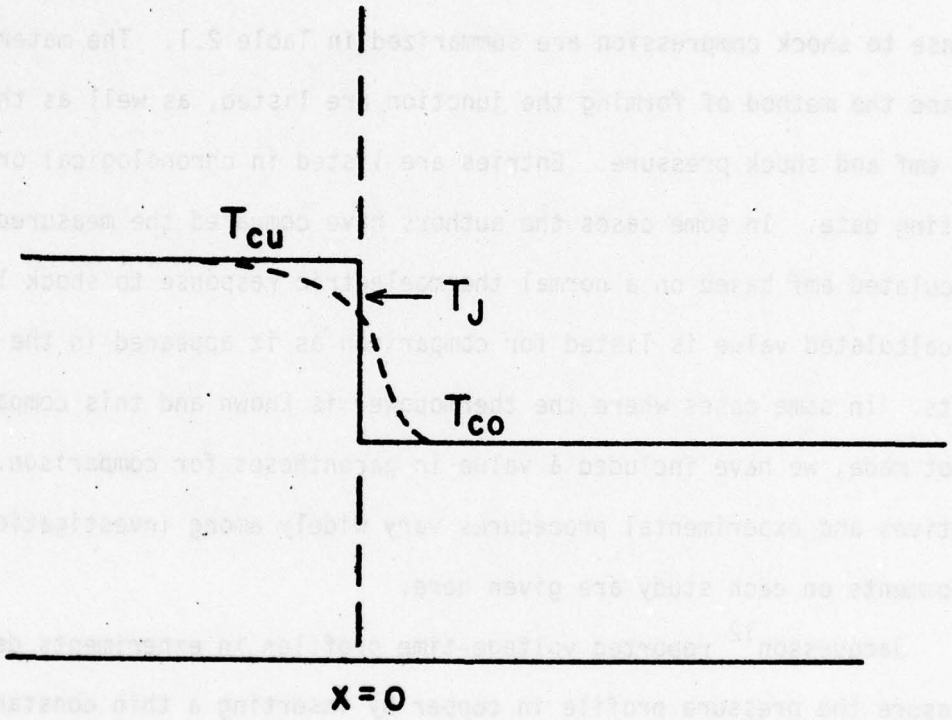

Fig. 1.6.--Temperature Profile Near Junction Just after Shock Compression. The dotted line represents the temperature profile due to heat conduction. The temperature T_J is independent of time.

CHAPTER 2

REVIEW OF PREVIOUS WORK

Experimental results from previously reported studies of junction response to shock compression are summarized in Table 2.1. The materials used and the method of forming the junction are listed, as well as the measured emf and shock pressure. Entries are listed in chronological order by reporting date. In some cases the authors have compared the measured emf to a calculated emf based on a normal thermoelectric response to shock loading. This calculated value is listed for comparison as it appeared in the original reports. In some cases where the thermopower is known and this comparison was not made, we have included a value in parentheses for comparison. Since objectives and experimental procedures vary widely among investigations, a few comments on each study are given here.

Jacquesson[12] reported voltage-time profiles in experiments designed to measure the pressure profile in copper by inserting a thin constantan ribbon between pieces of copper. He concluded that the emf was very large compared with normal thermoelectric response, but that some indication of the pressure-time profile could be obtained qualitatively. The actual emf trace, however, includes large positive and negative excursions and in general cannot be correlated with the expected pressure-time profile.

Ilyukin and Kologrivov[13] conducted a series of experiments in which a disk of nickel was soldered to the back of a larger disk of copper with no radial support. The emf values observed correspond to a temperature of

TABLE 2.1.--Results of Previous Investigations

Author	Date	Junction Materials	Pressure (kbar)	Measured Emf (mv)	Predicted Emf (mv)	Junction Surface Condition	Comments
Jacquesson[12]*	1962	Copper-Constantan	300	-250	-9	Not Characterized	
Ilyukhin[13] et al.	1962	Copper-Nickel	130	-26 ± 10	(-1.1)	Soldered	Several experiments at each pressure
			300	-39 ± 10	(-3.6)		
Doran and Ahrens[14]	1963	Copper-Constantan	400	-133 ± 10 -73 ± 4 -70 ± 5 -84 ± 5 -80 ± 3	-13.7	Flat surfaces in contact	Two different constantan compositions with different thermopowers were used. This explains the different predicted emfs for the same pressure.
			165	-90 ± 4	-3.1		
			370	-72 ± 4	-13.7		
			175	-23 ± 4	-3.4		
		Aluminum-Constantan	380	-82 ± 5 -88 ± 5 -100 ± 5 -100 ± 13	-14		
		Copper-Iron	360	-30 ± 10			
		Copper-Aluminum	220	-20 ± 10	-0.93		
		Copper-Copper	390	<5	0		
		Copper-Constantan	400	-42 ± 4	-15.4	Partial diffusion weld	
			175	-23 ± 4	-3.4		

TABLE 2.1.--Continued

Author	Date	Junction Materials	Pressure (kbar)	Measured Emf (mv)	Predicted Emf (mv)	Junction Surface Condition	Comments
Palmer and Turner[15]	1964	Copper-Constantan	300	-57	(-11)	Constantan wire soldered to copper plate	Junctions were soldered with a torch using a silver bearing solder.
			260	-52	(-8.5)		
			190	-40	(-5)		
			150	-28	(-3.5)		
			120	-22	(-2.7)		
			90	-18	(-2)		
			60	-8	(-1.2)		
			40	~-2	(-0.8)		
Crosnier et al.[16]	1965	Copper-Constantan	100	-30	-1.88	Not characterized	Emf is related to pressure in a graph as $\phi(mv) = 0.143P(kbar)+10$ More data are indicated in graphs. These data are those given in tabular form.
			180	-43	-3.9		
			400	-73	-11.8		
			1160	-180	---		
		Copper-Aluminum	150	-10	(0.2)		
		Copper-Nickel	400	-35	(-6)		
			1160	-90	---		
		Copper-Bismuth	180	+11	---		
			400	-100	---		
			1160	-170	---		
		Copper-Chromel	180	+10	(+1.8)		
			1160	0	---		
		Copper-Zinc	1160	-90	---		
		Iron-Constantan	100	-35	(-2.5)		
			130	-50	(-3)		
			360	-500	(-13.5)		
		Iron-Chromel	130	+20	(+2)		

TABLE 2.1.--Continued

Author	Date	Junction Materials	Pressure (kbar)	Measured Emf (mv)	Predicted Emf (mv)	Junction Surface Condition	Comments
Conze et al.[18]	1967	Copper-Constantan	1300	-300	---		Junction perpendicular to shock front.
Bushinskii and Samylov[19]	1969	Copper-Nickel	460	11.2 11.2 17.3 18 14.2 16.0 16.5 17.3 18.3 10.3 13.7 14.0 17.3	9	Polished or diffusion welded	No distinction is made in the tabular results as to which junctions were welded.
Jacquesson et al.[21]	1970	Copper-Constantan					Emf is related to pressure as $\phi(mv) = 0.145P(kbar) + 11$
Mineev et al.[22]	1970	Aluminum-Ytterbium	120	-134 -40	--- ---	Not characterized	
			200	-370 -280	--- ---		
			380	-160 -135	--- ---		
			780	130	---		

TABLE 2.1.--Continued

Author	Date	Junction Materials	Pressure (kbar)	Measured Emf (mv)	Predicted Emf (mv)	Junction Surface Condition	Comments
Mineev et al. (continued)		Aluminum Europium	170	66	---		
				73	---		
				43	---		
			320	170	---		
			670	150	---		
		Aluminum Cerium	120	15	---		
			210	15	---		
			390	-15	---		
Bordzilovskii[23]	1972	Copper-Nickel				Not characterized	Emf is related to pressure as ϕ(mv) = (.153 ± .008) P(kbar) ± 20.
		Duralumin-Nickel				Not characterized	ϕ(mv) = (.6 ± .05)P(kbar) + 7 ± 2.
Migault et al.[25]	1972	Copper-Constantan	60	-16	(-1.1)	Not characterized	
			188	-38	(-4.1)		
			310	-56	(-9.3)		
Bordzilovskii[26]	1974	Copper-Constantan				Not characterized	Emf is related to pressure as ϕ(mv) = (0.11 ± 0.01) P(kbar) + 4 ± 6.
Nesterenko[28]	1974	Copper-Nickel	50	-10 ± 1	(-0.4)	Coarse emery polish	
			130	-10 ± 1	(-1.2)		
			240	-19 ± 2	(-2.75)		
			400	-19 ± 3	-7		
			700	-40 ± 4	(-20)		
			400	-11 ± 3	-7	Mirror finish	

TABLE 2.1.--Continued

Author	Date	Junction Materials	Pressure (kbar)	Measured Emf (mv)	Predicted Emf (mv)	Junction Surface Condition	Comments
Nesterenko[28] (continued)		Copper-Tungsten	530	-10 ± 1	---	Coarse emery polish	
			310	-6 ± 1	---		
			170	-6 ± 1	---		
		Copper-Molybdenum	140	+5 ± 1	(+0.23)		
			260	+5 ± 1	(+0.7		
			450	+8 ± 1	(+2.8)		

*Superscripts refer to references following Chapter 5.

1000°C for a set of experiments in which the pressure was 130 kbars and 1600°C for experiments at 300 kbars. It was assumed that the indicated temperature closely approximated the actual temperature rise in the solder. This interpretation, which assumes no fundamental anomaly of the Seebeck effect in the shock environment, may be valid; however, the ratio of the "measured temperatures" in the two sets of experiments is too small compared with the ratio of pressures for any reasonable equation of state for solder.

Doran and Ahrens[14] reported data for a series of experiments in which the junction area was varied from 0.2 mm^2 to 285 mm^2 and the materials making up the junction were varied. Signal amplitudes for different couples were reported to be in the same ratio as their zero pressure thermopowers, but a close correlation is not obvious from the reported data. No definite relationship between junction area and amplitude was found. A partially successful diffusion-welding process of the junction resulted in a lower emf in one of two experiments. The authors concluded that the emf is probably of the same origin as the normal thermoelectric effect and that it is more nearly proportional to pressure than temperature. In these experiments, as in the previous study by Jacquesson, only the peak amplitude was reported and compared with the expected emf. This is due primarily to the use of explosive shock generation in which only the initial pressure is well known.

Palmer and Turner[15] conducted a series of experiments in which a constantan wire was soldered to the back surface of a copper plate being impacted from the front. The pressure behind the shock was varied from 40 kbars to 300 kbars. The voltage-time profile reported shows a 2 μsec rise time of the initial voltage and a 20 μsec pulse with random excursions of up to 50% of the peak value. The authors concluded that the emf was a function of final shock pressure and thereby could be used to indicate shock strength

qualitatively. It is not obvious that the reported voltage profile can be interpreted in this way. The high shock pressure in a soldered junction of this type should last only a few hundredths to a few tenths of a microsecond, depending on dimensions and configuration of the solder connection.

Crosnier et al.[16] reported data for several different couples. The junctions were formed by placing a disc of one material on the back surface of the other with no radial support, or by placing a rod of one material in an insulated hole in the other. The authors concluded that the emf was due to a voltage source of low internal resistance, and that the junction behaved qualitatively like a normal thermocouple. It was concluded that the emf was proportional to the pressure up to 1600 kbars, and that the emf was of such large magnitude that no classical interpretation was possible. It was proposed that the emf could be due to the formation of an electronic hot gas with a much higher temperature than the crystal lattice. Although these experiments were done with and without radial pressure support behind the shock wave in the active element, no mention is made of the effect this has on the observed emf.

In 1967, Migault and Jacquesson[17] proposed a theoretical explanation for the abnormally large emfs observed in their previous experimental program. The theory is based on the radiation pressure exerted on the conduction electrons by phonons created in the shock front. An estimate is made of this effect assuming all of the increase in internal energy is in the form of longitudinal phonons polarized in the shock propagation direction. This theory is said to explain the experimental results in the pressure range from 80 kbars to 300 kbars.

Conze et al.,[18] proposed another theoretical explanation of the abnormally high emfs in this type of experiment. The theory is based on an

elevated temperature of the electrons above the lattice temperature coupled with an electronic imbalance due to phonons created in the shock front. Several experiments were also conducted, including one in which mercury was used to make the contact in the junction. Results of this experiment were reported to be identical to those in which the surfaces were simply pressed together. The one reported data point is given in Table 2.1.

Buzhinskii and Samylov[19] conducted a series of experiments on a copper-nickel junction made from disks by polishing the mating surfaces or diffusion-welding the disks together. No distinction was made in the reported data between these two types of junctions. Results are given in the table for thirteen separate experiments at the same pressure. The diameter of the junction was varied from 20 mm to 32 mm with no significant change in the output. The mean measured temperature was reported to be 60% greater than the calculated temperature. Although a lot of scatter is present in the data, which may be partially due to differences in shock pressure, the lowest reported emf values are within 15% of the expected value. No indication is given as to which experiments were done with the welded junctions. These results suggest that the higher emf values observed previously may be due to an experimental artifact rather than to a fundamental phenomenon such as a high electron gas temperature.

Lascar and Duage[20] conducted a series of experiments on the copper-constantan junction to localize the source of the abnormal emf. In one series of experiments, the constantan was preheated to reduce the final temperature difference between the materials. This had only a "slight effect" from 0°C to 150°C preheating. In another series, the junction was diffusion welded with an interdiffusion layer of 100 μ and an alumina ceramic insulator was used around the copper element, which was inserted in a hole in the

constantan. No actual data are given for these experiments. The authors do not draw any specific conclusions from this experiment, but the qualitative sketch of the voltage-time profile shows a relatively small initial step in emf followed by a ramping. Without more specific data, an interpretation of the significance of these results in terms of our observations is impossible. The authors conclude that the abnormal emf is not localized at the junction or in the shock front and therefore, the emf source must be distributed in the bulk of the materials making up the junction. This conclusion does not appear to be justified by the qualitative results reported.

In 1970 Jacquesson et al.,[21] reviewed the results of previous experiments in this area, and reiterated the conclusion that the emf has a linear pressure relation in this type of experiment in the form E(mv) = 0.145P (kbars) + 11. No reference was made to the generally lower results of Buzhinskii and Samylov. Some new experiments were conducted in which the plane of the advancing shock front was perpendicular to the junction plane. In these experiments, the emf increased monotonically with time and reached a maximum when the entire junction was pressurized. The final emf was reported to be the same as in the case where the shock front and junction plane are parallel.

The results by Mineev et al.,[22] on the lanthanides ytterbium, europium and cerium are included in Table 2.1. The junctions were made by pressing 1-2 cm disks of the sample on the back of an aluminum buffer plate. The authors conclude that the measured emf is not connected with contact potential effects and is principally due to volume redistribution of charge in the shock front.

Bordzilovskii et al.,[23] conducted a series of experiments in which the angle between the plane of the junction and the plane of the shock wave

was varied. The rise time of the measured emf was equal to the time necessary for the shock wave to sweep across the junction. The authors conclude that the emf is due to an internal contact potential difference mechanism. The data reported for copper-nickel and duralumin-nickel, where the incidence angle was zero, are included in Table 2.1. In another set of experiments[24] using an external shunt of low impedance, the authors concluded that internal resistance of this emf source was about 10^{-2} Ω for a contact area of 78.5 mm^2 and was inversely proportional to the area. The objective of these studies was to characterize the electrical response of a junction in order to use it as a pressure-time profile transducer. No attempts were made to determine the cause of the large emf as compared with the normal thermoelectric response.

In 1972 Migault et al.,[25] gave a modified theoretical treatment of the response of a bimetallic junction to shock compression. The theory takes account of the radiation pressure of the phonon gas generated by the shock. The resultant effect is found by a resolution of a coupled set of linearized Boltzmann equations for phonon and electron distributions. The proposed theory purportedly explains the high observed emfs in the pressure range from 0 to 300 kbars. Again, no reference is made to the lower emf values observed by Buzhinskii and Samylov, which would not agree with this theory.

In 1974, Bordzilovskii et al.,[26] reported using a copper-constantan junction to measure a pressure profile in copper. The pressure wave in copper was produced by impacting a flyer plate on an intermediate layer consisting of polystyrene foam, liquid nitrogen or liquid hydrogen. The junction was made by pressing a constantan disk of 6 mm diameter on the back surface of the copper plate. The emf-pressure calibration curve which was used is given in Table 2.1 and was apparently measured in a separate set of

experiments. The authors conclude that the recording method is satisfactory to within 10-15%. However, the authors did note a discrepancy of as much as 65% between the calculated and measured final pressures. The reported voltage-time profiles do not appear to be consistent with the conclusion that a direct measurement of pressure was being made.

Nesterenko et al.,[27] and Nesterenko[28] conducted a series of experiments using various pairs of metals. In one series on copper-nickel at 400 kbars, half of the experiments were done with emery-polished surfaces and the other half were done using "rough" surfaces. The polished surfaces resulted in 40% reduction in amplitude. The authors conclude that the high emf measured in this type of experiment is due to a high nonequilibrium contact temperature.

In summary, the results of previous studies in this area are confusing, but some conclusions can be drawn. The emf is of the appropriate sign to be interpreted on the basis of a normal thermoelectric response to an elevated temperature. The emf observed in every case is higher than predicted on a thermoelectric basis, but the discrepancy varies from as little as 15% in some experiments by Buzhinskii et al.,[19] and Nesterenko[28] to as much as a factor of twenty or more. This also indicates the general nonreproducibility which is evident both among different investigations and within any particular investigation. Nesterenko has shown that when polished surfaces are used at the interface, the resultant emf is lower than when rough surfaces are used. The results of diffusion-welding the junction are not conclusive but suggest a lower resultant emf. Signals are generally not steady in time and are usually noisy. The investigations which have been undertaken up to this point have been directed toward either the characterization of this effect to make it useful as a pressure transducer or toward the resolution of the

conflict between the predicted and observed results. In the first case the nonreproducibility among investigators puts the results in doubt; and in the second case, the results and conclusions among authors vary widely and no general resolution of the problem exists.

CHAPTER 3

SOURCES OF ANOMALOUS EMF

In the first phase of the present program an experimental configuration was developed in which the measured emf could be predicted by direct comparison with the idealized experiment of Chapter 1. This was done by recognizing and eliminating any mechanism that would cause an emf to be measured which was not associated with the junction response to shock compression as discussed in Chapter 1. Only the fruits of this effort, specifically the three mechanisms which were isolated, will be described in this chapter. The details of the associated experiments will be included in Appendices C, D, and E. The final configuration will be described in Chapter 4.

3.1 Electrical Noise Observed When Circuit Is Completed during Shock Experiment.

We have observed that when a low impedance circuit (~0.1 ohm) is completed during a shock experiment electrical noise is observed in the circuit. In a thermoelectric experiment the two possibilities for this to be observed are when part of the eventual circuit is in the projectile, or when a small gap between components is closed by a shock wave. In either case the resulting noise interferes with the measurement of the thermoelectric emf.

Buzhinskii and Samylov[19] observed that when a shock wave passes through a series of disks that are nominally in contact, and electrically in series with the recording instrument, a noise spike is observed for each interface. The details of the experiment and the amplitude of the noise

were not given. In much of the previous work (see Chapter 2) the thermoelectric circuit was prepared by simply holding the elements in contact. In studies where only the initial peak signals were reported, the values may be anomalous because of the simultaneous noise.

In experiments done here, this type of noise was observed when attempts were made to complete the circuit at impact. The objective was to have one part of the bimetallic pair in the projectile and thus produce symmetric shock waves in the two metals as in the idealized experiment of Chapter 1. Several experiments were conducted to investigate the problem and the details are given in Appendix C. Although the fundamental source of this noise is not well understood, we consistently observed a non-zero signal from as much as 5 μsec before impact. At impact a positive and/or negative spike greater than 100 mv was observed and a high frequency (>50 mHz) noise persisted for up to 0.5 μsec after impact. Initially our efforts were directed toward minimizing or eliminating this problem using electrical and magnetic shielding techniques, but we eventually concluded that closure of the circuit at impact must be avoided completely to eliminate this problem.

3.2 Effect of Shock Demagnetization.

In several earlier studies involving the shock loading of bimetallic junctions, a ferromagnetic material, iron or nickel, was used as one of the active elements.[13,14,16,19,27,28] It has been shown in numerous investigations that ferromagnetic materials undergo a demagnetization process upon the passage of a strong shock wave.[29-33] It is necessary, therefore, to determine what effect the change in magnetic state has on the results of such experiments.

The following mechanisms for shock induced demagnetization have been identified:[29]

1. First-order phase transitions from ferromagnetic to nonferromagnetic phases such as in iron.
2. Second-order phase transitions between ordered and disordered states in combination with a lowering of the Curie temperature and shock heating.
3. Strain induced magnetic anisotropy in which the direction of shock propagation becomes an easy axis. This leads to an effective demagnetization in the transverse direction.

Iron was used in only two previous investigations[14,16] and was not given primary consideration in either study. Since no work was done here involving iron, attention will be focused on the shock demagnetization of nickel. There are no known first-order phase transitions in nickel below 500 kbars thus eliminating the first possible mechanism.

Experimental evidence of some form of demagnetization process in nickel was seen by Wong[34] at 23 kbars in the form of an eddy current spike in a resistivity measurement. It would not be possible to conclude from this type of experiment which of the two mechanisms listed above is active.

Although no study of the third mechanism has been done using nickel, a realignment of the magnetization along the shock propagation direction has been observed for other materials, including nickel ferrite and yttrium iron garnet.[29,30]

Grady et al.[31] have shown for polycrystalline materials that the direction of magnetization is determined by a minimizing of the internal energy expressed as

$$E = -\vec{H}_e \cdot \vec{M} + B\sin^2\theta \qquad (3.1)$$

where E is the internal energy, $\vec{H}_e$ is the external magnetic field, $\vec{M}$ is

the magnetization, e is the uniaxial strain, θ is the angle between the direction of the applied field and the direction of the magnetization, and B is a constant defined as

$$B = (-3/5)[(C_{11} - C_{12})\gamma_{100} + 3C_{44}\gamma_{111}] . \qquad (3.2)$$

Here C_{ij} and γ_{ijk} are the elastic and magnetostrictive constants, respectively. The internal energy, E, is a sum of the mechanical elastic energy, the magnetoelastic energy, and the energy due to interaction of the external magnetic field and the magnetization.

The experiments to measure this effect are done by magnetizing the sample in a direction perpendicular to the shock propagation direction with an external field. When the shock propagates through the material the magnetization direction changes to minimize the energy in Eq. (3.1). When B is positive, as is the case for nickel ferrite, YIG, and nickel, the second term in Eq. (3.1) is minimized when θ is 90°, thus tending to realign the magnetization direction with the shock propagation direction. This is observed as a demagnetization in the transverse direction. In the special case where no external magnetic field is applied, a complete realignment is expected along the shock propagation direction.

A series of 8 experiments was conducted in our study of the demagnetization process and its effect on bimetallic junction experiments.* The details of these experiments are given in Appendix D. The experimental program was initially undertaken to determine whether or not shock compression

---

*The term "bimetallic junction experiment" is in reference to the type of experiment that is indicated schematically as the idealized experiment of Chapter 1. This could include a number of specific configurations, but each would have in common a closed circuit of low internal impedance (~0.01 Ω), two metals to form the junction with a shock wave traveling in each, and a recording system sensitive to the small expected emfs (0.1 - 50 mv).

of a bimetallic junction in which both metals are the same would produce a null result. A null result is predicted by every previously proposed theory. In the first such experiment (76-032) the recorded emf was not zero. At this point we proposed several possible causes for the non-zero signals, and the next three shots (76-037, 76-039, 76-040) were conducted before we realized that the emf was probably due to demagnetization.

Three shots 76-051, 76-054,* and 76-062 were done specifically to determine whether or not a demagnetization of the nickel did occur under the experimental conditions of interest, and if this process would interact with the recording circuit and result in the characteristic signals. In shots 76-051 and 76-054 the magnetization of the nickel was controlled. In 76-051 the nickel was used as received and had a magnetic field just outside the body of about 0.8 Gauss in directions parallel and perpendicular to the shock propagation direction. In 76-054 the nickel was demagnetized with a field just outside the body of less than 0.05 Gauss in any direction. The recorded emf was about -40 mv in the first of the shots and about -7 mv in the second. (See Fig. D.5.) Therefore a reduction of the pre-shot magnetization in the nickel by a factor of 16 reduced the signal amplitude by about a factor of 6. This effect of the initial magnetization would be expected if the signals were caused by a shock demagnetization.

In another shot, 76-062, the active element was changed from nickel to Nichrome V† (80% nickel 20% chromium) which is not ferromagnetic. The experiment was the same in all other respects as shot 76-032. In shot 76-032 an emf of less than -100 mv was observed and in 76-062 no emf was observed during the time

---

*The author wishes to acknowledge the efforts of Dr. Jerry Dick who guided the work in this area and conducted shots 76-051 and 76-054.

†Trademark of the Driver Harris, Co., Harrison, New Jersey.

of shock transit through the target to within the recording capability of the instrumentation system of 0.01 mv. (See Fig. D.1 and D.5.)

Results of these experiments show conclusively that an emf is observed in this type of experiment when one of the active elements is ferromagnetic. The emf is due to shock demagnetization of that element. This puts the results of any previous work done with nickel or iron in doubt. It also precludes the use of ferromagnetic materials in this type of experiment unless this effect can be completely nullified in some other way.

3.3 Effect of Surface Layer between Elements.

In most of the work previously reported in which the response of a bimetallic junction to shock loading has been investigated, the observed emf is 2 to 15 times that predicted assuming a thermoelectric source and reasonable shock compression temperatures. One possible contributing factor to these erratic but consistently high results is that the interface between the two materials reaches a much higher temperature than the bulk material. If indeed a thermoelectric source is responsible for the emf recorded, the inferred temperature would be the local temperature in the immediate vicinity of the boundary between the two materials. In this case, the temperature rise of the interface above the bulk shock compression temperature would be zero only if a perfect plane separated the two materials. Urtiew and Grover[35] have studied the possible distribution of temperature in both distance and time near an interface between two materials under shock loading conditions. Two models were proposed, one in which the intermediate zone was characterized by a gap as might be the case for highly polished surfaces and another in which the intermediate zone is considered as a porous solid. Evidence is given for the acceptance of the porous material model as the more

correct even for highly polished surfaces for which the interface zone is on the order of one micron thick.

It was shown in experiments involving heat generation due to the friction of sliding by Bowden and Tabor[36] that hot spots on the order of a micron or less would produce an emf in a thermoelectric circuit. A diagram of the type of experiments conducted is seen in Fig. 3.1a. In Fig. 3.1b, the surfaces in contact are shown microscopically. It was proposed that in the small regions which make contact, a very high temperature was produced due to friction, and the purpose of the experiments was to determine if this was true by measuring the thermoelectric response of a constantan rod rubbing on a copper disk. Transient temperatures on the order of 1000°C were measured for time of less than one millisecond. These results indicate that the thermoelectric circuit involved in the shock experiments would respond to a region of high temperature on the order of several microns at the junction interface.

Consider a plane interface between copper and constantan with the following properties:

1. The intermediate region will be treated as a porous layer of thickness 2a.
2. The porous material will have the properties of copper foam.
3. Complete compaction is achieved in the first shock transit.

Figures 3.2 and 3.3 show that the pressure-particle velocity state reached in the porous layer after one reflection may be nearly the same as the initial state in the solid. However, the temperature in the interface region is higher than that of the bulk material.

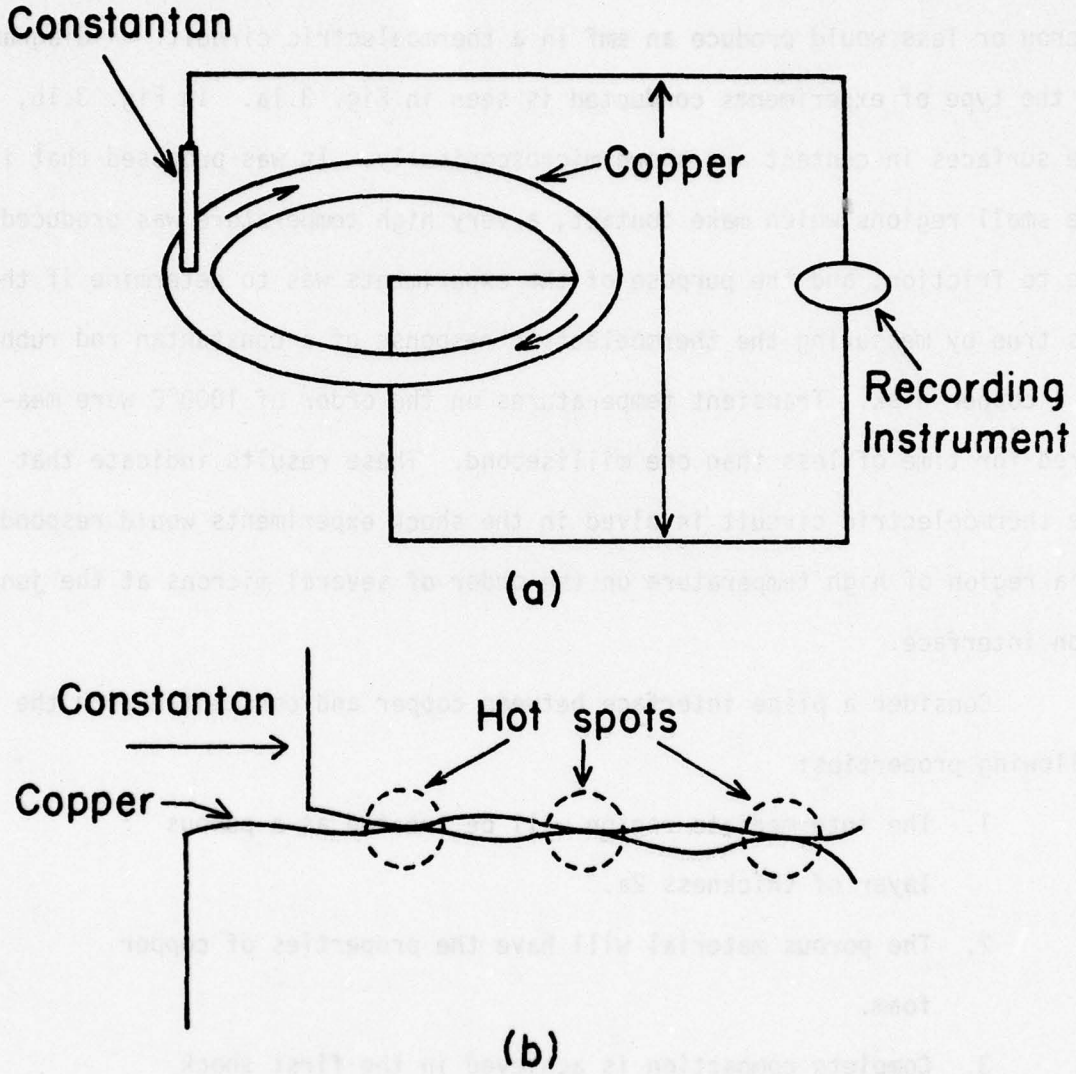

Fig. 3.1.--Illustration of Experiments by Bowden and Tabor[36] on Friction. (n (a) an experiment to measure the temperature produced locally by friction is illustrated, and in (b) a microscopic view of the sliding surfaces is shown.

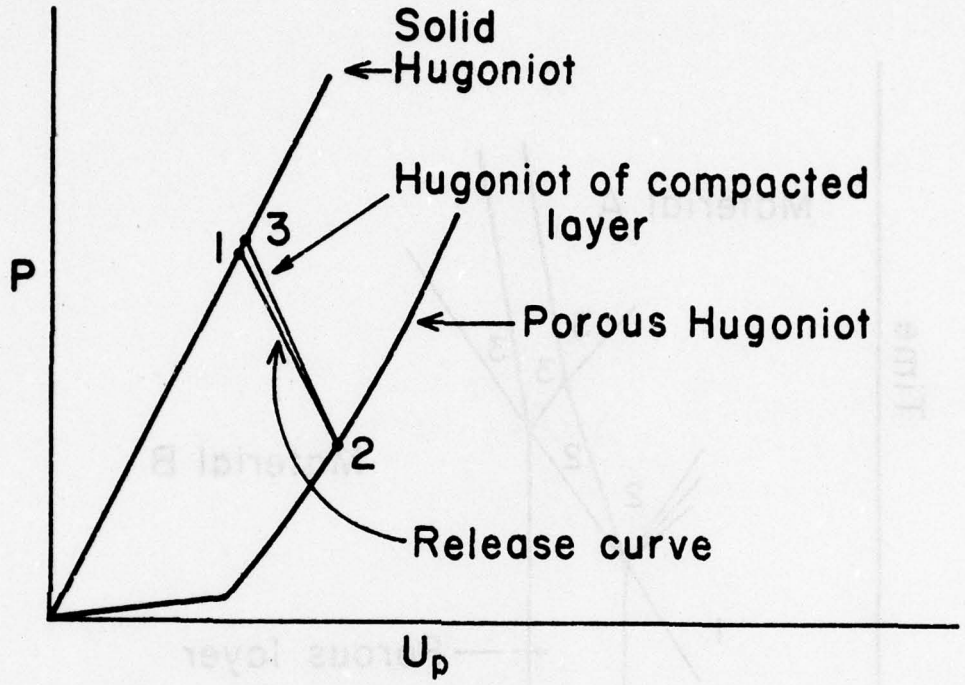

Fig. 3.2.--Pressure-Particle Velocity Diagram for Shock Wave Interactions in a Porous Layer between Solid Regions.

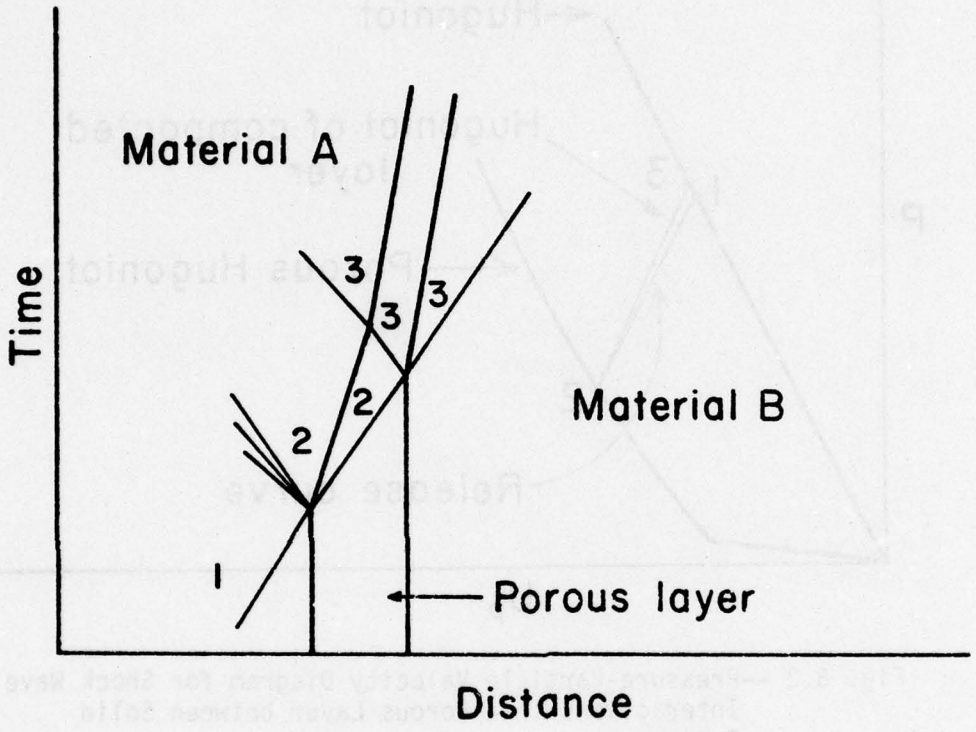

Fig. 3.3.--Position-Time Diagram for Shock Wave Interactions with a Porous Layer between Solid Regions.

The temperature in the porous material can be estimated using a Christian and Walsh technique (see section 1.3), in which the Hugoniot of the porous material is characterized before compaction by the relation

$$P = A - b\chi \tag{3.3}$$

where P is the pressure and χ is the compression defined by

$$\chi = \frac{\text{present volume}}{\text{full density volume at zero pressure}}$$

Here A and b are positive constants. This straight line pressure-volume curve is used until it intersects the principal Hugoniot of the full density material, which is assumed to occur when compaction to full density is complete. A more nearly exact relation for $P(v)$ can be obtained using the P-α equation of state of Herrman.[37] However, for temperature calculations the difference is less than 10% up to 500 kbars and the P-α form is much more difficult to manipulate. It is also assumed that C_v, γ, and ρ are the same as for the zero pressure full density material at the point where compaction is complete.

After compaction is complete, the Hugoniot for the porous layer can be calculated from the full density Hugoniot by using the Grüneisen equation of state to take into account the added internal energy due to irreversible work done in compaction (see Boade).[38] Consider two independent shock situations for the porous and full density materials. To each of these single shocks one may apply the Rankine-Hugoniot equation

$$E_P - E_{Po} = \frac{1}{2} P_P(v_{Po} - v_P) \tag{3.4}$$

$$E_S - E_{So} = \frac{1}{2} P_S(v_{So} - v_S) \tag{3.5}$$

where the subscripts P and S refer to porous and full density material, respectively. Now to find $P_P(v)$ we use the Grüneisen equation

$$P_P - P_S = (\gamma/v)(E_P - E_S) \tag{3.6}$$

which is just a relation between two equilibrium states of the same material at constant volume. Substituting from Eqs. (3.4) and (3.5), Eq. (3.6) becomes

$$P_P - P_S = (\gamma/v)\,\tfrac{1}{2}\,[P_P(v_{Po} - v_P) - P_S(v_{So} - v_S)] \tag{3.7}$$

where it is assumed $E_{Po} = E_{So}$. To find the relation for $P_P(v)$ for a given $P_S(v)$ which is known, let $v_P = v_S = v$, so that

$$P_P = \frac{P_S(v)[v_{So} - v - \frac{2}{G}]}{(v_{Po} - v - \frac{2}{G})} \tag{3.8}$$

where $\gamma/v \equiv G$ = constant. With the Hugoniot just constructed, it is possible to estimate the temperature in the porous layer by a numerical integration method outlined in section 1.3. Temperature rise in a single shock to various pressures and from various initial densities is given in Table 3.1 for copper. These temperatures are as much as a factor of 20 higher than shock compression temperatures in the solid. It should also be noted that the temperatures in the porous layer are roughly proportional to the shock pressure for a given initial porosity.

The temperature profile just after the shock wave passes through the interface is shown in Fig. 3.4. Evolution of this initial profile in time must be considered in terms of the relative time for decay of the temperature profile and the lifetime of the experiment. The maximum temperature, which will always be at y = 0, decreases with time. Depending on the relative time

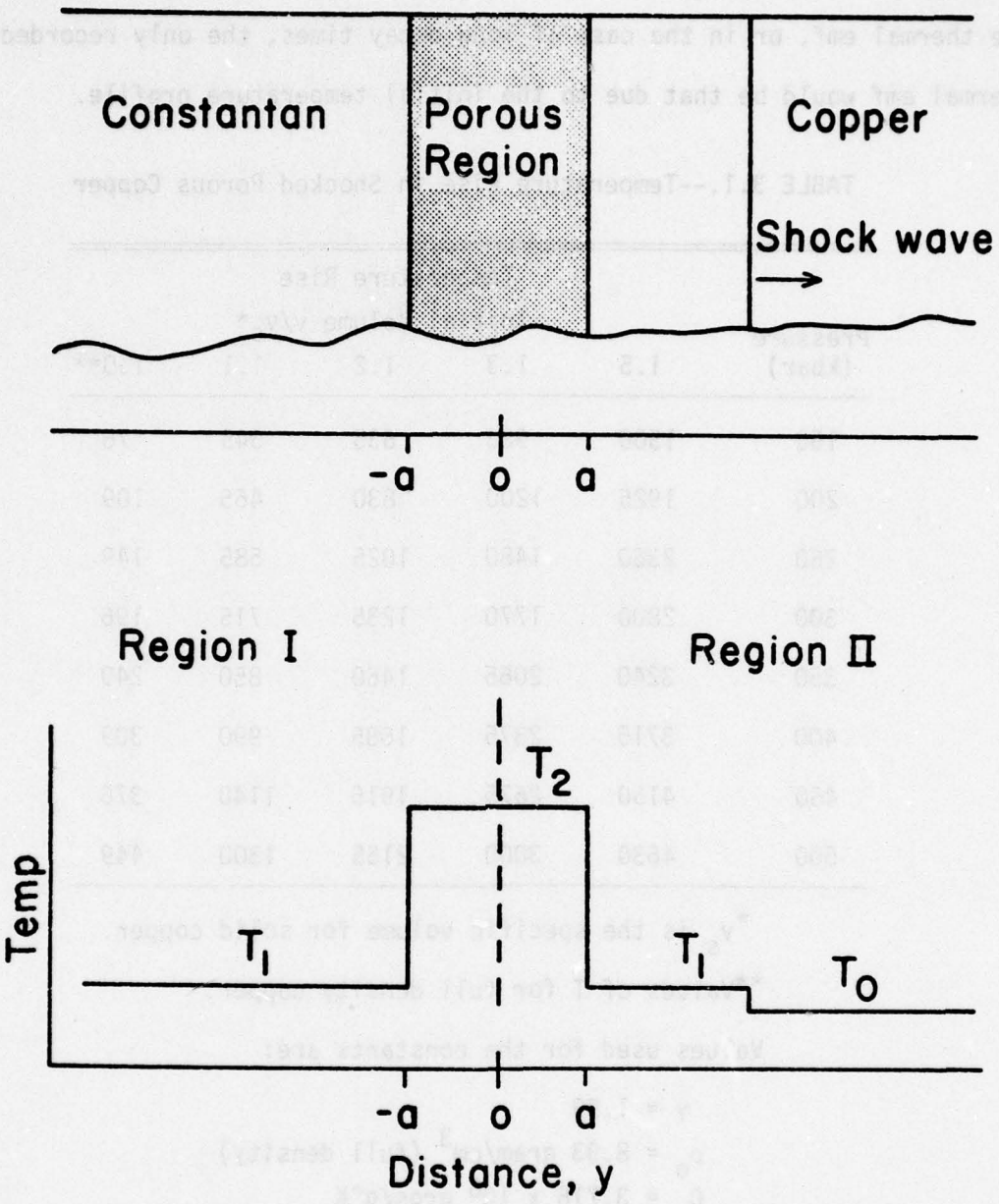

Fig. 3.4.--Temperature Profile Just after the Shock Compression of a Porous Layer.

dependence, one would expect either to see a predictable rate of decay of the thermal emf, or in the case of long decay times, the only recorded thermal emf would be that due to the initial temperature profile.

TABLE 3.1.--Temperature Rise in Shocked Porous Copper

Pressure (kbar)	Temperature Rise Initial Volume v/v_s* 1.5	1.3	1.2	1.1	1.0**
150	1500	920	635	345	76
200	1925	1200	830	465	109
250	2360	1480	1025	585	149
300	2800	1770	1235	715	196
350	3240	2065	1460	850	249
400	3715	2375	1685	990	309
450	4150	2675	1915	1140	376
500	4630	3000	2155	1300	449

*v_s is the specific volume for solid copper.

**Values of T for full density copper.

Values used for the constants are:

$\gamma = 1.99$

$\rho_o = 8.93$ gram/cm^3 (full density)

$C_v = 3.718 \times 10^6$ ergs/g°K

$C_o = 3.94$ mm/μsec

$S = 1.489$

where $U_s = C_o + S\,U_p$ for full density material.

The time dependence of the initial distribution can be studied using the one dimensional heat flow equation. It can be shown (see Appendix E) that the temperature at $y = 0$, $T(0,t)$, is

$$T(0,t) = T(0,0)[\tfrac{1}{5}\,\mathrm{erf}(2\sqrt{\tau/t}) + \tfrac{4}{5}\,\mathrm{erf}(\tfrac{1}{2}\sqrt{\tau/t})] \qquad (3.9)$$

where $\tau = a^2/D_{Cu}$ and D_{Cu} is the diffusivity of copper. The time constant τ takes on the values 0.01 μsec, 0.25 μsec, and 1 μsec for porous layers of 1 μ, 5 μ, and 10 μ, respectively. A plot of $T(0,t)/T_2$ versus τ is given in Fig. 3.5. Typical experiment life times are about 1 μsec in most previous work. Therefore, if an effective porous layer of 10 μ existed at the interface, the temperature would decay less than 40% during the experiment.

To show the importance of the temperature at $y = 0$, consider an experiment in which plane impact occurs between slabs of copper and constantan. The receding shock in constantan and the advancing shock in copper are indicated in Fig. 3.6 along with a temperature profile which includes a high temperature region about the origin. Using Eq. (1.2b) the emf measured between a and b in this circuit is given by

$$\phi_{a-b} = -\int_{T_0}^{T_2} S_{Cu}\,dT - \int_{T_2}^{T_0} S_{Co}\,dT\,. \qquad (3.10)$$

If we assume for simplicity that S_{Cu} and S_{Co} are independent of temperature and pressure this becomes

$$\phi_{a-b} = -S_{Cu}(T_2 - T_0) - S_{Co}(T_0 - T_2)$$

$$\phi_{a-b} = (S_{Co} - S_{Cu})(T_2 - T_0)\,. \qquad (3.11)$$

The emf observed in such a circuit is independent of T_1 and T_3, which represent the shock compression temperatures, and is a function only of T_2, which is $T(0,t)$ given in Eq. (3.9). This is true even if T_2 is only slightly higher than the shock compression temperature.

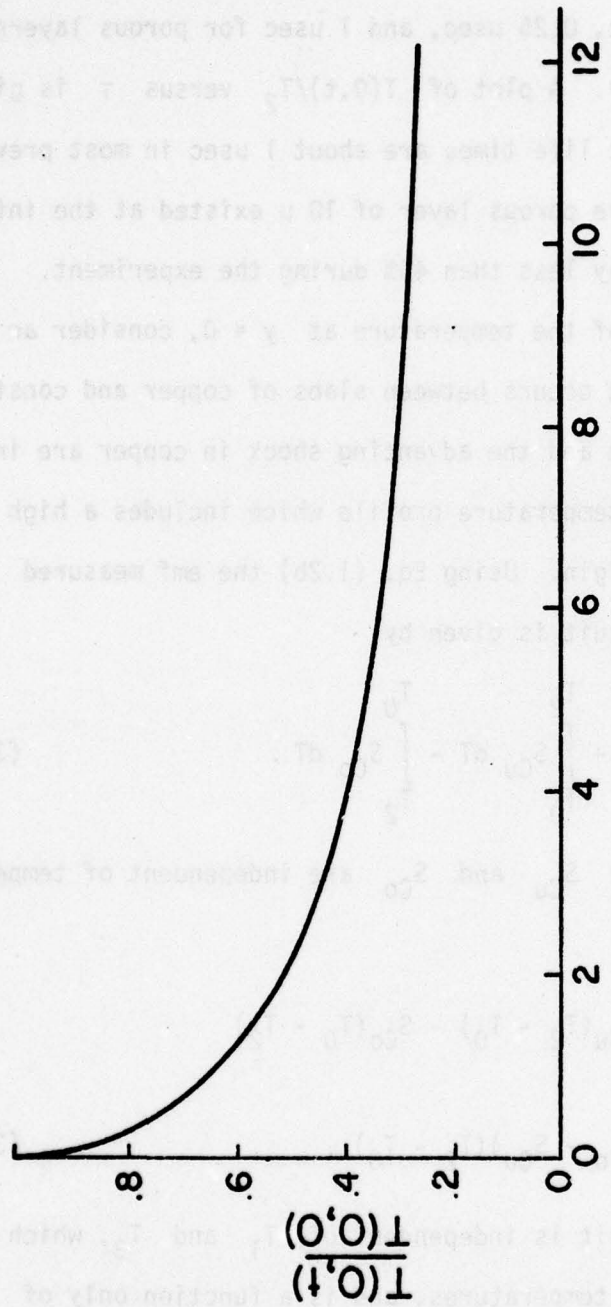

Fig. 3.5.--Temperature vs. Time in a Porous Layer Heated by Shock Compression. $T(0,0) = T_2$ of Fig. 3.4.

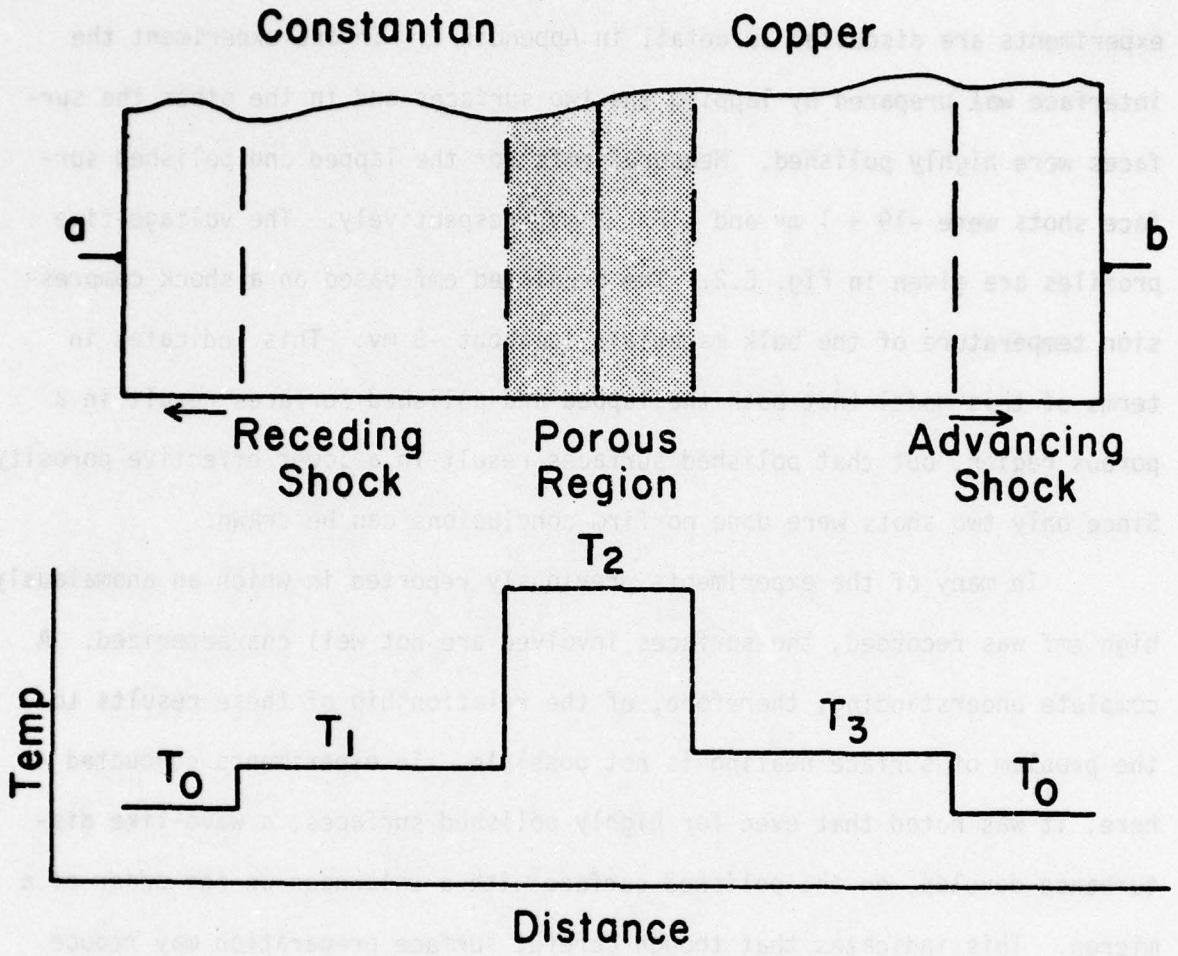

Fig. 3.6.--Thermoelectric Circuit and Associated Temperature Profile with Porous Interface Layer.

Two experiments were conducted to investigate the effect of surface preparation on measured emf in a copper-constantan junction experiment. The experiments are discussed in detail in Appendix E. In one experiment the interface was prepared by lapping the two surfaces and in the other the surfaces were highly polished. Measured emfs for the lapped and polished surface shots were -19 ± 1 mv and -16 ± 2 mv, respectively. The voltage-time profiles are given in Fig. E.2. The predicted emf based on a shock compression temperature of the bulk materials is about -3 mv. This indicates in terms of this model that both the lapped and polished surfaces result in a porous region, but that polished surfaces result in a lower effective porosity. Since only two shots were done no firm conclusions can be drawn.

In many of the experiments previously reported in which an anomalously high emf was recorded, the surfaces involved are not well characterized. A complete understanding, therefore, of the relationship of these results to the problem of surface heating is not possible. In experiments conducted here, it was noted that even for highly polished surfaces, a wave-like disturbance develops on the polished surface with a thickness on the order of a micron. This indicates that though careful surface preparation may reduce the problem, it would not be possible to completely eliminate these effects. Bowden and Tabor[36] have shown through surface resistance measurements that the actual area in contact between two surfaces can be more than an order of magnitude less than the geometrical area even for highly polished surfaces. This too indicates that even under the best of conditions, a region in which there are voids must exist between the two bulk materials of interest.

Results of our experiments indicate that polished surfaces at the junction may result in a lower emf than when rough surfaces are used. We have shown that the "measured temperature," or the temperature to which the

junction as a thermocouple responds, is the temperature in the immediate vicinity of the junction, and is independent of the temperature behind the shock front. Finally, we have shown that if the interface region is treated as a porous solid, the temperatures reached by a shock compression are high enough to explain the anomalously large emfs observed previously. It seems quite reasonable to conclude that the measured response to shock loading of a bimetallic junction, in which the specimens are simply held in contact, is partially or perhaps totally due to the conditions at the junction interface.

CHAPTER 4

EXPERIMENTAL TECHNIQUE

The experimental configuration and techniques described here were developed to avoid the problems discussed in Chapter 3 and still retain the essential conditions of the idealized experiment of Chapter 1. The actual experiments will be described first followed by a discussion of how the specific problems were avoided. Finally, a comparison will be made between the real experiments and the idealized experiment.

4.1 Experimental Configuration.

The basic impactor and target assemblies are illustrated in Fig. 4.1. The constantan is diffusion-welded to the copper buffer as shown, with a ceramic and copper guard ring surrounding it for lateral support. The ceramic was machined to a close tolerance, and fitted between the copper and constantan, by a process described in section 4.4. The copper leads are attached as indicated with solder. The copper guard ring is in intimate contact with the buffer plate, but is not involved in the thermoelectric circuit. Nominal dimensions are listed in Fig. 4.1 for each of the components.

Shock pressure is generated by plane high velocity impact of a copper or tungsten alloy impactor on the copper buffer. The plane shock wave travels through the copper buffer, and uniformly loads the copper-constantan junction. A shock wave also travels out radially from the edge of the impactor toward the outer edge of the copper buffer. The dimensions here were chosen so that no pressure disturbance reaches the point on the buffer where the measurement

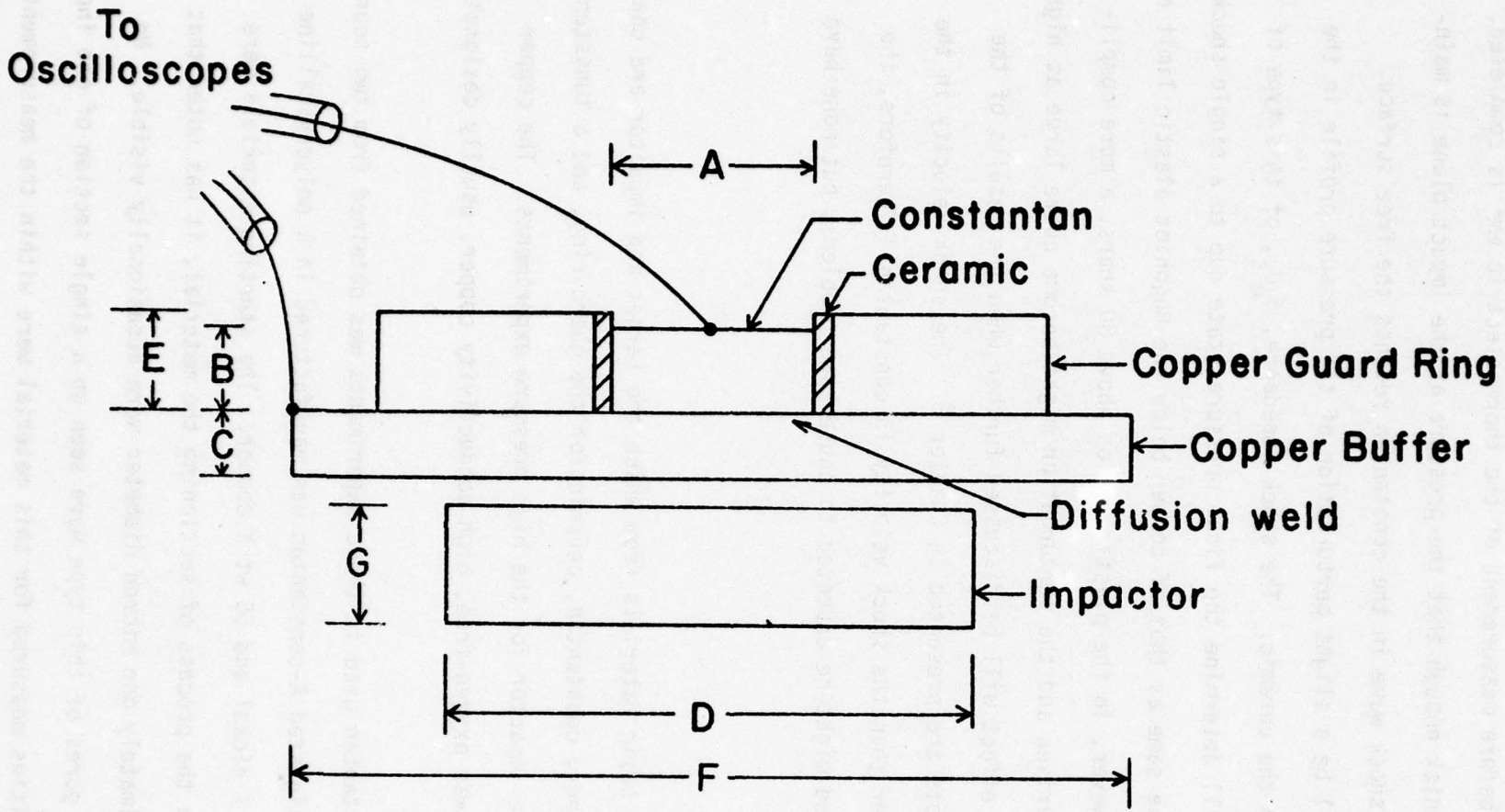

Fig. 4.1.--Configuration for Uniaxial Strain Experiments. Nominal dimensions: A = 15 mm, B = 5 mm, C = 4 mm, D = 40 mm, E = 6 mm, F = 63.5 mm, G > 5 mm.

lead is attached before measurement of the thermoelectric emf is completed. The impactor is thick enough that the pressure at the impact plane is maintained until the shock wave in the constantan reaches the free surface.

There will be a slight perturbation of the pressure profile in the constantan due to the ceramic. The shock impedance, $\rho_o U_s$, of this type of ceramic, which will determine the final pressure state due to a single shock, is essentially the same as that of copper below the Hugoniot elastic limit of the ceramic. However, in the plastic region above 80 kbars, a more complicated situation arises and the perturbation might become quite large at high pressures. This effect will be discussed further when the results of the high pressure shots are presented in Chapter 5. The shock velocity in the ceramic is greater than the shock velocity in constantan. Therefore, the wave running ahead might be expected to cause some problems, but none have been identified.

4.2 Materials.

The four basic materials from which the target and impactor are constructed are copper, constantan, ceramic for the guard ring, and a tungsten alloy used as the impactor for the high pressure experiments. The copper used throughout was oxygen-free, high conductivity copper, usually designated OFHC copper.

The constantan used in these experiments was obtained from two sources. The material designated A-constantan was manufactured in a polycrystalline form from 45 wt % nickel and 55 wt % copper. The starting materials were 99.99% pure. In the process of sectioning the material, it was noted that voids of approximately one micron diameter were occasionally visible. No more than 10-15 pores of this type were seen on a single section of one inch diameter. Densities measured for this material were within the measurement

error of the expected value of 8.9 gram/cm^3. More information for this and the following materials is included in Table 4.1.

TABLE 4.1.--Materials Used

Supplier	Material Type	Identification Used Here	Analyzed Composition
Metals Research*	45 wt% Nickel 55 wt% Copper Alloy	A-Constantan	44.4 wt% to 46.9 wt% Nickel
U.S. Bureau of Mines†	44.5 wt% Nickel 55.5 wt% Copper 1% Manganese Alloy	B-Constantan	54.2% Copper 44.2% Nickel 1% Manganese 0.3% Carbon
Teledyne**	17-D Densalloy	Tungsten Alloy	90.91% Tungsten 4% Iron 3% Copper 2% Nickel

*Metals Research Ltd. Melbourn, Royston, Herts SG8 6EJ, England.

†U.S. Bureau of Mines, Albany, Oregon.

**Teledyne Powder Alloys, Clifton, New Jersey.

The material designated B-constantan was supplied by the U.S. Bureau of Mines. This material was manufactured in a polycrystalline form from 54.5 wt% copper, 44.5 wt% nickel, and 1 wt% manganese. The starting materials were commercially pure, but the alloying was done in a carbon vessel and later analysis shows 0.3% carbon exists in the material. The density of this material measured 8.82 ± 0.05 g/cm^3.

The ceramic used for the guard ring was supplied by Coors Porcelain Company, and is designated AD-998 Alumina. The ceramic was supplied as a tubing and is nominally 99.8% Al_2O_3.

The tungsten alloy which was used as the impactor for the higher pressure shots was supplied from two different production lots. The

properties measured such as density, alloy composition, and yield strength, are not significantly different between lots. Hugoniot data for this material are given in Appendix B. The concentration of the various components is 90.91% tungsten, 4% iron, 3% nickel, and 2% copper. The density for the two lots was 17.0 g/cm^3 and 17.2 g/cm^3.

4.3 Preparation Technique.

The first step in preparing a target is the diffusion welding of the junction. The pieces a and b (see Fig. 4.2) are machined to the following dimensions:

(a) 63.5 mm diam. x 4 mm thickness

(b) 22.2 mm diam. x 6.4 mm thickness.

The flat surfaces of the disks are then lapped flat and parallel to within 1 micron over the entire area. At this point, the surfaces have a damage layer due to lapping of between 5 and 15 microns thickness. The surfaces to be welded are now carefully polished in three stages on a Buehler* polishing wheel. The objective in the first stage is to completely remove the damage layer due to lapping. This is done using a nylon polishing cloth loaded with 15 μ diamond polishing paste and light oil designed for this purpose. The quality of the results depends, to a great extent, on the pressure applied to the specimen, and on the amount of oil and diamond paste used. At the completion of this stage, the surface should appear under a 400x microscope as a uniform "scratched" surface where only the damage due to polishing is visible.

In the second polishing stage 6 μ diamond polishing paste is used and the finished surface should again have a uniform scratched appearance, but with much smaller scratches. Final polishing is done with 0.05 μ alumina

*Buehler Ltd., Evanston, Illinois.

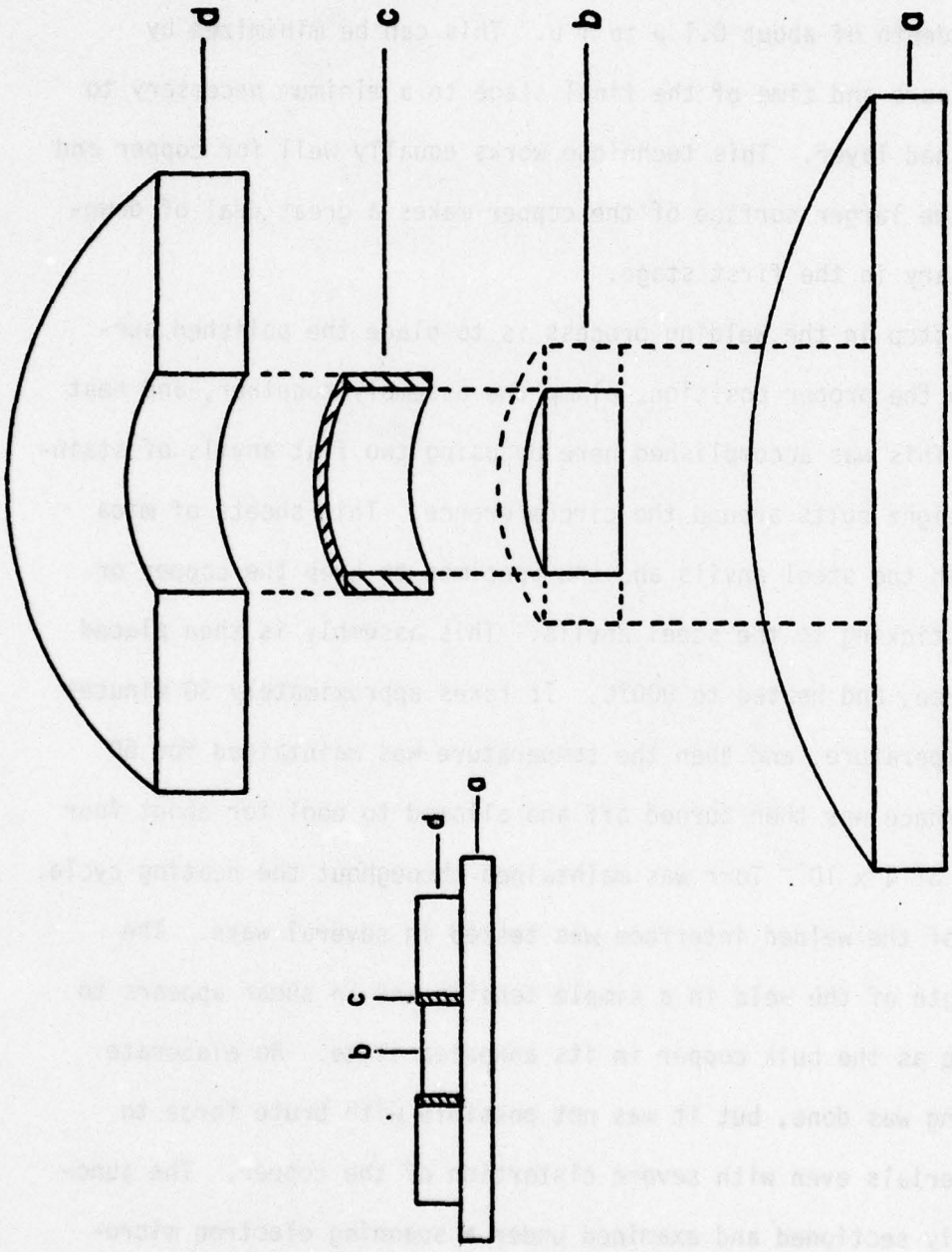

Fig. 4.2.--Exploded View of Target Assembly. (a) Copper buffer, (b) Constantan, (c) Ceramic Insulator, (d) Copper Guard Ring.

polishing powder and water in the form of a slurry. A napped cloth is used in this stage with very little pressure. After this final polish, the surface under a 400x microscope appears free of scratches and polishing damage. There is a slight waviness which develops on the surface with a wavelength of 10-50 μ and a depth of about 0.1 μ to 1 μ. This can be minimized by reducing the pressure and time of the final stage to a minimum necessary to remove the scratched layer. This technique works equally well for copper and constantan, but the larger surface of the copper makes a great deal of downward force necessary in the first stage.

The next step in the welding process is to place the polished surfaces together in the proper position, clamp the assembly together, and heat it in a vacuum. This was accomplished here by using two flat anvils of stainless steel with eight bolts around the circumference. Thin sheets of mica are placed between the steel anvils and the specimen to keep the copper or constantan from sticking to the steel anvils. This assembly is then placed in a vacuum furnace, and heated to 800°C. It takes approximately 30 minutes to reach this temperature, and then the temperature was maintained for 60 minutes. The furnace was then turned off and allowed to cool for about four hours. A vacuum of 4×10^{-5} Torr was maintained throughout the heating cycle.

Quality of the welded interface was tested in several ways. The mechanical strength of the weld in a simple tension and in shear appears to be about the same as the bulk copper in its annealed state. No elaborate mechanical testing was done, but it was not possible with brute force to separate the materials even with severe distortion of the copper. The junction was carefully sectioned and examined under a scanning electron microscope and no damage or impurities were detected.

An estimate can be made of the depth of interdiffusion from known diffusivities of nickel in copper. Consider the situation in which the

copper and constantan are separated by a plane at $x = 0$. If the constantan (45% nickel) is to the left of the dividing plane, Crank[39] gives for the concentration of nickel for $x > 0$

$$C(x,t) = \frac{1}{2} C_o \operatorname{erfc} \frac{x}{2\sqrt{Dt}} .$$

Here D is the diffusivity of nickel in copper and C_o is the concentration of nickel at $t = 0$ and $x < 0$. Jost[40] gives the value for D at 800°C as 4.84×10^{-11} cm^2/sec. Figure 4.3 is a plot of $C(x, t = 1\ hr)$ for a temperature of 800°C.

After the welding process is completed, the assembly must be lapped square again due to a slight deformation of the copper. The piece is then carefully aligned in a lathe, and the constantan is machined to a dimension two to five microns larger on the diameter than the inside dimension of the ceramic tube. This dimension is nominally 15.25 mm, which allows only the central portion of the initial weld to be used, thus reducing effects due to rounding of the edges of the constantan during polishing. The ceramic and copper guard ring is assembled by a heat-shrinking process. The inside diameter of the copper ring, d, is machined to a dimension two to five microns smaller than the outside diameter of the ceramic. The ceramic tube had been previously machined round to a tolerance of less than 2.5 microns. The copper is then heated about 200°C or until the copper and ceramic slip together easily. The guard ring assembly is then assembled with the welded copper-constantan piece by cooling the copper-constantan piece in liquid nitrogen and slipping them together. Care is taken throughout this process to maintain the parallelism among pieces. The entire process is illustrated in Fig. 4.2.

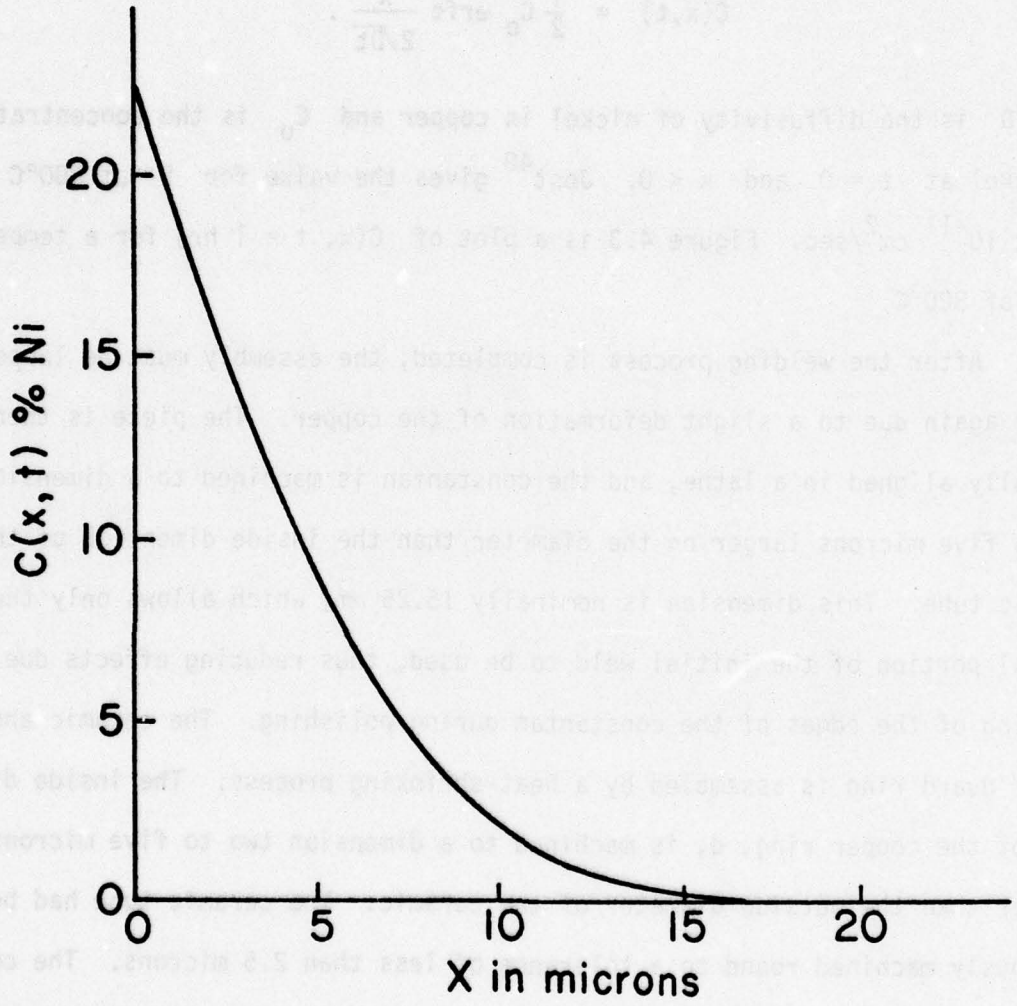

Fig. 4.3.--Concentration of Nickel in Copper Near the Welded Junction of Copper and Constantan.

4.4 Impact Technique.

The impact experiments were done using the four inch gas gun facility at Washington State University.[41] The impactor piece was mounted on the front of an aluminum projectile as illustrated in Fig. 4.4. The recess which is indicated on the front of the projectile is necessary to avoid contact between the aluminum projectile face and the copper buffer during the useful time of the experiment. For projectile velocities greater than 0.8 mm/μsec a nylon and syntactic foam projectile was used.* The design of this projectile is only slightly modified from that reported by Peterson et al.[42] Projectile velocity is measured with a set of four electrically charged pins which are contacted by the projectile just before impact.

The target assembly, described in the previous section, was potted into an aluminum target ring with a calcium carbonate filled casting epoxy. A void was allowed in the epoxy around the soldered oscilloscope lead on the copper buffer to avoid a pressure disturbance in this area during the experiment. A grounded pin and an electrically charged trigger pin contacted the projectile before impact and were used to start the oscilloscopes.

Signals in the one to twenty millivolt range must be measured with care to avoid ground loops and extraneous noise. The signals were measured using differential amplifiers in a system illustrated in Fig. 4.5. This type of system has a 50 Ω input impedance in each leg with respect to ground, thus giving a 100 Ω net input impedance. The analysis of the thermoelectric effect in Chapter 3 assumes an open circuit or infinite impedance measurement of the emf. The effect of this difference is negligible due to the very low internal impedance of the emf source. As was stated in Chapter 1, the emf source here can be treated as a voltage source with an associated internal

*Material used here was Scotchply XP-241-34 Syntatic Foam supplied by 3M Co., St. Paul, Minnesota.

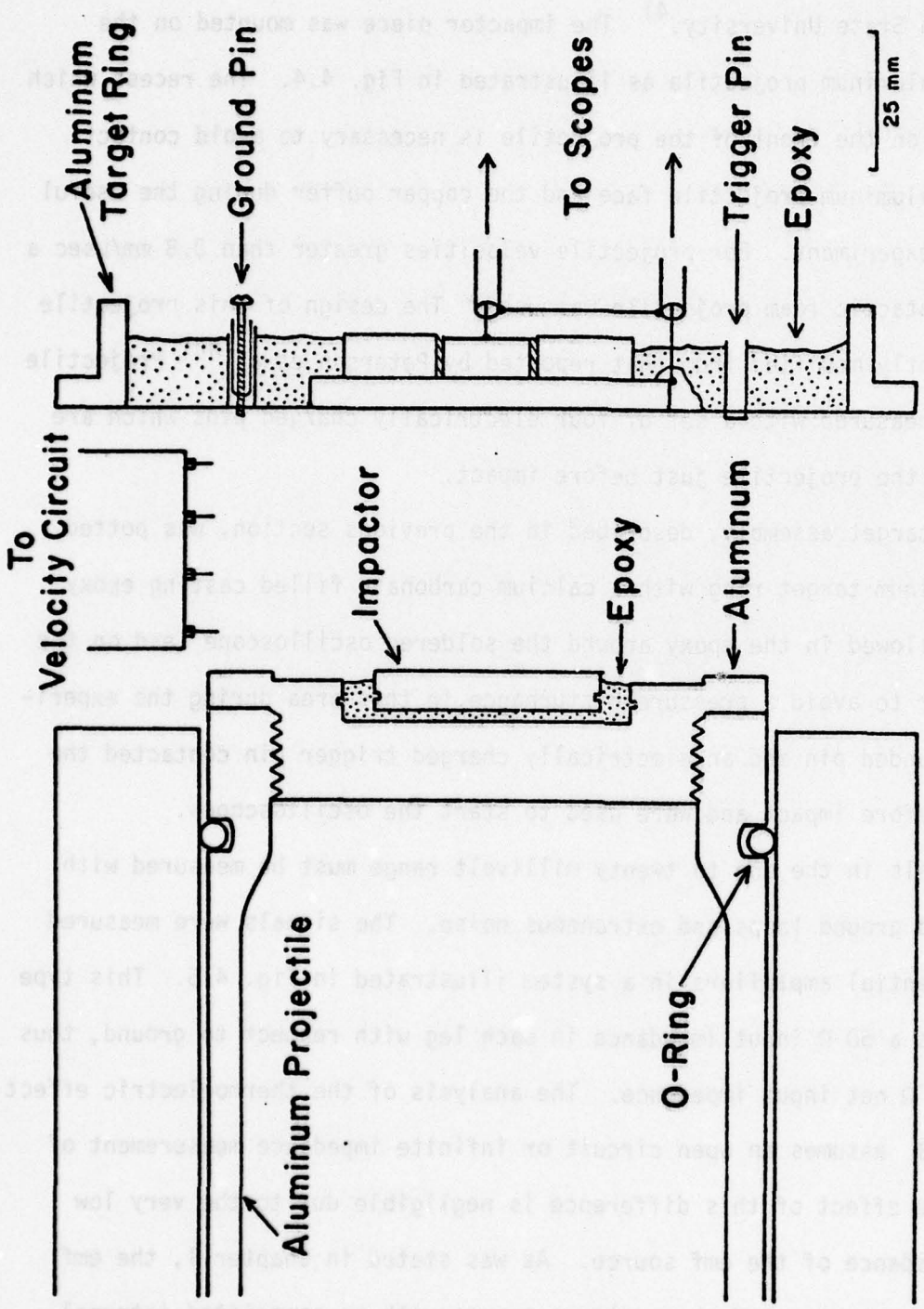

Fig. 4.4.--Illustration of Impact Experiments. Drawn to scale.

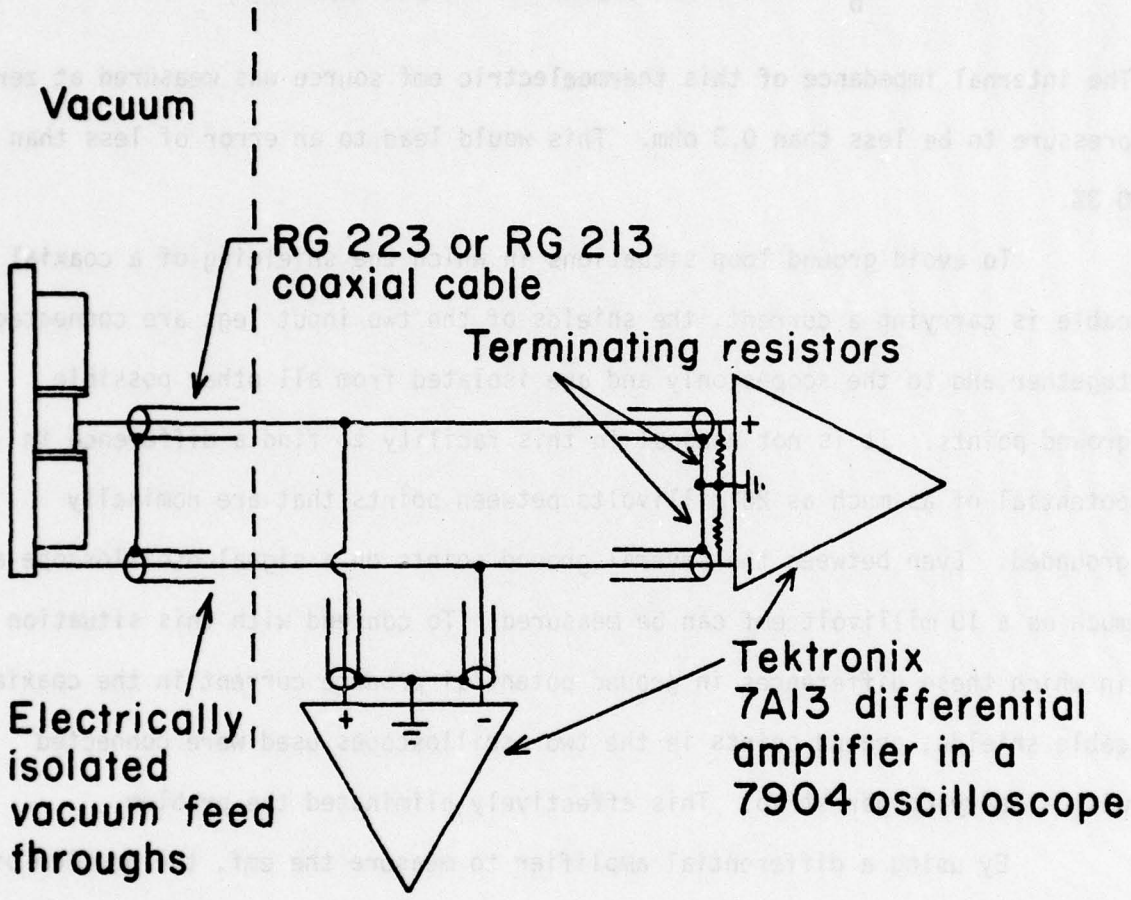

Fig. 4.5.--Schematic Drawing of Recording System.

impedance. The ratio of the measured voltage in this circuit to that which would be measured in an open circuit system is

$$\frac{V}{V_o} = \frac{\text{Input Impedance}}{\text{Internal Impedance + Input Impedance}}$$

The internal impedance of this thermoelectric emf source was measured at zero pressure to be less than 0.3 ohm. This would lead to an error of less than 0.3%.

To avoid ground loop situations in which the shielding of a coaxial cable is carrying a current, the shields of the two input legs are connected together and to the scopes only and are isolated from all other possible ground points. It is not unusual in this facility to find a difference in potential of as much as 20 millivolts between points that are nominally grounded. Even between the several ground points on a signal oscilloscope as much as a 10 millivolt emf can be measured. To contend with this situation in which these differences in ground potential produce current in the coaxial cable shields, ground points in the two oscilloscopes used were connected with a heavy copper strap. This effectively eliminated the problem.

By using a differential amplifier to measure the emf, the problem of noise on the scope ground is minimized. Not only is there a difference in potential between various ground points, but there is also as much as five millivolts of 60 cycle noise on the entire chassis ground of the oscilloscope system. Since in a differential input system the deflection on the oscilloscope is proportional to the difference between the two inputs and independent of the ground, this problem can be completely avoided. Using Tektronix model 7A13 amplifier plug in units in model 7904 mainframes, clean signals could be measured down to one millivolt.

4.5 Comparison of the Actual Experiments with the Idealized Experiment.

The actual configuration described in section 4.1 and the idealized experiment are shown for comparison in Fig. 4.6. The similarities of these two configurations are:

(1) A plane shock wave is advancing in a cylinder of constantan away from the junction.

(2) The copper-constantan junction is in a pressurized region and the pressure is uniform and constant over the entire junction.

(3) Pressure relief from the edges of the constantan behind the shock front is avoided. (Assumed condition in idealized experiment.)

(4) The emf is measured between unshocked regions in the copper and constantan.

The primary differences between the two configurations are:

(1) The shock wave in the copper is not a simple plane wave traveling in a cylinder, but is rather the rounded edge of a plane wave traveling radially outward in the copper disk.

(2) The symmetry with respect to the junction is not maintained in the real experiment.

(3) The pressure in the copper near the junction is attained by a large transmitted shock and a small reflected shock from the copper-constantan interface. The reflected shock is very small because the shock impedances of copper and constantan are very nearly equal (see Appendix B).

The effects of these differences are minimized because the thermo-
power of constantan is a factor of 20 greater than that of copper. The

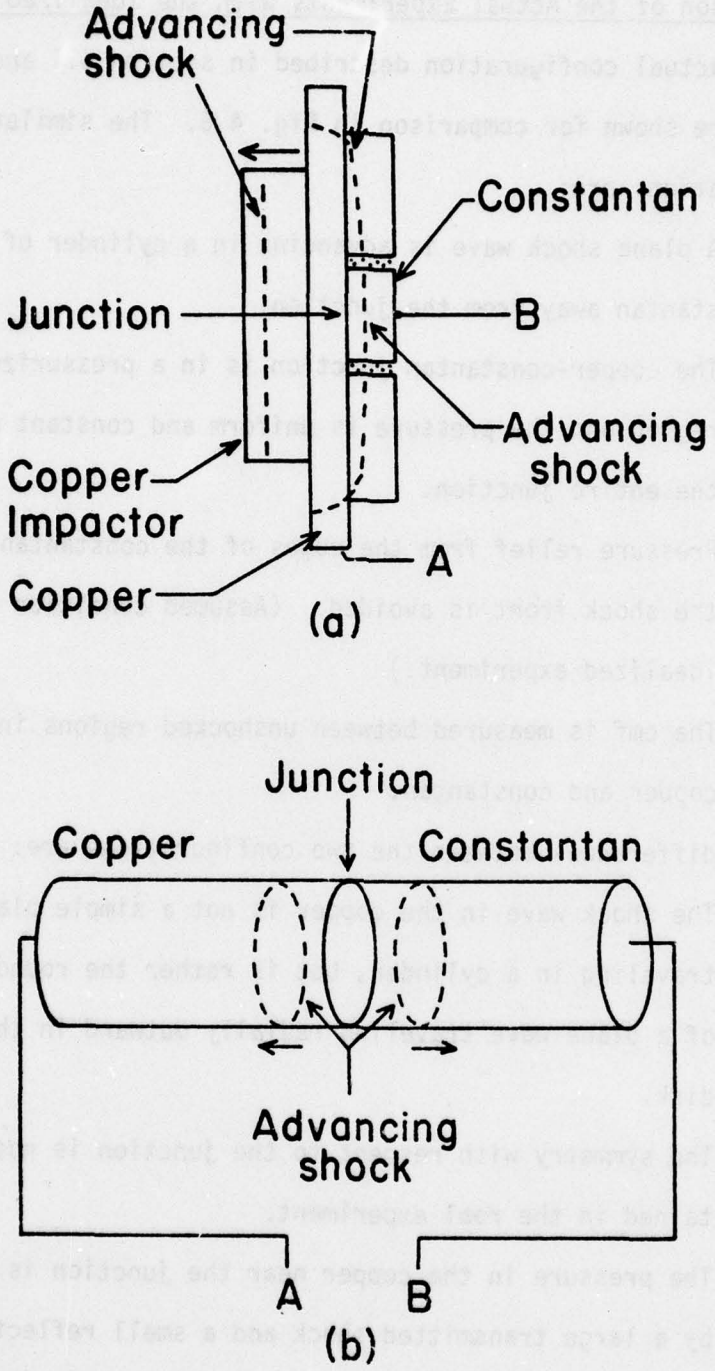

Fig. 4.6.--Actual Experimental Configuration Compared with the Idealized Configuration.

experiment was designed to preserve the ideal conditions in the constantan and make any necessary compromises in the copper.

The experimental problems of Chapter 3 were avoided in these experiments in the following way:

(1) Electrical noise upon circuit closure was avoided by having the recording circuit complete before the shot. All connections are either soldered or welded to ensure good contact.

(2) Demagnetization effects were avoided by choosing nonferromagnetic materials. Constantan has a relatively high thermopower of about 50 μv/°C at and above room temperature and is nonferromagnetic. The primary disadvantage to the use of this material arises because it is an alloy. Since thermopower is somewhat affected by impurities and composition, the obvious problem of reproducibility among samples of different manufacture could arise.

(3) A superheated region at the interface was avoided or minimized by diffusion welding the junction. This type of junction has very little, if any, porosity.

CHAPTER 5

EXPERIMENTAL RESULTS AND DISCUSSION

Results presented here are divided into two parts. In the first part the guard ring was modified or completely eliminated. This allowed for pressure relief radially behind the shock wave in the constantan. In the second part the results of a set of experiments in which the guard ring was used to maintain one-dimensional flow behind the shock will be presented. Finally, our conclusions and a proposal for further study will be given.

5.1 Results of Experiments without Guard Ring.

Consider again the idealized experiment of Chapter 1. If the edges of the rod in which the shock wave is traveling were free surfaces, relief waves would advance inward from the edges behind the shock wave to reduce the pressure. It was assumed in the analysis that no pressure relief of this type was allowed. We have observed that this restriction has a significant effect on the measured emf. Four experiments were conducted in which the effects of this restriction can be seen. The experimental parameters and the results of these shots (77-005, 77-026, 77-037, and 77-074) are summarized in Table 5.1, and Fig. 5.1. A short discussion of each shot will follow.

77-005 and 77-026. These experiments were conducted as described in Chapter 4 except that no guard ring was used, and the diameter of the constantan was 19 mm ± .1 mm. The second shot (77-026) was done to duplicate the first, and was identical to the extent possible. Shock pressure was calculated from the projectile velocity of .7 mm/μsec to be 144 ± 4 kbars in

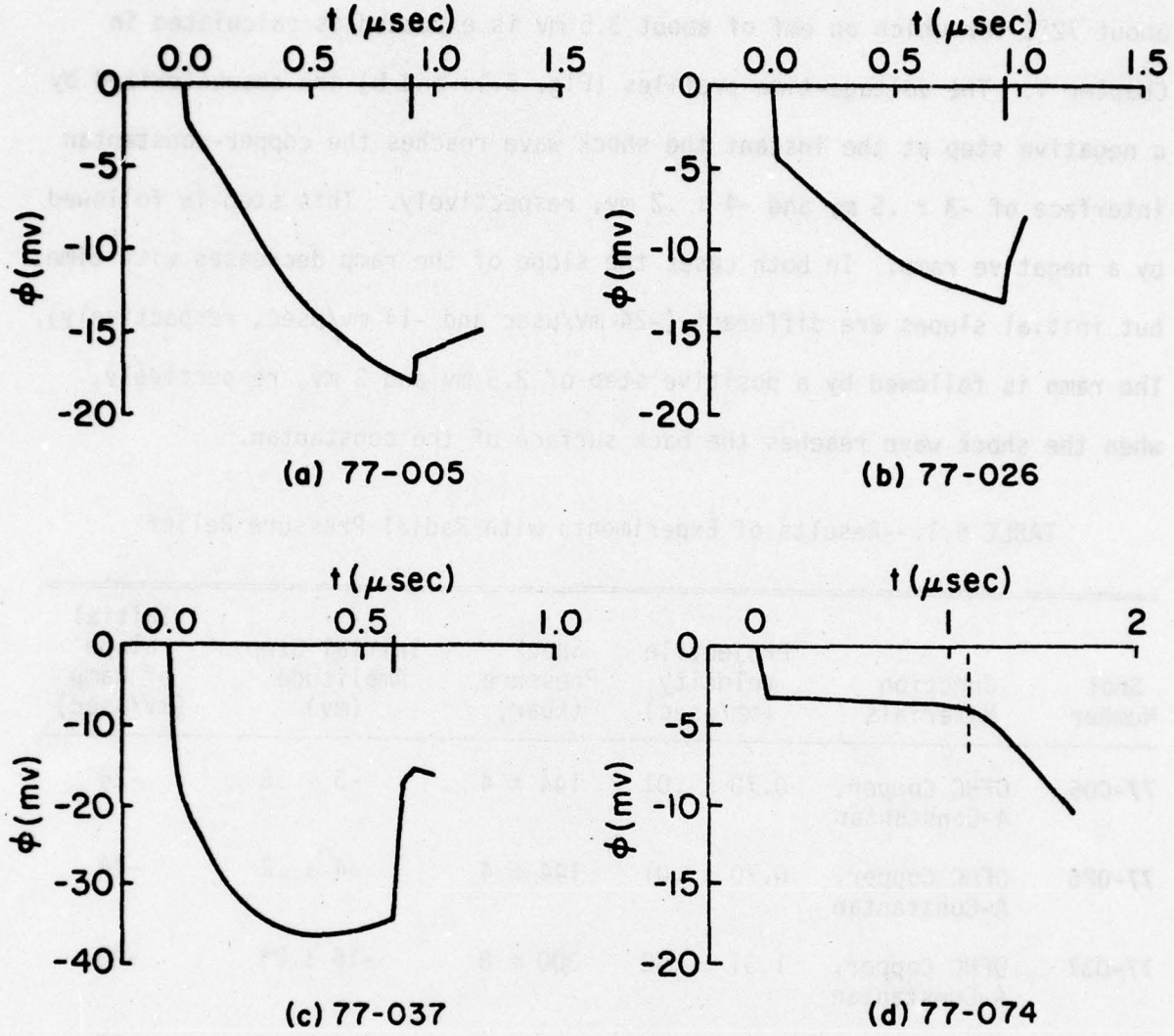

Fig. 5.1.--Voltage-Time Profiles for Shots 77-005, 77-026, 77-037, and 77-074. The large tick marks in (a), (b), and (c) indicate the time at which the shock wave reached the back surface of the constantan. The dotted line in (d) indicates the time at which the shock wave in the constantan advanced past the guard ring.

both shots. This would give a temperature rise in the shock compression of about 72°C for which an emf of about 3.5 mv is expected as calculated in Chapter 1. The voltage-time profiles (Fig. 5.1a and b) are characterized by a negative step at the instant the shock wave reaches the copper-constantan interface of -3 ± .5 mv and -4 ± .2 mv, respectively. This step is followed by a negative ramp. In both cases the slope of the ramp decreases with time, but initial slopes are different (-24 mv/μsec and -14 mv/μsec, respectively). The ramp is followed by a positive step of 2.5 mv and 3 mv, respectively, when the shock wave reaches the back surface of the constantan.

TABLE 5.1.--Results of Experiments with Radial Pressure Relief

Shot Number	Junction Materials	Projectile Velocity (mm/μsec)	Shock Pressure (kbar)	Initial Step Amplitude (mv)	Initial Slope of Ramp (mv/μsec)
77-005	OFHC Copper, A-Constantan	0.70 ± .01	144 ± 4	-3 ± .5	-24
77-026	OFHC Copper, A-Constantan	0.70 ± .01	144 ± 4	-4 ± .2	-14
77-037	OFHC Copper, A-Constantan	1.31 ± .02	300 ± 8	-15 ± 2*	-75
77-074	OFHC Copper, B-Constantan	0.70 ± .01	144 ± 4	-3.2 ± .2	-13

*The step height is difficult to determine due to the steepness of the following ramp.

77-037. The projectile velocity was increased in this experiment and was measured to be 1.31 ± .02 mm/μsec. The dimensions of the target and impactor were scaled down to facilitate the high projectile velocity. The constantan diameter was the same at 19 mm, the impactor diameter was 25 mm, the copper buffer diameter was 35 mm, and the copper buffer thickness was

1.7 mm (nominal dimensions with .1 mm tolerance). The pressure was calculated to be 300 ± 8 kbars which would give a temperature rise in the shock compression of about 194°C and an estimated thermal emf of about 9.5 mv. The voltage-time profile (Fig. 5.1c) is quite different for this shot than for the previous two shots. A step in emf is not clearly distinguishable from the following ramp. In the original data trace a slight change in slope can be seen at about -15 mv. The magnitude of the emf does not increase monotonically during the shock transit through the constantan as in shots 77-005 and 77-026, but reaches a maximum of -36.5 mv about .2 μsec before the shock wave reaches the back surface of the constantan.

77-074. In this shot the guard ring of ceramic and copper described in Chapter 4 was used, but unlike the configuration in Fig. 4.1 the constantan thickness (B) was 13 ± .03 mm and the guard ring thickness (E) was only 5.16 ± .03 mm. We had tentatively determined at this time that the ramping in shots 77-005, 77-026, and 77-037 was related to the violation of the one-dimensional strain restriction of the idealized experiment. This was supported by the steady emf (no ramping) observed in another shot 77-064 in which the guard ring was used as described in Chapter 4 (see section 5.2). The specific purpose of 77-074 was to determine whether the pressure relief at the junction itself causes the ramping, or if it could be observed when the radial flow was allowed just behind the shock front, but not at the junction. The projectile velocity and shock pressure were the same as for shots 77-005, and 77-026. The resulting voltage-time profile (Fig. 5.1d) shows an initial step of -3.2 ± .2 mv at the instant the shock wave reaches the copper-constantan interface and a steady emf until the shock wave reaches the back surface of the guard ring. At that point a ramping of -13 mv/μsec is observed. This indicates that the ramping is associated with the relief process

at the edges in the constantan, and is not due to the interaction of the relief waves with the copper-constantan interface.

These results indicate that in the case where simple uniaxial strain conditions exist, the net emf around the thermoelectric circuit is constant as the shock wave progresses through the constantan. In the case where two-dimensional flow exists behind the shock front in constantan due to relief at the edges, the emf around the circuit is greater in magnitude and unsteady, at least under these experimental conditions. In the experiments where no guard ring was present, the emf measured when the shock first pressurizes the junction, and before relief waves from the edges are established, compares directly with the steady emf measured when a guard ring was used, as shown in Table 5.1.

We propose three possible causes for this difference in electrical response between these two types of experiments.

(1) High velocity radial flow due to radial pressure relief which would tend to rapidly change the self-inductance of the current-carrying conductor. The entire circuit then, when taken as a unit, would have an unsteady current flow even for a constant emf source.

(2) Relativistic effects usually neglected in a moving conductor. This is unlikely because of the small speeds involved, but is included for completeness.

(3) Some unknown transport property of the electron-lattice system making up the conductor when two-dimensional flow is present behind the shock front.

Calculations have been done in Appendix F which indicate that the effects mentioned in the first two possible explanations are far too small in magnitude to account for the observed response.

A serious study of the possibilities involved in the third suggested explanation has not yet been undertaken. It should be noted, however, that the absolute thermopower is affected to varying degrees by both hydrostatic pressure and one-dimensional strain in static situations. Both of these effects can be understood at least qualitatively on the basis of modern transport theory as it applies to thermoelectric phenomena. We feel that further study of this problem is warranted on the basis of these results.

5.2 Results of Experiments with Guard Ring.

Six additional measurements were made with the experimental design of Fig. 4.1 and 4.4, including the ceramic and copper guard ring. The only parameters that were varied in these experiments were the shock pressure and the constantan material.* The results of one additional shot, 77-074, mentioned in section 5.1, in which the constantan was longer than the guard ring, compare directly for times less than the shock transit time through the guard ring, and will be included in these results.

Results of these experiments are listed in Table 5.2. The pressure behind the shock was calculated for each of the shots using the Rankine-Hugoniot jump conditions and empirical U_s-U_p relations for both copper and constantan (see Appendix B). The uncertainties indicated for the measurements are based on the quality of the record and its character; i.e., where records are noisy, or the emf is not steady but varies slightly with time, the uncertainty attributed is larger. The uncertainties in each case are larger than could be attributed to the recording system or data handling system; therefore, the uncertainty listed reflects only the character of the observed signals rather than our ability to record the signal.

---

*In shot 77-064 a disk of copper was welded to the back surface of the constantan as an electrode instead of simply soldering a copper wire onto the constantan. This accounts for the uncharacteristic slow decay of the emf after shock transit in the constantan.

TABLE 5.2.--Results of Experiments with Uniaxial Strain

Shot Number	Projectile Velocity (mm/μsec)	Impactor Material	Junction Materials	Pressure (kbar)	Measured Emf (mv)	Rise Time (nanosec)
77-064	0.71 ± .01	OFHC Copper	OFHC Copper, B-Constantan	146 ± 4	- 3.8 ± .4	26 ± 5
77-074	0.70 ± .01	OFHC Copper	OFHC Copper, B-Constantan	144 ± 4	- 3.0 ± .2	50 ± 5
77-076	0.70 ± .01	OFHC Copper	OFHC Copper, B-Constantan	144 ± 4	- 3.7 ± .7	7 ± 5
77-079	1.22 ± .02	Tungsten Alloy*	OFHC Copper, A-Constantan	362 ± 7	-17.2 ± .4	50 ± 10
77-084	0.70 ± .01	OFHC Copper	OFHC Copper, A-Constantan	144 ± 4	- 4.9 ± .4	30 ± 5
77-085	0.77 ± .01	OFHC Copper	OFHC Copper, A-Constantan	162 ± 4	- 4.5 ± .2	25 ± 5
77-092	0.95 ± .02	Tungsten Alloy*	OFHC Copper, A-Constantan	270 ± 5	-10.4 ± .2	107 ± 5

*Tungsten alloy is described in section 4.3 and Appendix IV.

The voltage-time profiles for all of these experiments are given in Figs. 5.2 and 5.3. The initial negative step in emf in each of the records takes place when the shock wave reaches the copper-constantan junction. In the shots done near 150 kbars, the emf remains approximately constant until the shock wave reaches the back free surface of the constantan. The rise times for the initial voltage step are included in Table 5.2 for each shot. The rise times vary considerably, but the short rise time of 7 ns observed in shot 77-076 indicates that the response time of the thermoelectric circuit is short compared with the typical value observed for rise time. A great deal of care is taken in an effort to maintain parallelism between the advancing plane shock and the junction plane. However, neither the tilt of the projectile with respect to the target nor the actual parallelism between target face and junction were measurable in these experiments.

In the two highest pressure shots, 77-079 and 77-092, the emf became unsteady and increasing in magnitude after about 300 ns. This has been attributed to the mechanical behavior of the ceramic insulator which makes it a poorer impedance match to the copper and constantan at high pressures than at low pressures as discussed in section 4.2. The lower pressure in the ceramic allows pressure relief at the edges of the constantan and produces an effect similar to that seen in the unsupported shots.

5.3 Comparison of Results with Theory and Discussion.

The emfs observed for the experiments discussed in section 5.2 can now be compared directly with calculations based on the thermoelectric theory, known empirical relations for thermopower, and temperature estimates discussed in Chapter 1. The initial emf step for the experiments of section 5.1, in which no radial support is used, can be considered the result of a

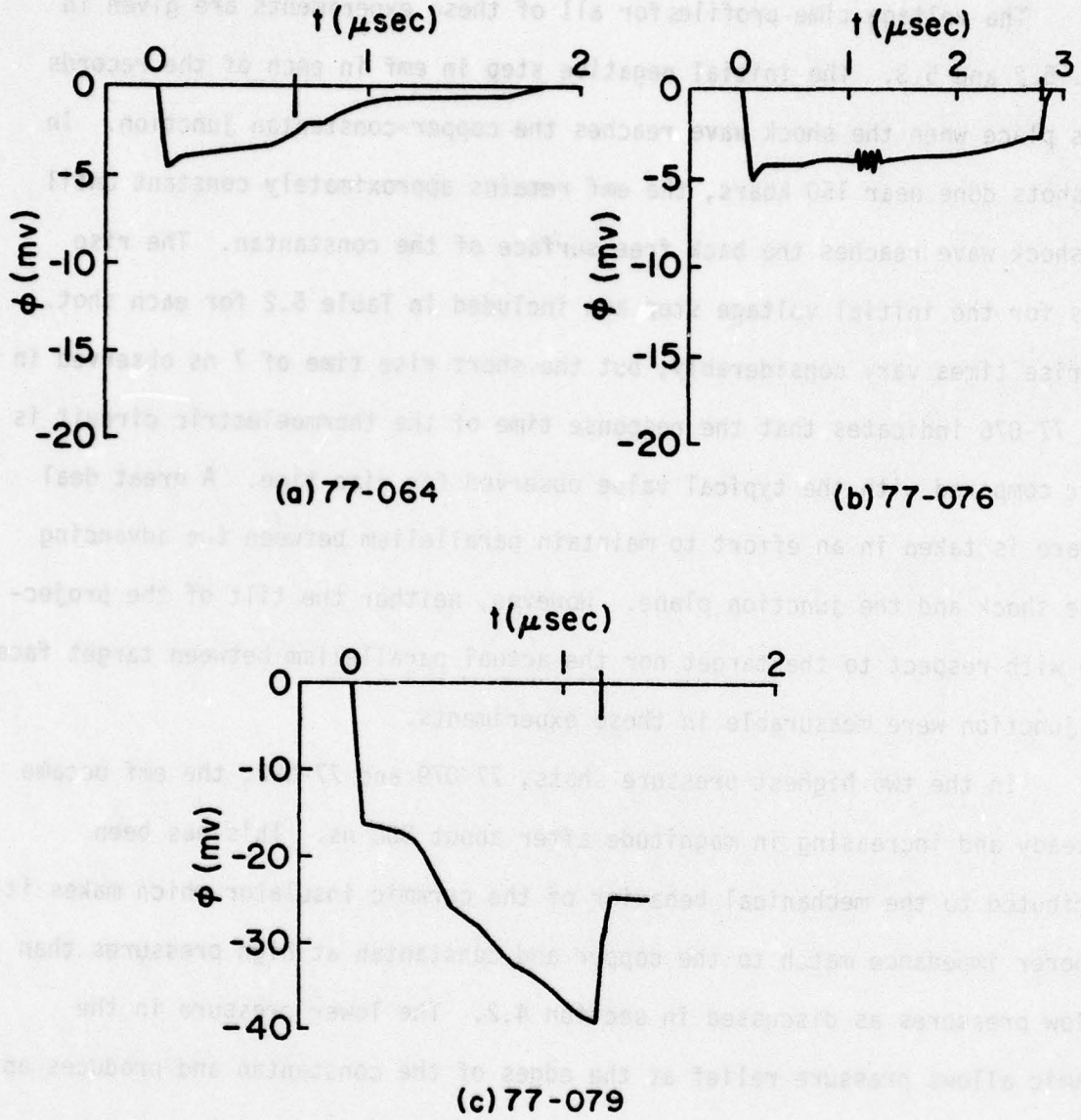

Fig. 5.2.--Voltage-Time Profiles for Shots 77-064, 77-076, and 77-079. The large tick marks indicate the time at which the shock wave reached the back surface of the constantan.

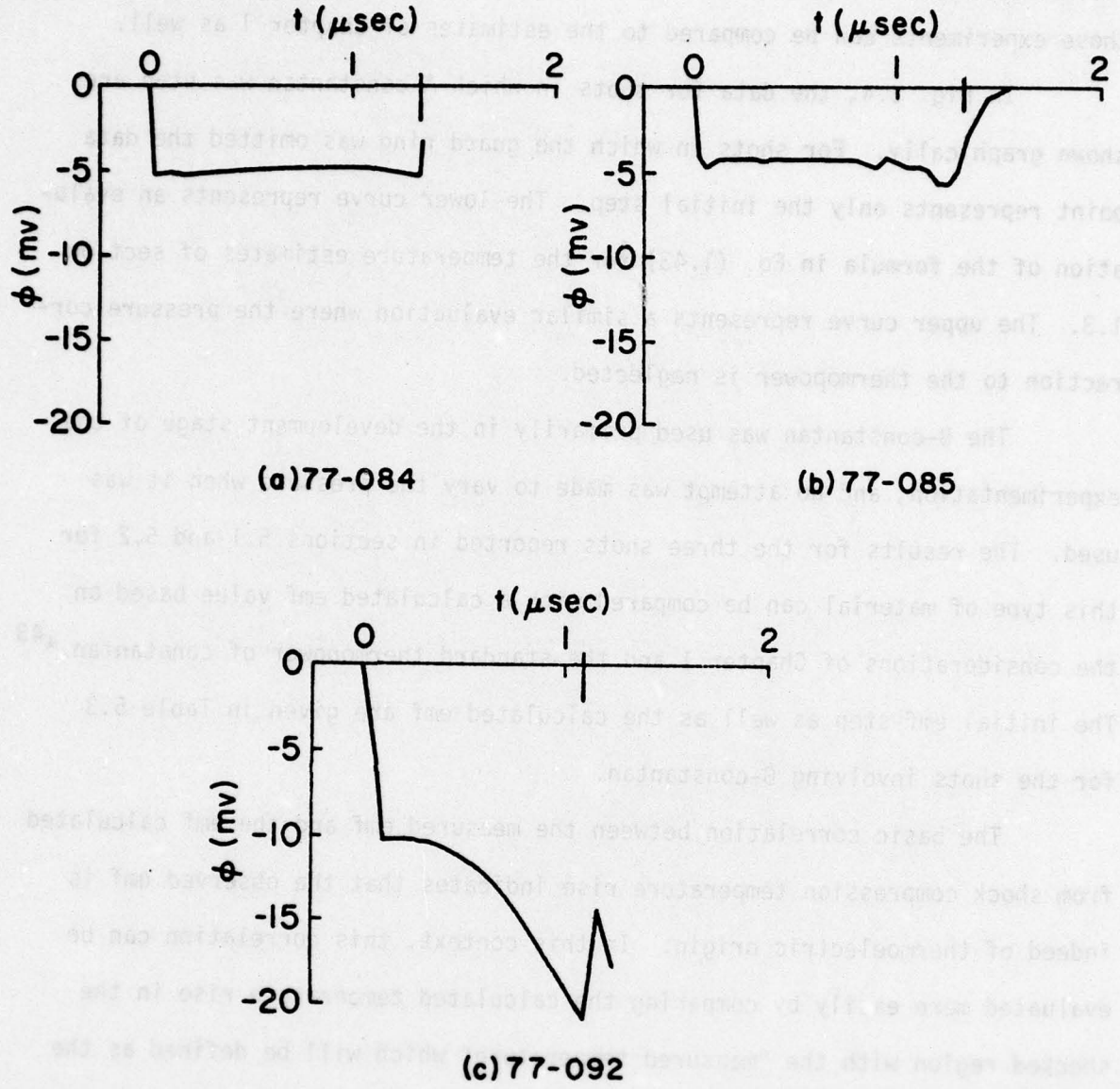

Fig. 5.3.--Voltage-Time Profiles for Shots 77-084, 77-085, and 77-092. The large tick marks indicate the time at which the shock wave reached the back surface of the constantan.

one-dimensional loading of the junction. Therefore, the initial steps for those experiments can be compared to the estimates of Chapter 1 as well.

In Fig. 5.4, the data for shots in which A-constantan was used are shown graphically. For shots in which the guard ring was omitted the data point represents only the initial step. The lower curve represents an evaluation of the formula in Eq. (1.43) for the temperature estimates of section 1.3. The upper curve represents a similar evaluation where the pressure correction to the thermopower is neglected.

The B-constantan was used primarily in the development stage of the experimentation, and no attempt was made to vary the pressure when it was used. The results for the three shots reported in sections 5.1 and 5.2 for this type of material can be compared with a calculated emf value based on the considerations of Chapter 1 and the standard thermopower of constantan.*[43] The initial emf step as well as the calculated emf are given in Table 5.3 for the shots involving B-constantan.

The basic correlation between the measured emf and the emf calculated from shock compression temperature rise indicates that the observed emf is indeed of thermoelectric origin. In this context, this correlation can be evaluated more easily by comparing the calculated temperature rise in the shocked region with the "measured temperature" which will be defined as the temperature rise necessary to give the observed results if the junction acts as a thermocouple. In Table 5.3, the "measured temperature," based on a pressure corrected thermopower as discussed in section 1.2, is given for each shot along with the shock compression temperature calculated by the technique outlined in section 1.3. The average discrepancy between the calculated

*The composition of this material matches that of commercial constantan to which the referenced table applies. The thermopower was measured and found to be within one percent of the table value for temperatures between 0°C and 70°C.

AD-A053 693 WASHINGTON STATE UNIV PULLMAN SHOCK DYNAMICS LAB F/G 14/2
ELECTRICAL RESPONSE OF A BIMETALLIC JUNCTION TO SHOCK COMPRESSI--ETC(U)
MAR 78 D D BLOOMQUIST, G E DUVALL, J J DICK F49620-77-C-0034
UNCLASSIFIED AFOSR-TR-78-0728 NL

2 OF 2
AD
A053 693

END
DATE
FILMED
6-78
DDC

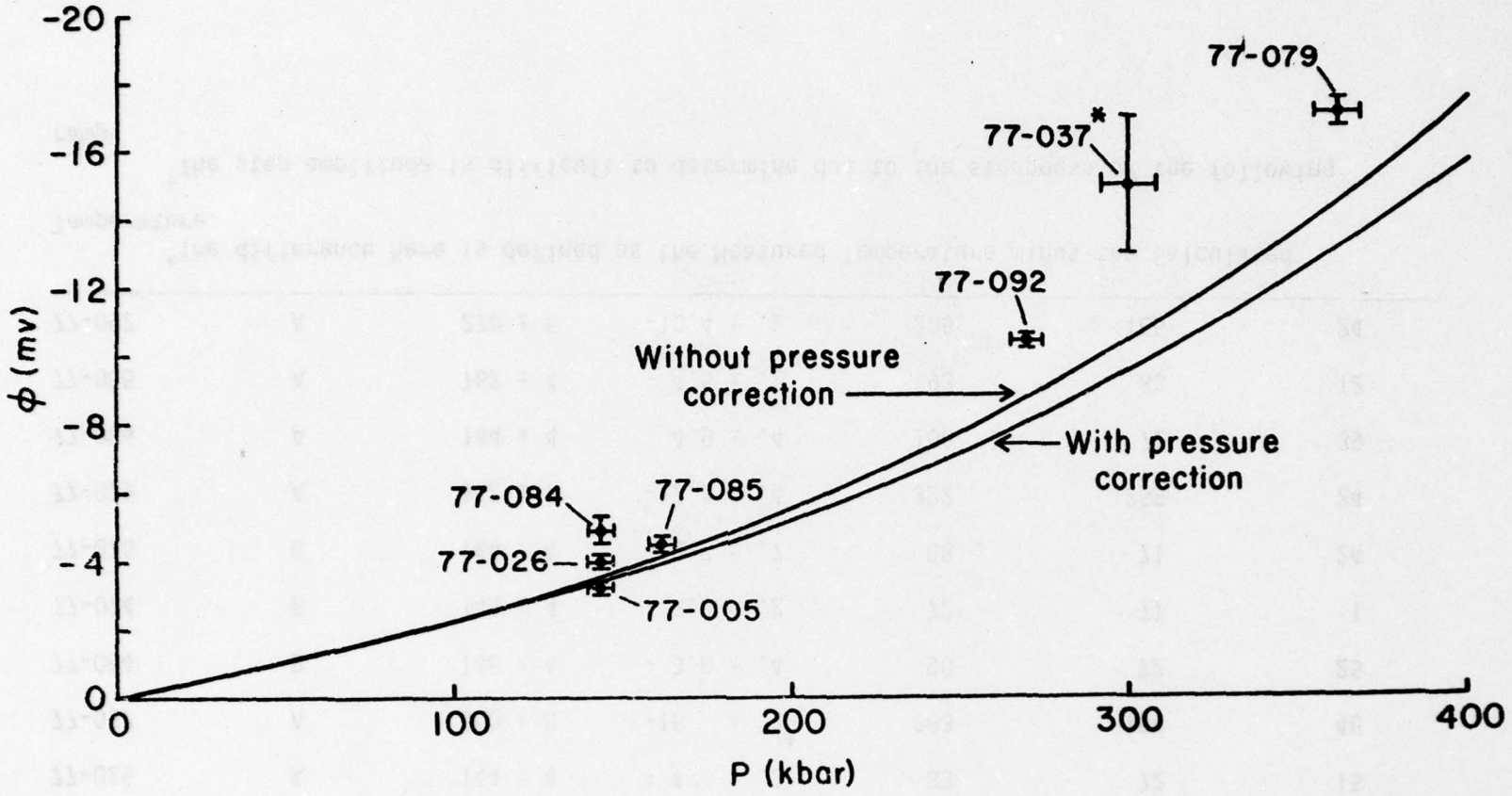

Fig. 5.4.--Comparison of Measured Emf Data with the Predicted Emf as a Function of Pressure.
*The step amplitude is difficult to determine due to the steepness of the following ramp.

TABLE 5.3.--Comparison of Calculated and Measured Temperatures

Shot Number	Constantan Type (A or B)	Pressure (kbar)	Measured Emf (mv)	Measured Temp. Rise (°K)	Calculated Temp. Rise (°K)	Percentage* Difference
77-005	A	144 ± 4	- 3 ± .5	63	72	-13
77-026	A	144 ± 4	- 4 ± .2	83	72	15
77-037	A	300 ± 8	-15 ± 2†	283	194	46
77-064	B	146 ± 4	- 3.8 ± .4	90	72	25
77-074	B	144 ± 4	- 3.0 ± .2	72	71	1
77-076	B	144 ± 4	- 3.7 ± .7	88	71	24
77-079	A	362 ± 7	-17.2 ± .4	322	259	24
77-084	A	144 ± 4	- 4.9 ± .4	100	72	39
77-085	A	162 ± 4	- 4.5 ± .2	93	83	12
77-092	A	270 ± 5	-10.4 ± .2	205	155	24

*The difference here is defined as the Measured Temperature minus the Calculated Temperature.

†The step amplitude is difficult to determine due to the steepness of the following ramp.

temperature and the "measured temperature" is 22%.* Three possible sources of error involved in this comparison are the error in the measured emf, the uncertainty in the calculated shock compression temperature, and the validity of the pressure correction to the thermopower. Only the errors involved in the emf measurement for each shot are indicated explicitly as an uncertainty in the "measured temperature." The shock compression temperature calculation using the assumptions that γ/v and C_v are constant is believed to be correct within about 10%. The temperature in the shocked region could be as much as 5% higher than the value given due to plastic work if the yield stress were significantly larger than the value obtained from quasistatic measurements. The pressure correction to the thermopower is extrapolated from hydrostatic thermopower corrections measured to 72 kbars. The actual magnitude of this correction at any given pressure would depend somewhat on the pressure dependence of temperature in the shock front (see section 1.2). However, since this correction is based theoretically on the effects of the change in atomic volume, the fact that the pressure is reached through a shock mechanism rather than hydrostatically should not make the correction completely invalid. At 150 kbars this correction increases the "measured temperature" by only 5%.

Considering the 10% uncertainty in the calculated temperature, the measured emf in the experiments corresponds to a temperature that may be within 10% of the actual shock compression temperature. At least three possible explanations exist with respect to the remaining discrepancy. First, it is possible that the calculated temperature is 10-20% lower than the actual value and that the "measured temperature" is more accurate than the calculated value. Attempts have been made to determine the shock compression

*This is the RMS value neglecting shot 77-037.

temperature of opaque materials by measuring the residual temperature after expansion to zero pressure.[44-46] The techniques used are based on measuring the surface radiation temperature or resistivity of the unloaded material. Sufficient data are not available at this time to adequately examine this possibility. Secondly, the 10-20% discrepancy may be due to a slight change in the thermopower in shock compression. This would represent a change in the heat transport properties of the conduction electrons, and/or the crystal lattice from the static situation. Finally, the temperature in the immediate vicinity of the junction interface may be somewhat higher than the bulk temperature. We have shown in section 3.3 that the temperature measured in this type of thermoelectric circuit may be that which exists within a few microns of the interface rather than in the bulk material behind the shock.

It is our belief that the interface temperature could easily be 10-20% higher than the bulk temperature, and that this is the most probable explanation of the discrepancy between the calculated and measured values of temperature. The diffusion welding process used here reduces the difference between a real junction and an ideal junction, but some imperfections undoubtedly exist which could lead to a higher temperature in this region. In this context, the diffusion welded junction is one step closer to the ideal junction in which a plane divides the two materials.

5.4 Conclusions and Recommendations.

5.4.1 Conclusions

The initial objective to determine whether the previously reported anomalous and generally nonreproducible results were due to experimental artifacts or fundamental principles has been achieved. Our results indicate that any fundamental anomaly which exists for one dimensional strain is less than 10-20% of the observed signals in the pressure range from 140-360 kbars.

In a study of the effects of an imperfect interface layer between the metals due to surface preparation, we have shown that the measured emf in a thermoelectric circuit is sensitive to the junction interface temperature, which might be several times greater than the shock compression temperature of the bulk material. We therefore conclude that the large emf values previously reported, as well as the general nonreproducibility among experiments, were due primarily to the effects of poor junction interface conditions. Using a model of a porous layer between the materials, it was shown that the temperature in this region is nearly proportional to the pressure in a single shock compression. This may explain the linear emf pressure relations previously observed. In studies by Buzhinskii et al.,[19] and Nesterenko,[28] in which particular attention was given to surface preparation, some of the resulting emf values are within 20% of the predicted values and although a great deal of scatter in the data is present in both studies, this evidence supports the conclusion that no fundamental anomaly exists and that high emf values are due to poor surface conditions.

We have shown that in experiments designed to measure the response of a bimetallic junction, it is possible to inadvertently measure an induced emf caused by shock demagnetization when a ferromagnetic material such as nickel is used as one of the elements. This may be responsible for some of the nonreproducibility evident in previous investigations in which ferromagnetic materials were used.

In experiments in which radial pressure relief was allowed behind the shock front, the emf was observed to be unsteady and increasing with time. No adequate explanation of this observation has yet been found. We have shown, however, that the unsteady emf is directly related to the two-dimensional flow caused by radial pressure relief behind the shock. This

effect, having now been isolated, may be considered as a possible source of the nonreproducibility present in some previous experiments. In particular, the relatively small emf followed by a ramping observed by Lascar and Duage[20] could be explained as a "normal" thermoelectric response coupled with this two-dimensional effect.

The one oscillogram reported by Buzhinskii *et al.*[19] does not indicate a ramping effect similar to that observed here. The same basic experimental geometry was used in that study as was used for the experiments reported here; however, in some experiments the nickel was in the shape of a 120° cone which would modify the relief wave situation. The authors do not indicate which experiments were done in this way or for which experiment the oscillograph was observed. Since the surfaces and geometry were varied and the data have a great deal of scatter, it is impossible at this point to determine how these results compare with those observed here.

Finally, we have shown that the voltage response of a carefully prepared and diffusion-welded copper-constantan junction to one-dimensional shock compression over a range in pressure from 145 kbars to 360 kbars is within 10-20% of the predicted value. This prediction is based on a pressure corrected thermoelectric response to the shock compression temperature of the bulk materials. Further study is necessary to determine conclusively whether this remaining discrepancy is due to the inaccuracy of the temperature calculation or of the temperature measurement. At this point we believe that the discrepancy is more probably due to a temperature at the junction interface which is higher than that of the bulk materials due to imperfections in the welded interface.

5.4.2 Recommendations

We recommend that further study be done to determine the cause of the decreasing unsteady emf observed when radial pressure relief is allowed behind the shock front. If this effect is indeed due to a fundamental change in the transport properties of the material under these conditions, characterization of this phenomenon could considerably advance basic understanding in this area.

Further study is also recommended to determine the cause of the remaining discrepancy between predicted and measured temperatures. Since the measured temperature is that which exists in the immediate vicinity of the junction interface, the possibility of a higher temperature due to defects at or near the weld should be eliminated. The use of a smaller junction area is recommended to facilitate the diffusion welding process.

The use of a highly compressible metal as one element in this junction would generate a much higher expected temperature and make the imperfections at the weld negligible. The discrepancy between the measured and predicted temperatures should then be smaller if this discrepancy is due only to defects at the interface.

Finally, we recommend that the feasibility be studied of using a thermocouple as a temperature transducer in shock compressed materials other than the thermocouple elements. We have shown that the thermoelectric effect is not altered to any large degree by a one-dimensional shock compression and therefore might be employed in a shock environment to determine the temperature of the shocked state in surrounding material.

REFERENCES

1. H. B. Callen, Thermodynamics (John Wiley & Sons, Inc., New York, 1960).

2. J. M. Ziman, Electrons and Phonons (Oxford University Press, London, 1960).

3. F. J. Blatt, P. A. Schroeder, C. L. Foiles, and D. Greig, Thermoelectric Power of Metals (Plenum Press, New York, 1976), Chap. 4.

4. N. F. Mott and H. Jones, The Theory of the Properties of Metals and Alloys (Dover Publications, Inc., New York, 1958), 2nd ed.

5. P. W. Bridgman, Proc. Am. Acad. Arts Sci. 53, 269 (1918).

6. F. P. Bundy, J. Appl. Phys. 32, 483 (1961).

7. E. Nagy and J. Toth, J. Phys. Chem. Solids 24, 1043 (1963).

8. J. M. Walsh and R. H. Christian, Phys. Rev. 97, 1544 (1955).

9. G. E. Duvall, Dynamic Response of Materials to Intense Impulsive Loading, Edited by P. C. Chou and A. K. Hopkins (U.S. Government Printing Office, 1973), Chap. 4, pp. 89-122.

10. M. H. Rice, R. G. McQueen, and J. M. Walsh, Solid State Phys. 6, 1 (1958).

11. H. S. Carslaw and J. C. Jaeger, Conduction of Heat in Solids (Oxford University Press, London, 1959), 2nd ed.

12. J. Jacquesson, Les Ondes de Detonation (Editions du Centre National de la Recherche Scientifique, 15 Quai Anatole-France-Paris (VII^{e}) 1962), pp. 415-422.

13. V. S. Ilyukin and Y. N. Kologrivov, Prikladnoi Mekhanika i Tekhnicheskaya Fizika [Applied Mechanics and Technical Physics], 5, 175 (1962).

14. D. G. Doran and T. J. Ahrens, "Electrical Effects of Shock Waves: Conductivity in CsI and KI. Thermoelectric Measurements in Metals," Final Report, Stanford Research Institute, Project PGU-4100 (1963).

15. E. P. Palmer and G. H. Turner, J. Appl. Phys. 35, 3055 (1964).

16. J. Crosnier, J. Jacquesson and A. Migault, Fourth Symposium on Detonation (Office of Naval Research, Washington, D.C., 1965), pp. 627-638.

17. A. Migault and J. Jacquesson, Behavior of Dense Media Under High Dynamic Pressure (Symposium on High Dynamic Pressure, 1967, Gordon and Breach, New York, 1968), pp. 431-440.

18. H. Conze, J. Crosnier and C. Bernard, Behavior of Dense Media Under High Dynamic Pressure (Symposium on High Dynamic Pressure, 1967, Gordon and Breach, New York, 1968), pp. 441-452.

19. O. I. Buzhinskii and S. V. Samylov, Fiz. Tverd. Tela. [Sov. Phys.-Solid State] 11, #10, 2332 (1970).

20. A. Lascar and G. Duage, C. R. Acad. Sci. (Paris) 270, 162 (1970).

21. J. Jacquesson, J. P. Romain, and H. Hallouin, Fifth Symposium on Detonation (Office of Naval Research, Washington, D.C., 1970), pp. 403-412.

22. V. N. Mineev, A. G. Ivanov, Yu. V. Lisitsyn, E. A. Novitskii, and Yu. N. Tyunyaev, Zh. Eksp. Teor. Fiz. [Sov. Phys.-JETP] 34, 131 (1972).

23. S. A. Bordzilovskii, S. M. Karakhanov, and V. V. Polyvdiv, Combustion, Explosion, and Shock Waves, Trans. from Fizika Goreniya i Vzryva, 8, 586 (1972).

24. S. A. Bordzilovskii and S. M. Karakhonov, Zh. Tekh. Fiz. [Sov. Phys.-Tech. Phys.] 18, 1246 (1974).

25. A. Migault and J. Jacquesson, J. Phys. (Paris) 33, 599 (1972).

26. S. A. Bordzilovskii, S. M. Karakhonov, and V. M. Titov, Combustion, Explosion, and Shock Waves, Trans. from Fizika Goreniya i Vzryva 10, 265 (1973).

27. V. F. Nesterenko and A. M. Staver, Combustion, Explosion, and Shock Waves, Trans. from Fizkia Goreniyz i Vzryva 10, 905 (1974).

28. V. F. Nesterenko, Combustion, Explosion, and Shock Waves, Trans. from Fizika Goreniya i Vzryva 11, 444 (1975).

29. E. B. Royce, Physics of High Energy Density (Proceedings of the International School of Physics 'Enrico Fermi,' Academic Press, New York and London, 1971), Course XLVIII, pp. 126-138.

30. D. E. Grady, J. Appl. Phys. 43, 1942 (1972).

31. D. E. Grady, G. E. Duvall, and E. B. Royce, J. Appl. Phys. 43, 1948 (1972).

32. R. A. Graham, J. Appl. Phys. 39, 437 (1968).

33. R. C. Wayne, J. Appl. Phys. 40, 15 (1969).

34. J. Y. Wong, J. Appl. Phys. 40, 1789 (1969).

35. P. A. Urtiew and R. Grover, J. Appl. Phys. 45, 140 (1974).

36. F. P. Bowden and D. Tabor, The Friction and Lubrication of Solids (Oxford University Press, London, 1950).

37. W. Herrman, J. Appl. Phys. 40, 2490 (1969).

38. R. R. Boade, Shock Waves and Mechanical Properties of Solids (Proceedings of the 17th Sagamore Army Materials Research Conference, Syracuse University Press, Syracuse, 1971), Chap. 12, pp. 263-285.

39. J. Crank, The Mathematics of Diffusion (Oxford Univ. Press, London, 1957), p. 37.

40. W. Jost, Diffusion in Solids, Liquids, Gases (Academic Press Inc., New York, 1960).

41. G. R. Fowles, G. E. Duvall, J. Asay, P. Bellamy, F. Feistmann, D. Grady, T. Michaels, and R. Mitchell, Rev. Sci. Instrum. 41, 984 (1970).

42. C. F. Peterson and J. T. Rosenberg, "Dynamic Properties of Rock Required for Prediction Calculations (V)," Stanford Research Institute Report for Defense Nuclear Agency DNA-3579F (1974).

43. National Bureau of Standards, Circular 561.

44. J. W. Taylor, J. Appl. Phys. 34, 2727 (1963).

45. W. J. Von Holle and J. J. Trimble, J. Appl. Phys. 47, 2391 (1976).

46. G. R. Hauver, Bull. Am. Phys. Soc. II, 20, 19 (1975).

47. G. R. Fowles, J. Appl. Phys. 32, 1475 (1961).

48. R. G. McQueen, S. P. Marsh, J. W. Taylor, J. N. Fritz, and W. J. Carter, High Velocity Impact Phenomena (Academic Press, New York, 1970), Chap. 7, pp. 293-417.

UNCITED REFERENCES

Neal Baum, Reynold Shunk and Robert Bunker, "Thermoelectric Thermopile Transducer (T^3) Development," Air Force Weapons Laboratory Report No. AFWL-TR-73-24 (1973).

S. Winkler, "Messung von Profilen schwacher Stosswellen," Vortrag, gehalten auf der Frühjahrstagung der Deutschen Physikalischen Gesellschaft, Fachausschuss Kurzzeitphysik, Hannover (1976).

S. W. Yuan and J. P. Billingsley, Appl. Sci. Res. 24, 431 (1971).

APPENDIX A

MEASUREMENT OF THE THERMOELECTRIC POWER OF AN OFHC COPPER AND A-CONSTANTAN THERMOCOUPLE

The thermoelectric power $S_{Cu-Co}(T)$ for the materials OFHC copper and A-constantan was determined by measuring the potential difference ϕ_{E-F} as in Fig. 1.5. The data taken for various values of T are given in Table A.1 where $T_o = 23 \pm 2°C$. The standard thermocouples were made from wire manufactured by Leeds-Northrop Co. with a rated accuracy of ± 3/4%.

TABLE A.1.--Thermopower Data at Zero Pressure

$(T-T_o)$ (°C)	ϕ_{E-F} (mv)
77	3.80
85	4.24
111	5.63
149	7.77
154	8.20
174	9.27
191	10.30
199	10.76
248	14.00
276	15.85
289	16.54
310	17.84

Using the method of least squares these data were fit to the expression

$$\phi_{E-F}(T-T_o) = Q(T-T_o) + R(T-T_o)^2$$

where

$$Q = 0.0475 \text{ mv/°C}$$

$$R = 3.4 \times 10^{-5} \text{ mv/°C}^2 .$$

The standard error of estimate is 0.095 mv. In Fig. A.1 the data taken for $\phi_{E-F}(T-T_o)$ and the associated least squares fit are given.

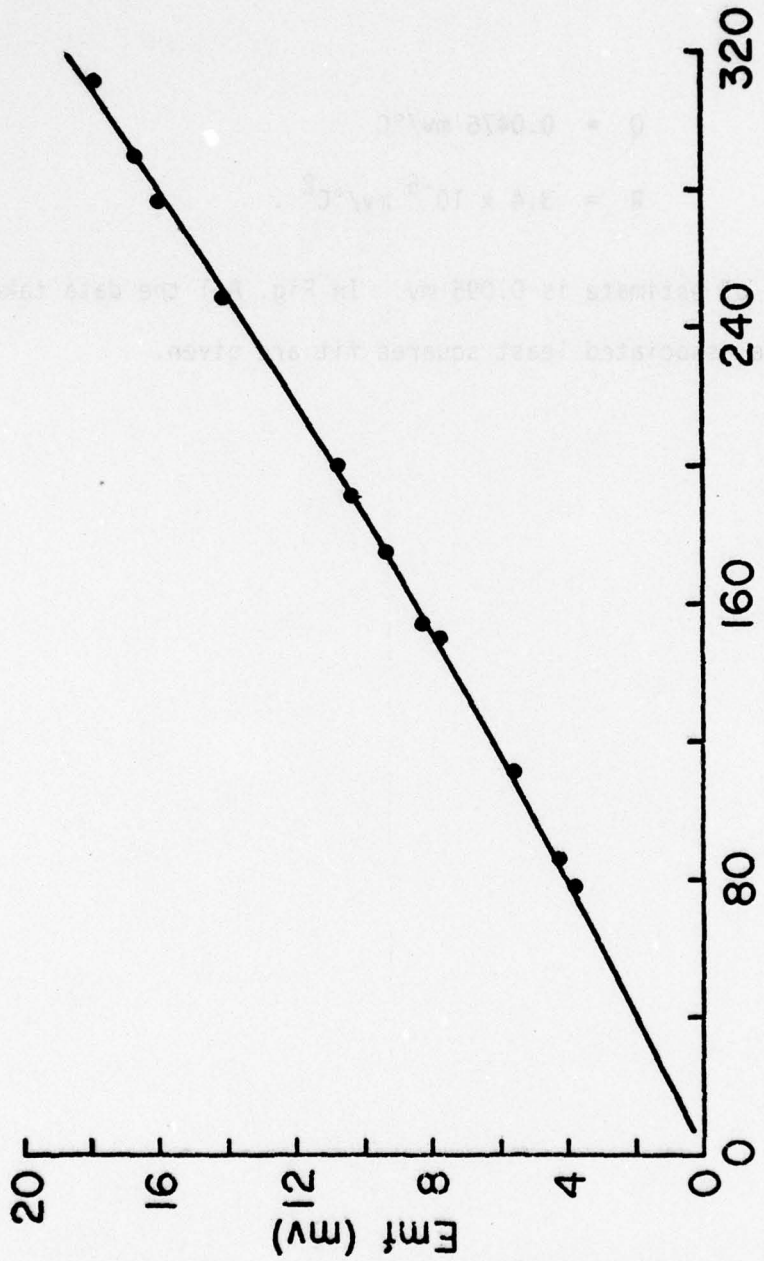

Fig. A.1.--Thermopower Data for Copper-Constantan Thermocouple at Zero Pressure. The solid line represents a least squares fit to the data.

APPENDIX B

TEMPERATURE CALCULATION

The temperature behind a single shock can be calculated as outlined in section 3.3. The temperature as a function of final shock pressure was found by numerically integrating the expression

$$T = e^{-G(v-v_o)}T_o + e^{-Gv}\int_{v_o}^{v} e^{Gv'}F(v')dv' \qquad (B.1)$$

where

$$G = \gamma_o/v_o ,$$

$$F(v) = \frac{4}{3}\frac{\tau}{C_v}\left(1 - \frac{v}{\mu}\frac{d\tau}{dv}\right) + \frac{1}{2C_v}\left(p_x - P_{x\ HEL}\right)\left]1 - \frac{v_{HEL} - v}{p_x - p_{x\ HEL}}\left(-\frac{dp_x}{dv}\right)\right] ,$$

$$\tau = (\sigma_x - \sigma_y)/2 \qquad \text{(maximum resolved shear stress)}$$

Here γ is the yield stress in uniaxial stress, μ is the shear modulus, p_x is the component of pressure in the shock propagation direction and C_v is the specific heat at constant volume. The subscript HEL refers to the value of the parameter at the Hugoniot elastic limit.

Work hardening can be included by letting τ be a function of volume. In simple uniaxial compressive stress the yield stress can be expressed as

$$Y = Y_o + H(\varepsilon_s - \varepsilon_s^o) \tag{B.2}$$

where ε_s is the natural strain in uniaxial stress and H is a constant. Fowles[47] has shown that

$$d\varepsilon_x = \frac{3}{2} d\varepsilon_s - \frac{dY}{6K} , \tag{B.3}$$

where ε_x is the natural strain in uniaxial strain and K is the isothermal bulk modulus. If the variation in K is neglected we have

$$\varepsilon_x - \varepsilon_x^o = \frac{3}{2} (\varepsilon_s - \varepsilon_s^o) - [(Y - Y^o)/6K] . \tag{B.4}$$

Equation B.2 can now be expressed as

$$(Y - Y_o)/2 = [\frac{H}{3} (\varepsilon_x - \varepsilon_x^o)]/(1 - \frac{H}{9K}) . \tag{B.5}$$

For reasonable values of H and K the term $\frac{H}{9K}$ is negligible compared to 1. The natural strain ε_x for the one-dimensional strain case can be expressed as a function of volume as

$$\varepsilon_x = \ln \frac{v}{v_o} . \tag{B.6}$$

Using the von Mises yield criteria for uniaxial strain,

$$Y = \sigma_x - \sigma_y \equiv 2\tau,$$

Eq. (B.5) becomes

$$\tau = \tau_o + \frac{H}{3} \ln \frac{v}{v_o} . \tag{B.7}$$

To calculate the temperature using Eq. (B.1) the pressure must be known as a function of volume along the Hugoniot. As the integration proceeds the values of p and dp/dv are calculated using a $U_s - U_p$ relation and the Rankine-Hugoniot relations. Using the relation

$$\rho_o U_s = p(U_s - U_p) \tag{B.8}$$

and a $U_s - U_p$ relation in the form

$$U_s = C_o + sU_p \tag{B.9}$$

we have

$$P = \frac{(v_o - v)C_o^2}{[v_o - (v_o - v)s]^2} . \tag{B.10}$$

The $U_s - U_p$ relations used for these calculations and to determine the final pressure in a given experiment are:

OFHC Copper[48]	C_o = 3.94 mm/μsec	s = 1.489
Tungsten Alloy	C_o = 3.97 mm/μsec	s = 1.11
A-Constantan	C_o = 4.24 mm/μsec	s = 1.55
B-Constantan	C_o = 4.20 mm/μsec	s = 1.55

The relation for the tungsten alloy was obtained by measuring the shock speed in two symmetric impact experiments at about 240 kbars and 355 kbars. Also the zero pressure intercept was estimated from ultrasonic sound speed measurements. The relation for A-constantan was obtained by measuring the shock speed in shots 77-005, 77-026, 77-037, 77-079, and 77-084. From the data trace (see Chapter 5) one can obtain the shock transit time through the constantan. With this and the known Hugoniot of copper one can determine the $U_s - U_p$ point for each experiment. The standard error of estimate for these five shots using the least squares fit given above is 0.05 mm/μsec. The relation for B-constantan was obtained by shifting the curve for A-constantan

to intercept the zero pressure bulk sound speed obtained from ultrasonic sound speed measurements.

The values for the remaining parameters necessary in this calculation which were used here are given in Table B.1. Temperatures calculated using Eq. (B.1) are given in Table B.2. For comparison, temperatures are listed with (A columns) and without (B columns) the work hardening correction. In the last column the calculated values of Rice et al.[10] for copper are included.

TABLE B.1.--Constants Used in Temperature Calculations

Parameter	OFHC Copper	A-constantan	B-constantan
γ*	1.99	2.26	2.06
v_{HEL}/v_o	0.99974	0.999382	0.99187
Y_o (kbar)†	-.2	-1	-1
τ_o (kbars)†	0.125	0.5	0.5**
H (kbars)†	15.5	3.74	3.74**
ξ (kbars)*	480.	810.	615.
ρ_o (g/cm^3)	8.93	8.93	8.82
C_v (10^6 ergs/gr°K)*	3.73	3.82	3.83
ν*	.35	.30	.32
ultrasonic longitudinal sound speed (mm/μsec)	4.81	5.60	5.187
ultrasonic transverse sound speed (mm/μsec)	2.32	3.01	2.64

*Derived from ultrasonic sound speed measurements done here and handbook values of C_p in the case of C_v.

†From quasistatic yield stress measurements done here.

**Value for A-constantan was used.

TABLE B.2.--Temperature Rise in a Shock

Pressure (kbar)	Temperature Rise (°C)						
	OFHC Copper		A-constantan		B-constantan		
	A*	B**	A*	B**	A*	B**	Copper†
50	24	24	23	23	21	21	--
100	48	48	45	45	43	42	43
150	76	76	70	70	67	66	69
200	110	109	99	99	96	95	101
250	151	159	134	134	130	130	138
300	198	196	175	174	170	170	181
350	252	249	221	220	216	216	235
400	312	309	273	272	268	268	291
450	380	376	330	329	327	326	353
500	454	449	393	392	390	389	424

*The "A" columns are values with work hardening.

**The "B" columns are values without work hardening.

†Reference 10.

APPENDIX C

ELECTRICAL NOISE AT IMPACT

Four experiments were done specifically to investigate the problem of electrical signals produced when a thermoelectric circuit is completed by the impact. The experimental configuration is illustrated in Fig. C.1, and the voltage time profile for each shot is given in Fig. C.2. Since each experiment was somewhat different a short description of each will follow.

76-073. The configuration is symmetric with respect to the impact plane except for the Nichrome V center element in the target. This material was used here to simulate the constantan since it has similar mechanical and magnetic properties and is more readily available. The impactor assembly was mounted on an aluminum projectile (see section 4.4). The oscilloscopes were triggered about 10 μsec before impact. The emf was measured between the inner and outer pieces of the target assembly with a differential measuring system as described in section 4.4. The magnetic field in the impact area was about 0.15 Gauss in a direction perpendicular to the direction of motion. The projectile velocity for this series of shots was 0.6 mm/μsec ± 0.02 mm/μsec.

76-075. In this experiment the magnetic field in the area of impact was lowered to less than 0.005 Gauss in any direction with Helmholtz coils. In all other respects the experiment was the same as 76-073.

76-078. The projectile in this shot was modified by placing a one inch plastic piece on the front of the projectile between the aluminum body and the copper active elements. This was done to reduce the effects of a

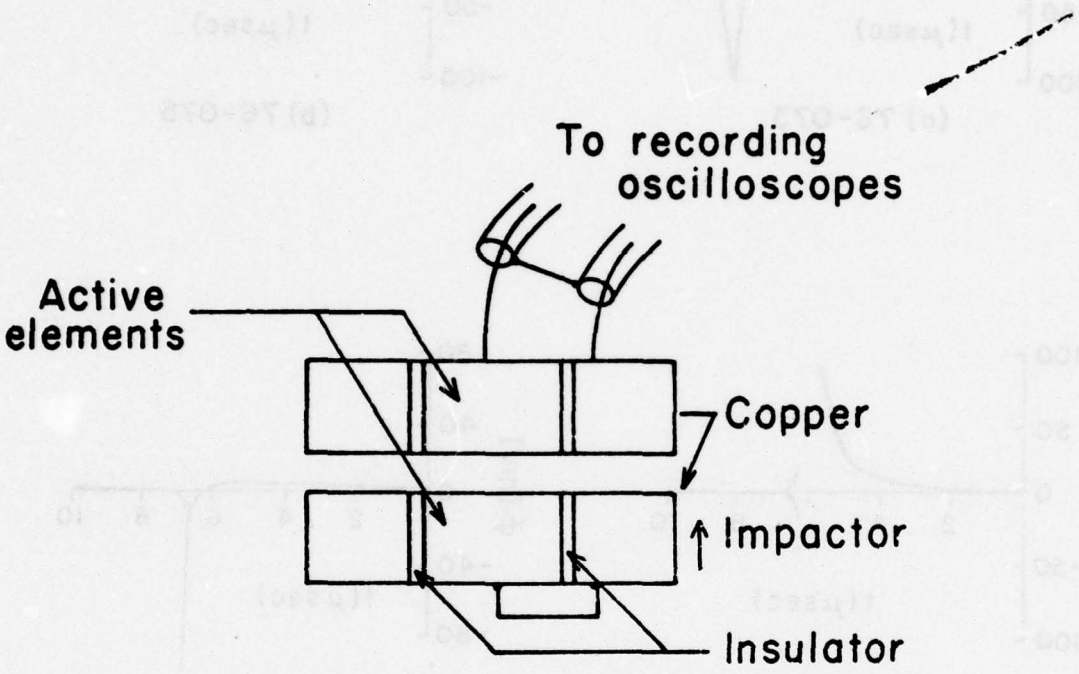

Fig. C.1.--Concentric Ring Experimental Configuration.

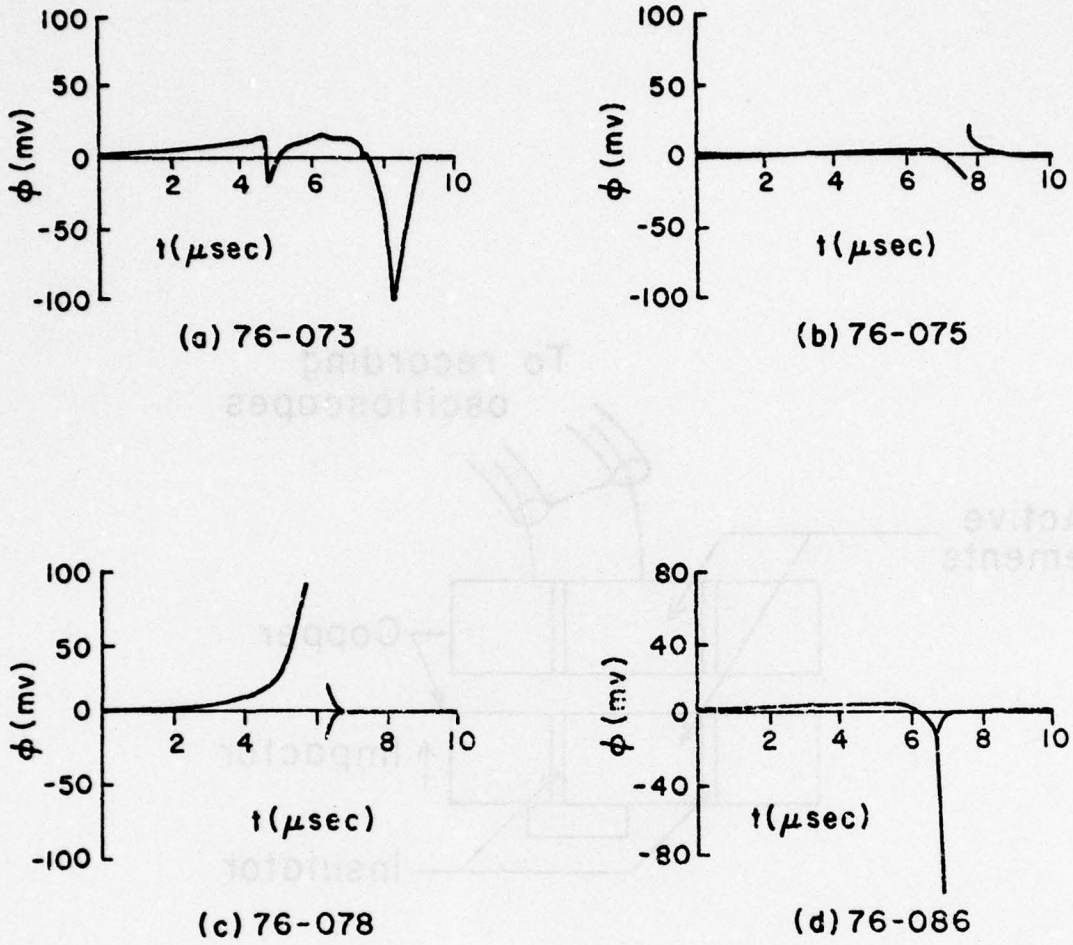

Fig. C.2.--Voltage-Time Profiles for Shots 76-073, 76-075, 76-078, and 76-086.

moving conductor in a magnetic field near the impact. In all other respects the experiment was the same as 76-073.

76-086. The center element of this target was made of copper which makes the projectile and target assemblies indentical. Again, the experiment was the same in all other respects as 76-073.

The objective of this study was to determine the cause of this type of noise and eliminate it if possible. By lowering the magnetic field in the impact area the amplitude of the signal was reduced as seen in 76-075. We concluded that the pre-impact signal and associated noise at and just after impact were probably due to an interaction of the moving conductors with the magnetic field. We determined that if the remaining signal observed in 76-078, where the field was reduced to 0.005 Gauss, is due to the residual magnetic field, it would be impossible to eliminate this type of noise in our facility.

APPENDIX D

SHOCK DEMAGNETIZATION

Eight experiments were conducted in a study of the effects of shock demagnetization in bimetallic junction experiments. The basic experimental technique, based on the use of a four-inch light gas gun, is detailed in section 4.4. Instrumentation involved a combination of oscilloscopes used in a differential mode as indicated in the schematic drawing of Fig. 4.5. The material used, except where noted, was nickel-200, formerly called "A" nickel, which is nominally 99.4% nickel. In all experiments, except 76-054 and 76-051, the magnetization state was not altered from the supplied condition and was assumed to be random in direction with respect to the axis of shock propagation. Since each of the experiments was performed with a different objective in view, a short description of each will follow, with the results summarized in Table D.1.

76-032. A concentric guard ring geometry was used as illustrated in Fig. C.1. The insulator used was machined from solid teflon. The outer ring used in this case for support and to complete the circuit, was made from OFHC copper. The configuration is symmetric with nickel impacting nickel as active elements so that no thermoelectric emf is expected. However, a non-zero signal was observed. The voltage versus time profile, as seen in Fig. D.1, indicates a zero voltage at impact with a continuously increasing magnitude of negative sign. This result represents the initial indication that nickel in this type of experiment would cause a non-zero signal.

TABLE D.1.--Summary of Data on Shock Demagnetization

Shot Number	Proj. Vel. (mm/μsec)	Pressure (kbar)	Impactor Material	Target Material(s)	Expected** Emf (mv)	Maximum Observed Emf (mv)	Experimental Configuration	Results
76-032	0.58	132 ± 2	Nickel	Nickel	0	-109	Fig. C.1	Fig. D.1
76-037	0.59	134 ± 2	Nickel	Nickel	0	-32	Fig. D.2	Fig. D.1
76-039	~0.5*	~114	Nickel	Nickel	0	+97	Fig. D.2	Fig. D.1
76-040	0.55	125 ± 2	Nickel	Nickel	0	+57	Fig. D.3	Fig. D.1
76-051	0.59	70 ± 2	Aluminum	Nickel	-1	-40	Fig. D.4	Fig. D.5
76-054	~0.6*	~70	Aluminum	Nickel	-1	-7	Fig. D.4	Fig. D.5
76-052	0.69	148 ± 2	Copper	Copper-Nickel	-1.5	-10 ± 2	---	Fig. D.5
76-062	0.60	155 ± 5	Nichrome V†	Nichrome V†	0	0 ± 0.1	Fig. C.1	Fig. D.5

*Velocity measurement failed.

†Nichrome V is a trademark of Driver Harris Co., Harrison, New Jersey.

**The "Expected Emf" is based on a thermoelectric response to shock compression temperature rise.

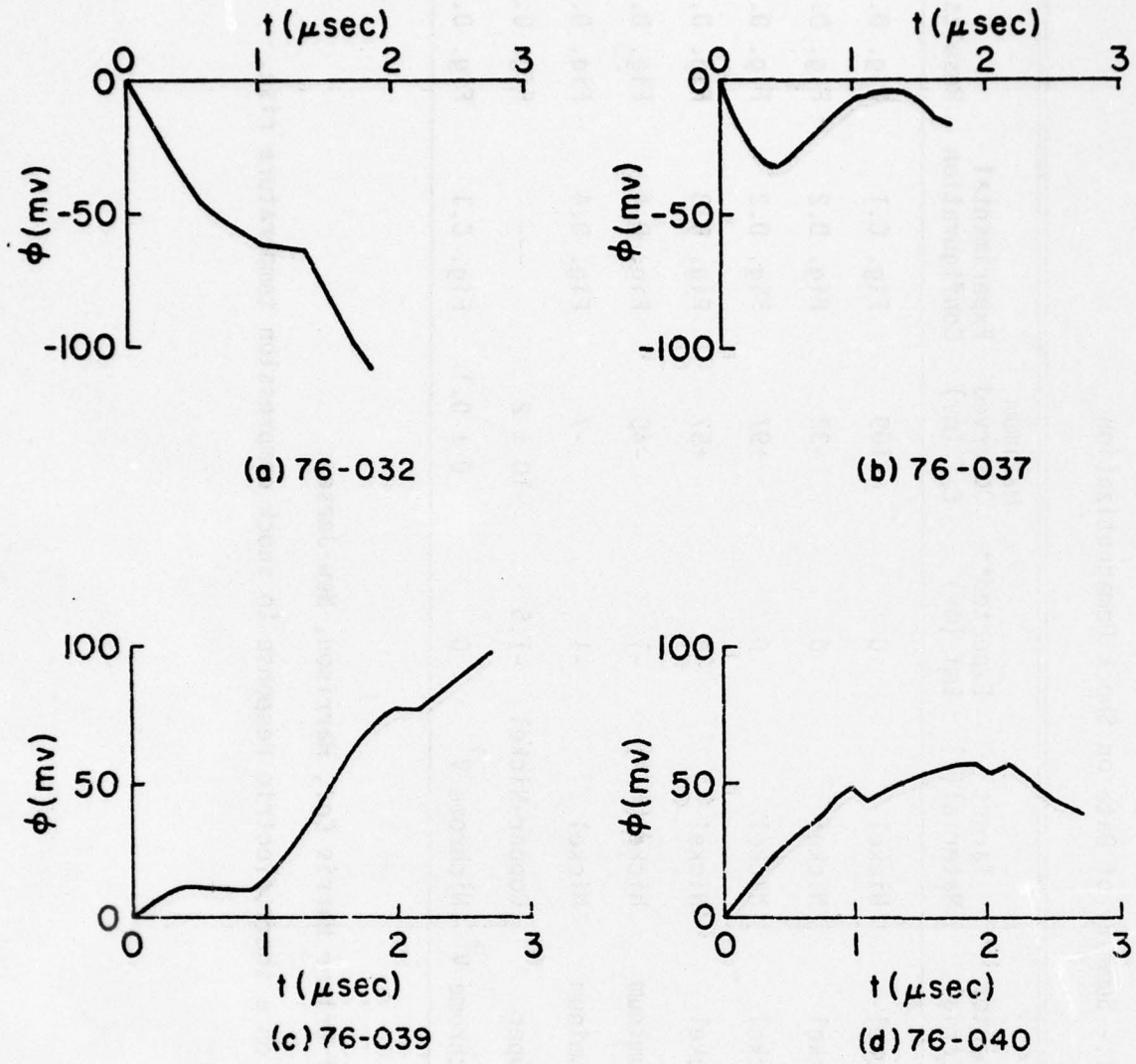

Fig. D.1.--Voltage-Time Profiles for Shots 76-032, 76-037, 76-039, and 76-040.

However, it was thought that the compression of the teflon insulator might contribute to the non-zero signal through a dielectric polarization mechanism.

76-037. In order to eliminate the ambiguity with respect to the insulator in shot 76-032, the geometry of this experiment was altered as shown in Fig. D.2. The return path for the signal is completely independent of the shock guard ring system, including the insulator. Direct measurement of any shock polarization is thus eliminated. Again a negative non-steady emf was recorded with an initial value of zero. (See Fig. D.1.) The time variation of the signal is entirely different from that of shot 76-032 for reasons unknown.

76-039. This experiment was designed to duplicate 76-037 except for the projectile design. The projectile used was machined from solid nylon in order to modify the pre-impact noise observed in this type of experiment in which the circuit is completed at impact. The resulting voltage-time profile, shown in Fig. D.1, is again initially zero but positive thereafter. This change in sign may be a result of the lack of characterization of the material with respect to magnetic properties.

76-040. The guard ring was completely eliminated in this experiment to clearly indicate an effect involving only the nickel active element (as seen in Fig. D.3). The resulting voltage-time profile is again positive (see Fig. D.1).

The next series of experiments was designed to show specifically whether or not the observed non-zero signals in this type experiment were due to demagnetization.

76-051. The geometry used for this experiment, where the nickel element is impacted directly by an aluminum projectile, is shown in Fig. D.4. This shot was done as a control experiment for the shot to follow, 76-054,

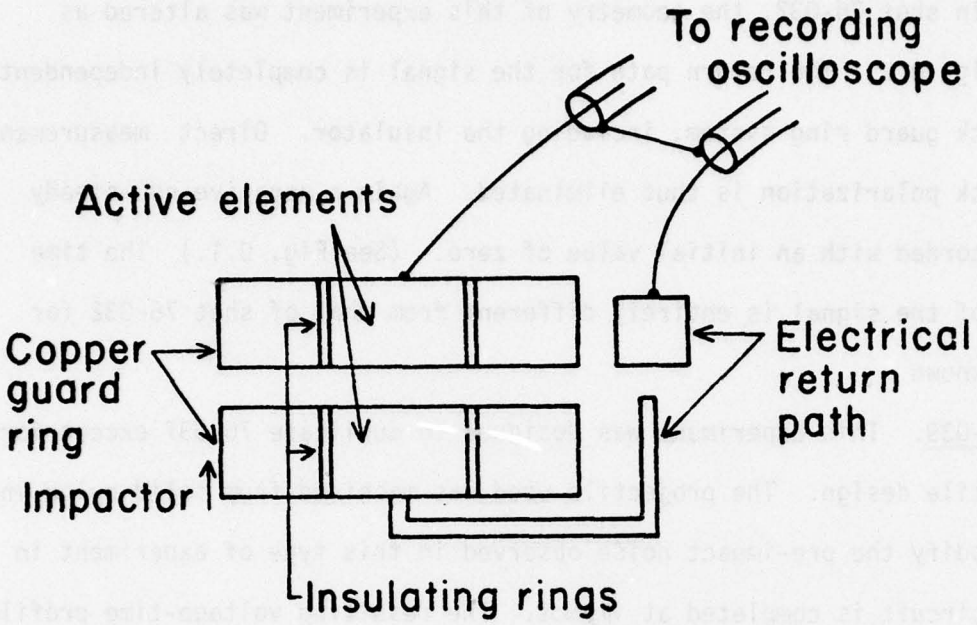

Fig. D.2.--Modified Concentric Ring Configuration Used in Shots 76-037 and 76-039.

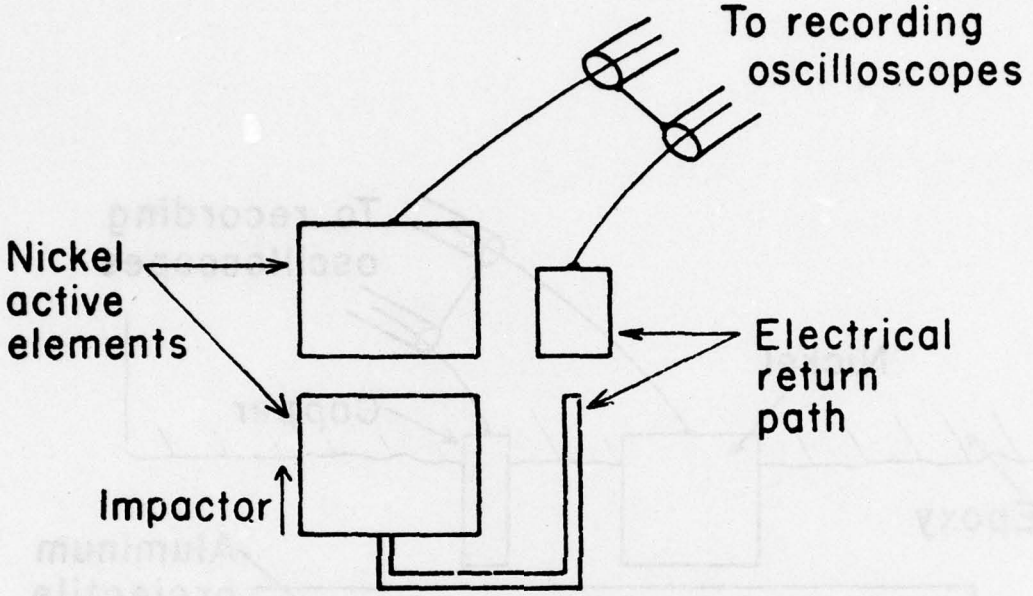

Fig. D.3.--Experimental Configuration Used in Shot 76-040.

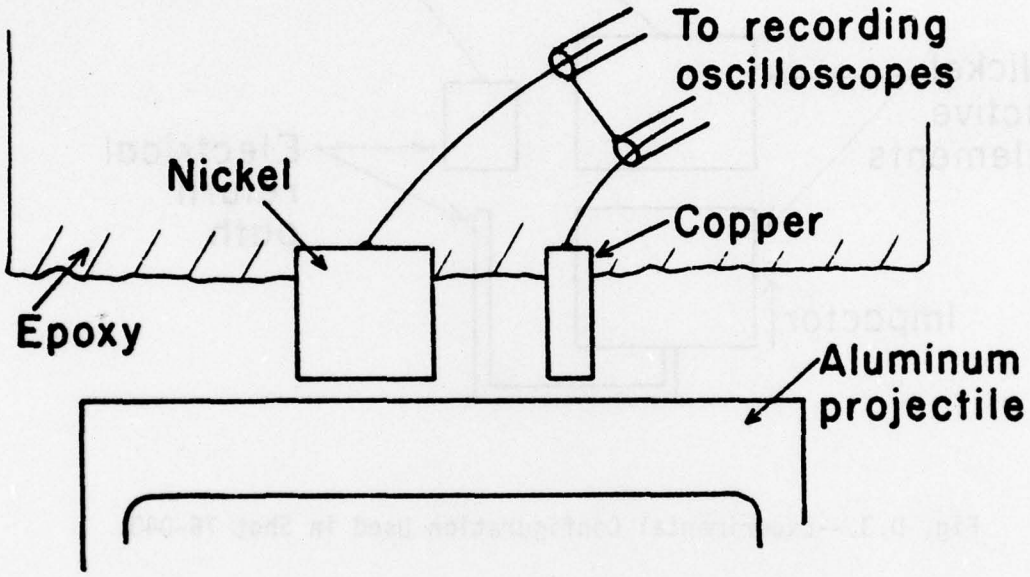

Fig. D.4.--Experimental Configuration Used in Shots 76-051 and 76-054.

and the modification in design from previous shots was for simplicity of construction and analysis. The magnetization state was not altered from its supplied configuration, and was characterized by measuring the magnetic field just outside the body. The magnetic induction $\vec{B}$ was approximately 0.8 Gauss with components in directions parallel and perpendicular to the shock propagation direction. The resulting data trace has much the same character as those of the previous series with an amplitude of -40 mv. (See Fig. D.3.)

76-054. In this experiment, the magnetization of the nickel was decreased by careful demagnetization, using an alternating field, to a value less than 0.05 Gauss in any direction. In all respects, the experiment was conducted in the same manner as shot 76-051. The resulting amplitude varied between 3 mv and 7 mv with an initial value of zero (see Fig. D.5). In these two experiments, a reduction in initial magnetization resulted in a corresponding reduction in the absolute value of the emf recorded.

76-062. This experiment involved the use of a concentric guard ring system as used in shot 76-032 and shown in Fig. C.1. The material used for the active center element was Nichrome V,* an alloy composed of 80% nickel and 20% chromium. The material was chosen because of the mechanical similarity to nickel, and because it is paramagnetic at room temperature and pressure. The voltage-time profile, shown in Fig. D.5, indicates no emf produced during the time of shock transit through the target to within the recording capability of the instrumentation system of 0.01 mv.

The final experiment to be considered, 76-052, was designed to duplicate the conditions in the experiments reported by Buzhinskii and Samylov.[19] The geometry involved is the same as that used to investigate the effects of surface preparation, and is discussed in Appendix E (see Fig. E.1). The emf

*Trademark of Driver Harris Co., Harrison, New Jersey.

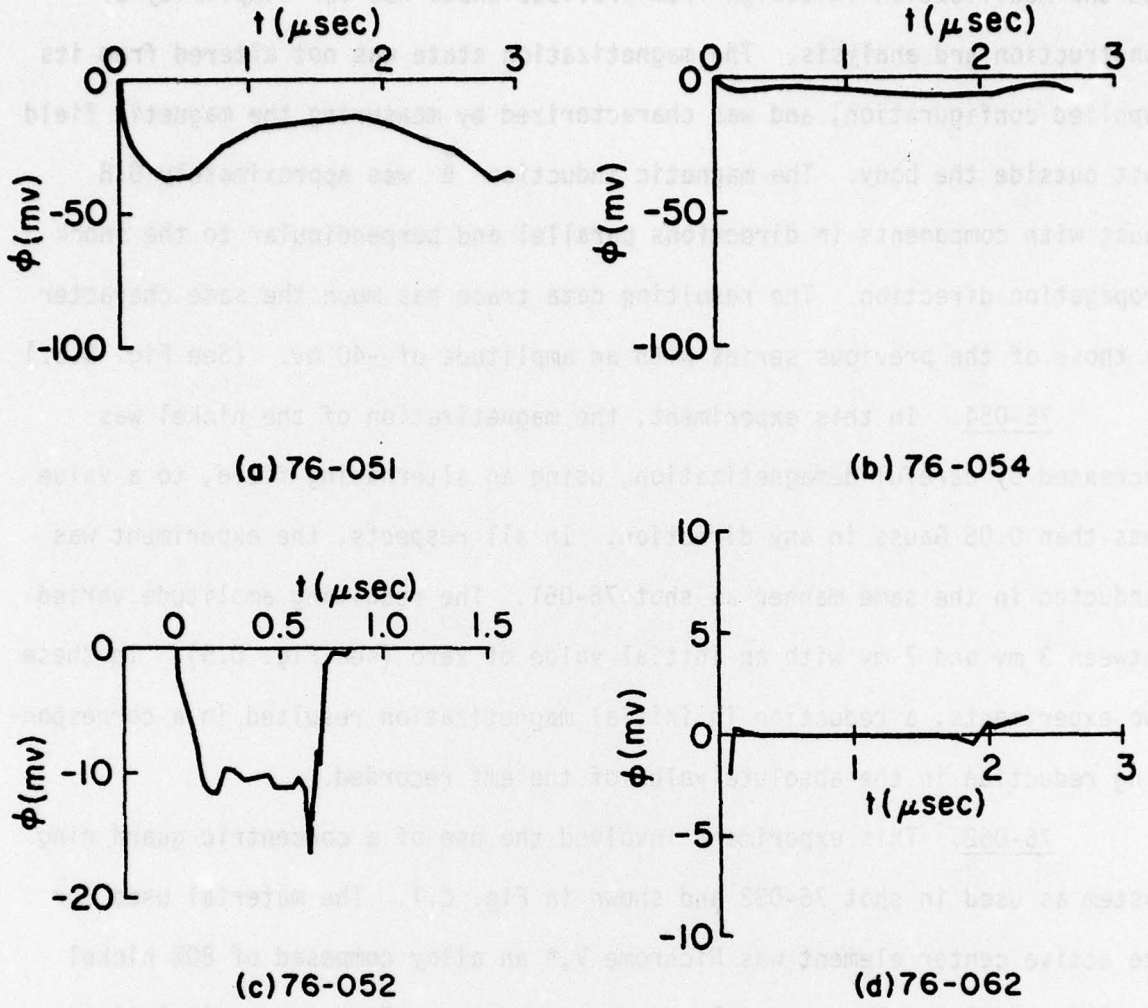

Fig. D.5.--Voltage-Time Profiles for Shots 76-051, 76-054, 76-052, and 76-062.

recorded is shown in Fig. D.5. It does not appear to be possible at this point to determine how the signals recorded in this way are affected by the demagnetization. This determination would involve separating the demagnetization effect from the normal response of a bimetallic junction under these conditions.

APPENDIX E

CALCULATIONS AND EXPERIMENTS INVOLVING THE SURFACE LAYER AT THE JUNCTION

Consider the temperature distribution of Fig. 3.4. The time dependence of the initial distribution can be studied using the one-dimensional heat flow equation. The appropriate solutions are most easily found using Green's functions. In one dimension, the diffusion equation for temperature is

$$\frac{\partial^2 T}{\partial x^2} = \frac{1}{D}\frac{\partial T}{\partial t} \qquad \text{(E.1)}$$

where

$D = \frac{\kappa}{\rho} C_v$

κ = thermal conductivity

ρ = mass density

C_v = constant volume specific heat.

The unit source function or Green's function for a unit source at position x' is given by Carslaw and Jaeger[11] as

$$G(D, x, x', t) = \frac{1}{2\sqrt{\pi D t}} \exp\left(-\frac{(x - x')^2}{4Dt}\right) . \qquad \text{(E.2)}$$

In a situation where two different metals with associated thermal properties are involved, as in Fig. 3.4, a more complex source function must be used. Carslaw and Jaeger[11] give the Green's function for a source in a

region 2 located a distance ℓ from the interface at the origin as

$$G_2(x, \ell, t) = \frac{2\alpha}{1+\alpha} G(D_1, x, \alpha\ell, t) \quad \text{for } x < 0$$

$$G_2(x, \ell, t) = G(D_2, x, \ell, t) + \frac{1-\alpha}{1+\alpha} G(D_2, x, -\ell, t) \quad \text{for } x > 0 . \tag{E.3}$$

Now for a source in region 1, again located a distance ℓ from the origin, we have

$$G_1(x, \ell, t) = G(D_1, x, \ell, t) + \frac{1-\beta}{1+\beta} G(D_1, x, -\ell, t) \quad \text{for } x < 0$$

$$G_1(x, \ell, t) = \frac{2\beta}{1+\beta} G(D_2, x, \beta\ell, t) \quad \text{for } x > 0 \tag{E.4}$$

where

$$\alpha = \frac{\kappa_1}{\kappa_2} (D_2/D_1)^{1/2} \simeq (\kappa_1/\kappa_2)^{1/2}$$

and

$$\beta = 1/\alpha$$

The effect of the interface on a source in region 1 is that in region 2 the source appears displaced to a position $\beta\ell$ and reduced in amplitude by a factor $2\beta/(1+\beta)$, while in region 1 an additional source appears in a reflected location and of amplitude $(1-\beta/1+\beta)$. A similar situation exists for a source in region 2. Now to find the temperature history due to a square initial temperature profile we have:

$$T = T_1 \quad |x| > a \ , \ t = 0$$

$$T = T_2 \quad -a \leq x \leq a \ , \ t = 0$$

$$T(x,t) = \int_{-a}^{0} T_2 \frac{2\beta}{1+\beta} G(D_2, x, \beta\ell, t)d\ell$$

$$+ \int_{0}^{a} T_2[G(D_2, x, \ell, t) + \frac{1-\alpha}{1+\alpha} G(D_2, x, -\ell, t)]d\ell \quad \text{for } x > 0 . \qquad (E.5)$$

For simplicity T_1 is taken to be the zero of temperature. A similar expression holds for $x < 0$; however, to find $T(x = 0, t)$ one need only solve for one half space. The solution is given in terms of error functions as

$$T(x,t) = T_2 \{ \frac{1}{1+\beta} \text{ erf } (\frac{x+\beta a}{\sqrt{4D_2 t}}) - \frac{1}{2} \text{ erf } (\frac{x-a}{\sqrt{4D_2 t}})$$

$$+ \frac{1}{2} (\frac{1-\alpha}{1+\alpha}) \text{ erf } (\frac{x+a}{\sqrt{4D_2 t}}) \} \quad \text{for } x > 0 . \qquad (E.6)$$

Of primary interest is the solution at $x = 0$ which is

$$T(0,t) = T_2 \{ \frac{\alpha}{\alpha+1} \text{ erf } (\frac{a}{\alpha\sqrt{4D_2 t}}) + \frac{1}{1+\alpha} \text{ erf } (\frac{a}{\sqrt{4D_2 t}}) \} \qquad (E.7)$$

If region 1 is taken to be constantan and region 2 is copper, $T(0,t)$ becomes

$$T(0,t) = T_2 \{ \frac{1}{5} \text{ erf } (2\sqrt{\tau/t}) + \frac{4}{5} \text{ erf } (\frac{1}{2}\sqrt{\tau/t}) \} \qquad (E.8)$$

where $\tau = a^2/D_2$.

Two experiments were conducted to determine the effects of surface preparation in a geometry in which the two surfaces making up the junction are held in contact before shock compression. The configuration for each of these experiments is given in Fig. E.1. In these two experiments the only

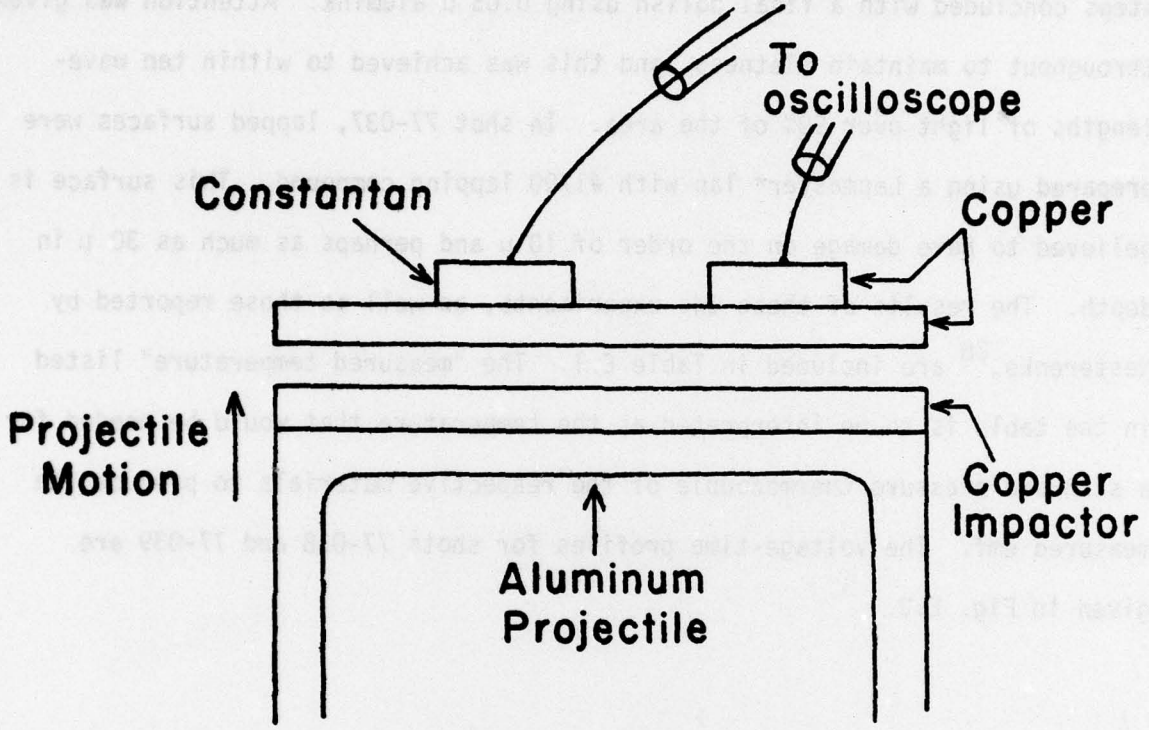

Fig. E.1.--Experimental Configuration Used in Shots 77-038, 77-039, and 76-052.

controlled difference was the surface on both the copper buffer and the constantan element. The materials used for the junction in both shots were B-constantan and OFHC copper as described in section 4.2. In shot 77-038, a highly polished surface was prepared using a series of diamond polishing steps concluded with a final polish using 0.05 μ alumina. Attention was given throughout to maintain flatness, and this was achieved to within ten wavelengths of light over 90% of the area. In shot 77-037, lapped surfaces were prepared using a Lapmaster* lap with #1700 lapping compound. This surface is believed to have damage on the order of 10 μ and perhaps as much as 30 μ in depth. The results of these two experiments, as well as those reported by Nesterenko,[28] are included in Table E.1. The "measured temperature" listed in the table is to be interpreted as the temperature that would be needed for a standard pressure thermocouple of the respective materials to produce the measured emf. The voltage-time profiles for shots 77-038 and 77-039 are given in Fig. E.2.

*Trademark of Crane Packing Co., Morton Grove, Illinois.

TABLE E.1.--Summary of Data in Surface Preparation Studies

Shot Number	Junction Materials	Area of Junction (mm^2)	Projectile Velocity (mm/μsec)	Pressure (kbar)	Emf (mv)	Measured Temp.* (°C)	Surface Condition
77-037	Copper-Constantan	284	0.70 ± .01	146 ± 3	19 ± 1	362	lapped
77-038	Copper-Constantan	284	0.70 ± .01	146 ± 3	16 ± 2	312	polished
Nesterenko[28]	Copper-Nickel	3.14	---	400	19 ± 3	780	"rough"
Nesterenko[28]	Copper-Nickel	3.14	---	400	11 ± 3	500	"mirror polish"

*The "measured temperature" is that temperature above room temperature which would give rise to the measured Emf in a thermocouple of the appropriate materials.

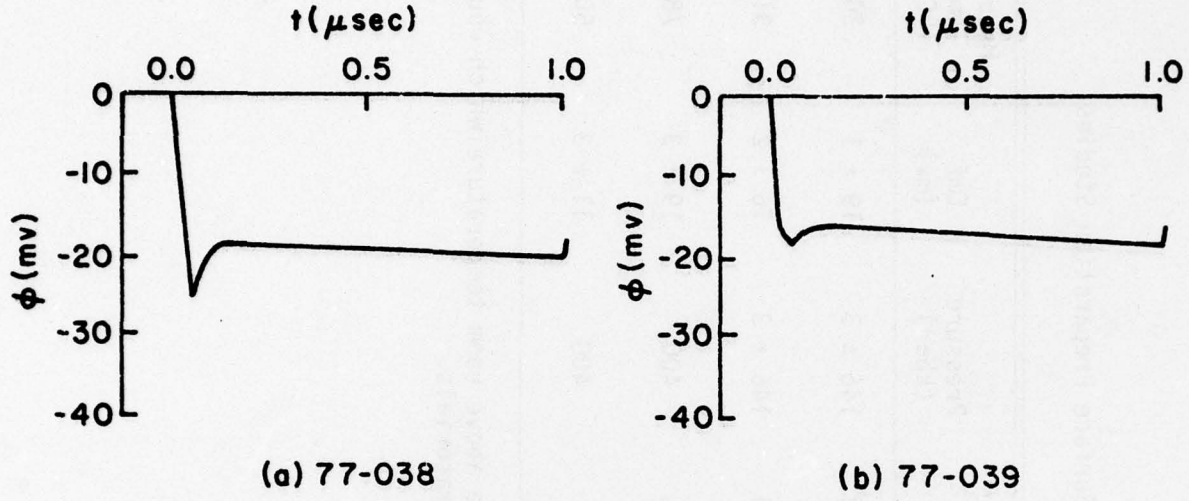

Fig. E.2.--Voltage-Time Profiles for Shots 77-038 and 77-039.

APPENDIX F

THE EFFECTS OF A CHANGING INDUCTANCE AND SPECIAL RELATIVITY WHEN RADIAL PRESSURE RELIEF IS ALLOWED

Consider the effect of the changing inductance in a thermoelectric circuit as a possible source of the ramping discussed in section 5.1. The pressure relief waves behind the shock will accelerate particles radially outward. The radius of the constantan will thus be increasing with time. As a model to investigate this problem consider a circuit with a constant emf source, ϕ, representing the thermal emf, a resistive element, R, representing the input impedance of the recording circuit, and an inductance, L. The inductance will have a component, L_1, which changes with time representing the changing inductance of the expanding conductor. The differential equation for the circuit is

$$L \frac{dI}{dt} + I \frac{dL_1}{dt} + IR = \phi \qquad \text{(F.1)}$$

At $t = 0$ we will assume the current has a value ϕ/R. This equation has the solution

$$I = Ae^{(-t/\tau)} + \frac{\phi}{R + \frac{dL_1}{dt}} \qquad \text{(F.2)}$$

where

$$A = \frac{\frac{dL_1}{dt}\phi}{R^2 + R\frac{dL_1}{dt}} \quad \text{and} \quad \tau = \frac{L}{R + \frac{dL_1}{dt}}$$

To estimate the value of $\frac{dL_1}{dt}$ we will model the expanding constantan cylinder by the solid center conductor of a coaxial transmission line. The inductance of a coaxial conductor of length ℓ in MKS units is

$$L_1 = \frac{\mu_o \ell}{2\pi} \left(\ln \frac{b}{a} + \frac{1}{2} \frac{\mu}{\mu_o}\right) \qquad (F.3)$$

where μ_o is the permeability in a vacuum, μ is the permeability of the conductor material, a is the radius of the center conductor and b is the radius of the outer conductor. Now if a increases with time, but b remains constant, the rate of change of the inductance is

$$\frac{dL_1}{dt} = -\frac{\mu_o \ell}{2\pi} \frac{1}{a} \frac{da}{dt} \qquad (F.4)$$

If a and ℓ are the radius and length (10 mm, and 5 mm) of the constantan and $\frac{da}{dt}$ has a value of 1 mm/μsec then $\frac{dL_1}{dt}$ has the value 1×10^{-4} henry/sec. Since Eq. (F.3) is derived assuming an infinitely long coaxial transmission line the value of L for the dimensions here will be inaccurate. However, this calculation should give a reasonably good approximation for $\frac{dL_1}{dt}$.

The time constant τ is 0.5 ns where $L = 0.05$ μhenry, $R = 100\ \Omega$, and $\frac{dL_1}{dt} = 1 \times 10^{-4}$ henry/sec. The value for R is the actual input impedance for our recording system and the value for L is an estimate of the total inductance of the experimental configuration. The effect on τ of the changing inductance is negligible.

The measured steady state emf will be

$$\phi_m = \frac{\phi}{1 + \frac{1}{R} \frac{dL_1}{dt}}$$

Using a binomial expansion this becomes

$$\phi_m = (1 - \frac{1}{R}\frac{dL_1}{dt} + (\frac{1}{R}\frac{dL}{dt})^2 + \ldots) \qquad (F.5)$$

The first term in $\frac{dL_1}{dt}$ has a value of 1×10^{-6} for the values given above which is obviously negligible compared to 1.

Although the assumptions made here to do this calculation are not valid, the estimate of the value of $\frac{dL_1}{dt}$ should be within 1 or 2 orders of magnitude. The effect of this changing inductance would still be negligible and could not account for the observed ramping.

To examine the relativistic effect on the electric field due to radial pressure relief in the experiments discussed in section 5.1 consider a conducting cylinder with a uniform current density $\vec{I}$, and electric field $\vec{E}$ in the direction of the cylinder axis. The pressure relief waves from the edges will accelerate the particles radially so that the velocity $\vec{v}$ will be perpendicular to the electric field everywhere. If the electric field is locally unchanged in the moving material, the electric field measured in the stationary laboratory frame is

$$\vec{E} = \gamma(\vec{E}' - \frac{\vec{v}}{c} \times \vec{B}') \qquad (F.6)$$

where $\vec{E}'$ and $\vec{B}'$ are measured in the moving frame, and

$$\gamma = \frac{1}{\sqrt{1 - \frac{v^2}{c^2}}} \qquad (F.7)$$

For a uniform radial particle velocity of 1 mm/μsec, which is larger than would be possible in any experiments done here, the value of γ is 1.00000167. The term in $\vec{B}'$ is negligible compared to $\vec{E}'$ so that $\vec{E}$ and $\vec{E}'$ are indistinguishable in this type of experiment.